Solvent-Free Electrode Fabrication Based on Polytetrafluoroethylene Fibrillation for Lithium-ion Batteries

by

Yang Zhang

Thesis submitted in fulfilment of
the requirements for the degree of
PHILOSOPHIAE DOCTOR
(PhD)

Faculty of Science and Technology
Department of Energy and Petroleum Engineering
2022

University of Stavanger
NO-4036 Stavanger
NORWAY
www.uis.no

ISBN: Click to enter ISBN.
ISSN: Click to enter ISSN.
PhD: Thesis UiS No. Click to enter PhD No.

ACKNOWLEDGEMENTS

First and foremost, I want to thank my PhD supervisor, Prof. Zhixin Yu from University of Stavanger. During the past three years, he offered me trust and freedom, which are guarantees for my successful study and research. His passion towards excellence will always be an inspiration to me. I also would like to offer my undying gratitude to my advisor Dr. Fengliu Lou from Beyonder AS. He devoted so much time and energy to offer me guidance both academically and industrially. I believe the skill and inspiration I got from him will help me all my life.

Special thanks to my colleague Song Lu in UiS. He gave me much help and enlightenment for my research. I'm grateful to my colleagues Frederik Huld and Obinna Egwu Eleri from Beyonder AS. As industrial PhD candidates in Beyonder, we had many memorable experiences both in office and after working. I also would like to express my gratitude to all my lab mates in Beyonder who helped me a lot in many ways. I am greatly appreciative for the help from the CEO and founder of Beyonder, Svein Kvernstuen, who offered me the opportunity to conduct my PhD research.

I would like to give my thanks to the financial support from Norwegian Research Council (NRC) for industrial PhD project under project number 310353.

My special appreciation is given to my parents and brother, for their everlasting love and unconditional support. Last but not the least, I would give my sincerest thanks to my fiancée Dr. Yongfang Zheng. Her understanding and encouragement are always the best support for me whatever difficulties encountered during last three years, especially during covid pandemic. Without her wholehearted supporting, I cannot image I would have courage to start this amazing journey.

Yang Zhang

Sep, 2022, Stavanger

Abstract

The commercial lithium-ion batteries (LiBs) electrodes are manufactured with slurry casting (SC) procedure, where a large amount of energy is consumed, increasing the manufacturing cost a lot. In addition, the SC procedure limits the fabrication of thick electrode caused by binder floating during drying process. Developing new procedures for electrode manufacturing to improve specific energy and lower cost is highly desired. One of the most promising technical routes to achieve the goal is solvent free (SF) procedure for electrode fabrication, where no solvent is involved, thus avoiding drawbacks of SC procedure. SF procedure for electrode fabrication has attracted tremendous attention both from academia and industry, especially polymer (polytetrafluoroethylene (PTFE)) fibrillation-based procedure, because the roll-to-roll process make the procedure compatible to commercial LiBs production line.

During this procedure, PTFE is fibrillated under high shear force to generate fibrils to bundle active materials together to form self-supporting electrode film when the fibrillated dry mixture is hot rolled. However, PTFE is instable under low voltage, making this procedure is not suitable for anode fabrication. On the other hand, the procedure works well with activate carbon or lithium nickel manganese cobalt oxide materials (NMC), but it cannot be used for lithium iron phosphate (LFP). In this project, we fabricated SF anodes with different active materials including graphite, hard carbon, and soft carbon. SF hard carbon and soft carbon electrodes with low volume variation during charge/discharge cycling showed good cycling life, while SF graphite electrode with big volume swelling and shrinking demonstrated fast capacity fading. With comprehensive study of different anodes, the failure mechanism of SF anodes was proposed that PTFE is reduced to amorphous carbon at first lithiation process. For the graphite electrode, the big volume swelling and shrinking makes the electrode lose the integrity and results in fast capacity fading. While the hard carbon and soft carbon electrodes can keep the integrity of electrodes even though the PTFE is reduced because the volume variation is small. Basing on insights of the failure mechanism, dual binder system was adopted to address the instability issue of PTFE fibrillation-based SF

graphite anode, where PTFE acted as self-supporting electrode formation aid reagent, while polyvinylidene fluoride (PVDF) acted as functional binder. With the help of PVDF, the SF graphite anode demonstrated good cycling stability

To further expand the application of PTFE fibrillation-based SF electrode manufacturing, LFP cathode was fabricated successfully with the help of carbon nanotubes (CNT). CNT on the one hand acted as conductive additive to increase the conductivity of the electrode. On the other hand, CNT played the role as LFP powders matrix to ensure further PTFE fibrillation, which is essential for self-supporting LFP electrode film formation. Finally, SF LPF/hard carbon full cells were assembled and demonstrated good stability with more than 95% of capacity retention after 50 cycles under 0.5 C in coin cells. With prelithiation, the initial coulombic efficiency (ICE) of full cell increased to close to 100%, which showed big advantage of prelithiation in specific energy enhancement.

List Publications

I. Revisiting Polytetrafluorethylene Binder for Solvent-Free Lithium-Ion Battery Anode Fabrication.

Yang Zhang, Frederik Huld, Song Lu, Camilla Jektvik, Fengliu Lou and Zhixin Yu.

Batteries. 2022, 8(6), 57.

II. Leveraging Synergies by Combining Polytetrafluorethylene with Polyvinylidene Fluoride for Solvent-Free Graphite Anode Fabrication.

Yang Zhang, Song Lu, Fengliu Lou and Zhixin Yu.

Energy Technology. 2022, 10.1002/ente.202200732.

III. Recent Technology Development in Solvent-Free Electrode Fabrication for Lithium-Ion Batteries

Yang Zhang, Song Lu, Zaisheng Wang, Vladislav Volkov, Fengliu Lou and Zhixin Yu.

Submitted

IV. Solvent-free Lithium Iron Phosphate Cathode Fabrication with the Fibrillation of Polytetrafluoroethylene

Yang Zhang, Song Lu, Fengliu Lou and Zhixin Yu.

Submitted.

This thesis is based on above four papers. Chapter 1, in part, is a reprint of the material of "Recent Technology Development in Solvent-Free Electrode Fabrication for Lithium-Ion Batteries", which has been submitted. The dissertation author was the primary investigator and author of this paper. Chapter 2, 3 and 4, in full, is a reprint of the material "Revisiting Polytetrafluorethylene Binder for Solvent-Free Lithium-Ion Battery Anode Fabrication" in ***Batteries*** 2022, 8(6), 57*,* "Leveraging Synergies by Combining Polytetrafluorethylene with Polyvinylidene Fluoride for Solvent-Free Graphite Anode Fabrication" in ***Energy Technology*** 2022, 10.1002/ente.202200732. and "Solvent-free Lithium Iron Phosphate Cathode Fabrication with the Fibrillation of Polytetrafluoroethylene" which has been submitted, respectively. The dissertation

author was the primary investigator and author of these paper. All experiment parts and corresponding writing were performed by the author. The author conducted all the experiment and data analysis and wrote the paper.

Additional Publications

V. Transition Metal-N_4@Graphene for Advanced Lithium-Sulfur Batteries: A First Principles Study

Yang Zhang, Song Lu, Kingsley, Ugochukwu, Fengliu Lou and Zhixin Yu. *Submitted*.

VI. Efficient Electrochemical Reduction of CO_2 to CO by Ag-Decorated B-Doped g-C_3N_4: A Combined Theoretical and Experimental Study

Song Lu, **Yang Zhang**, Mohamed F. Mady, Wakshum Mekonnen Tucho, Fengliu Lou and Zhixin Yu**.**

Ind. Eng. Chem. Res. 2022, 61, 29, 10400–10408.

VII. Sulfur decorated Ni−N−C catalyst for electrocatalytic CO_2 reduction with near 100% CO selectivity.

Song Lu, **Yang Zhang**, Mohamed F. Mady, Obinna Egwu Eleri, Wakshum Mekonnen Tucho, Michal Mazur, Ang Li, Fengliu Lou, Minfen Gu and Zhixin Yu.

ChemSusChem. doi.org/10.1002/cssc.202200870.

VIII. Non-precious metal activated $MoSi_2N_4$ monolayers for high-performance OER and ORR electrocatalysts: A first-principles study

Song Lu, **Yang Zhang**, Fengliu Lou, Kun Guo, Zhixin Yu

Appl. Surf. Sci 2022, 579, 152234.

IX. Transition metal single-atom supported on PC_3 monolayer for highly efficient hydrogen evolution reaction by combined density functional theory and machine learning study

Song Lu, Cao Jie, **Yang Zhang**, Fengliu Lou, Zhixin Yu

Appl. Surf. Sci 2022, 606, 154945.

X. Theoretical study of single transition metal atom catalysts supported on two-dimensional Nb_2NO_2 for efficient electrochemical CO_2 reduction to CH_4

Song Lu, **Yang Zhang**, Fengliu Lou, Zhixin Yu

J. CO_2 Util 2022, 62, 102069.

Patents

I. Method for manufacturing an electrode active material film.

Yang Zhang, Fengliu Lou, Zhixin Yu.

No. 20210502

II. Method for producing an electrode for an energy storage device.

Yang Zhang, Fengliu Lou, Zhixin Yu.

In Preparation

Conference Presentations

Yang Zhang, Song Lu, Fengliu Lou, Zhixin Yu

Revisiting Polytetrafluorethylene Binder for Solvent-Free Lithium-Ion Battery Anode Fabrication.

Poster presentation at International Meeting on Lithium Batteries 2022. Sydney, Australia, July, 2022.

TABLE OF CONTENTS

LIST OF FIGURES

LIST OF TABLES

Abbreviations

ABBSs	all-solid-state-batteries
BNEF	Bloomberg New Energy Finance
CE	coulombic efficiency
CNF	carbon nanofibrils
DOE	Department of Energy
DSD	dry spraying deposition
ESSs	energy storage systems
EVs	electric vehicles
FDM	fused deposition modelling
HNBR	hydrogenated nitrile butadiene rubber
ICE	initial coulombic efficiency
LCO	lithium cobalt oxide
LDM	liquid deposition modelling
LFP	lithium iron phosphate
LiBs	lithium-ion batteries
LiCs	lithium-ion capacitors
LLZTO	$Li_{6.5}La_3Zr_{1.5}Ta_{0.5}O_{12}$
LTO	lithium titanate
LUMO	the lowest unoccupied molecular orbital
MW	molecular weight
NCA	Lithium nickel cobalt aluminum oxide
N/P ratio	negative electrode capacity/positive electrode capacity
NMC	nickel manganese cobalt oxide
NMP	N-methyl pyrrolidone
PLA	polylactic acid
PP	polypropylene
PPC	polypropylene carbonate
PreLi	prelithiation reagents
PTFE	polytetrafluoroethylene
PVDF	polyvinylidene fluoride
PW	paraffin wax
SA	stearic acid
SC	slurry casting
SEs	solid electrolytes
SEM	Scanning Electron Microscopy
SF	solvent free
SLMP	stabilized lithium metal powder
VGCF	vapor grown carbon fiber
XPS	X-ray photoelectron spectroscopy
XRD	X-ray Diffraction

VITA

2015 Bachelor in Chemistry, ***Lanzhou University***, Lanzhou, China

2018 Master in Organic Chemistry, ***Fudan University***, Shanghai, China

2022 Doctor of Philosophy in Petroleum Engineering, ***University of Stavanger***, Stavanger, Norway.

Chapter 1: Introduction and Objectives

1. Background Introduction

Lithium-ion batteries (LiBs) dominate energy storge devices due to their high energy density, high power, long cycling life and reliability[1-3]. With continuous increasing of energy density and decreasing in manufacturing cost, LiBs are progressively getting more widespread applications, especially in electric vehicles (EVs) industry and energy storage systems (ESSs) for power grids[4, 5]. However, the boundaries of energy density and manufacturing cost should still be extended for further electrification of the transportation sector[6]. The United States Department of Energy (DOE) has stated a goal to reduce the cost of LiBs for their application in EVs to $80 per usable kWh within the next years[7]. The cost and performance of LiBs are determined by electrode manufacturing process to a great extent[8, 9]. An innovative, reliable, and cheap technology for electrode fabrication is essential to promote the electrification of transportation sector since LiBs are the most expensive components in EVs[10].

For the state-of-the-art commercial LiBs, slurry casting (SC) procedure is adopted for electrode manufacturing. The basic commercial electrode manufacturing procedure is shown in Figure 1.1, where the active material, conductive additives and polymer binders are homogenized with the help of solvents via a planetary mixer to make slurry with appropriate viscosity. In general, deionized water is used for anode, while organic solvent N-methyl pyrrolidone (NMP) is used for cathode. The prepared slurry is subsequently casted by a slot-die coating machine onto substrates (copper foil for anode and aluminum foil for cathode)[11, 12], and then dried with same coating machine.

The drying process is conducted at high temperatures, usually above 100 ^{o}C to evaporate solvents in a short time. A lot of energy is consumed in the drying step, accounting for more than 50% of total energy consumption for a 3.7 V, 2 ppm pouch cell production line[13]. In terms of cathode manufacturing, expensive and complicated NMP recovery system is required due to potential environmental hazards, which

increases the capital cost a lot. Finally, dried electrodes are compressed with a calendering machine to obtain the desired thickness and dense structure[14].

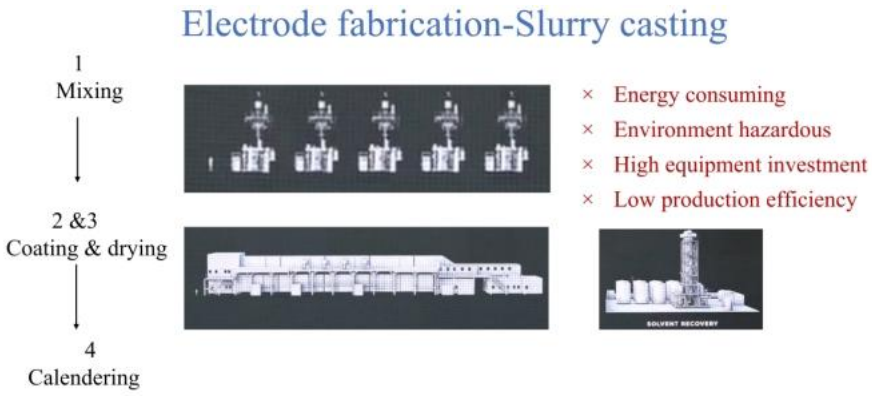

Figure 1.1 Overview of slurry casting procedure for electrode fabrication of commercial LiBs, where the drawbacks of SC procedure are highlighted.

LiBs with thick electrodes can not only increase the energy density but also lower the manufacturing cost, because more active materials are deployed within the same volume. Furthermore, less inactive auxiliary materials, such as current collectors, tabs, separators and packing materials, are required for the same capacity compared with thin electrodes.

The thickness of commercial electrodes is usually less than 100 μm[15], which is limited by the SC procedure. There are two main drawbacks to further increase electrode thickness utilizing the SC procedure. First is the uneven distribution of binder during the drying step. The implemented coating speed in mass production lines is very high (60 m/min). When high coating (drying) is combined with high mass loading, binder gradient occurs with rapid evaporation of the solvent[11]. The binder gradient is observed when the binder floats with solvent onto the electrode surface and thus results in low binder content within the electrode[16, 17]. Consequently, poor cohesion would be observed among the electrode particles, while the adhesion at the interface between electrode and current collector would also be impacted[18, 19]. Low cohesion and adhesion will further degrade the mechanical integrity of electrodes, resulting in reduced production yield and rapid capacity fading[20].

Another concern associated with thick electrodes is poor rate capability caused by

slow ion diffusion due to long ion transport path. For typical commercial electrodes with micro-sized active particles, the rate-limiting step is solid state diffusion of ions through active materials[21]. However, for electrodes with increased thickness, cell polarization along with mass transport become restrictive and could be rate-limiting, particularly at high C-rates[22-24].

In contrast to the SC procedure, fabricating electrode without solvent can potentially avoid all the above-mentioned limitations. With solvent free (SF) procedure, binder is dry homogenized together with active material and conductive additives. Therefore, a thick electrode could be fabricated without the risk of gradient binder distribution. The adoption of electrode with enhanced thickness can increase the energy density significantly since larger amounts of active material could be applied within the same cell volume.

Recently, as one of the most promising solutions to lower manufacturing cost and improve electrode quality, SF procedure is attracting increasing attention. In the past five years, many battery companies have dedicated tremendous efforts in SF procedure for electrode fabrication. For instance, Tesla declared to adopt SF procedure for their next generation 4680 cylindrical cell. Volkswagen has also claimed great progress in SF technology. Industrial research on SF electrode fabrication especially the dry powder spray deposition and polymer fibrillation is increasing rapidly, as demonstrated by the number of patents filed in the past decade (Figure 1.2). More exploration about SF procedure for electrode fabrication is conducted academically. For instance, Hawley et al. compared new generation electrode manufacturing processes including SF procedure[25]. Verdier et al. reviewed the challenges associated with SF procedures for manufacturing electrodes and electrolytes for lithium-based batteries[26]. Lu et al. presented the advantages of SF electrodes and electrolytes in the field of all-solid-state-batteries (ASSBs)[27]. Li et al. reviewed the history of dry film technology and the progress in SF procedures for batteries and supercapacitors, especially for dry spray and polymer fibrillation procedures[28].

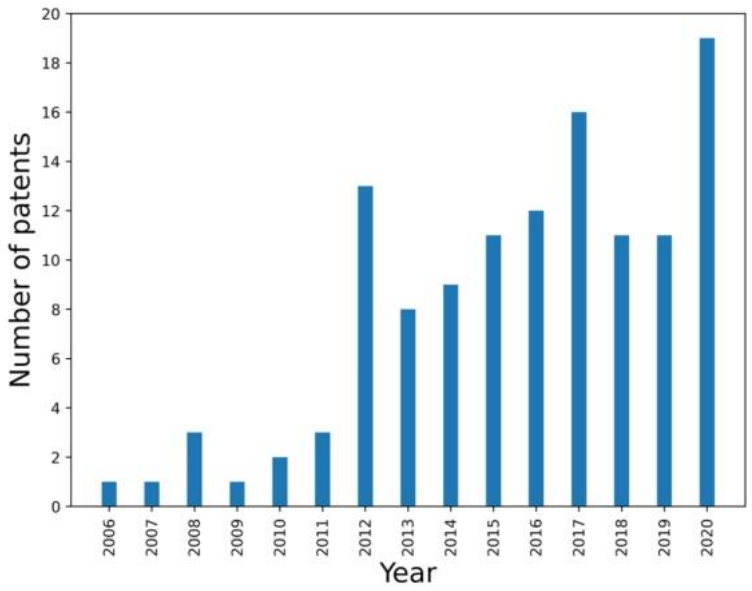

Figure 1.2 Number of patents filed for LiBs with dry spray deposition and fibrillation procedure.

2. Typical processes for SF procedure

As the significance of SF procedure is being recognized, various SF procedures for electrode fabrication have been developed. Generally, most of the SF electrode fabrication procedures have three steps, i.e., dry mixing, dry coating (dry deposition) and final pressing to achieve desired thickness and dense electrode structure. Electrode could also be compressed directly after dry mixing to avoid the dry coating process. The SF procedures could further be classified into six different categories according to their deposition process. Typical procedures for SF electrode manufacturing include polymer fibrillation, dry spraying deposition, vapor deposition, hot melting and extrusion, 3D printing and direct pressing. The schematic diagram of each procedure is presented in Figure 1.3.

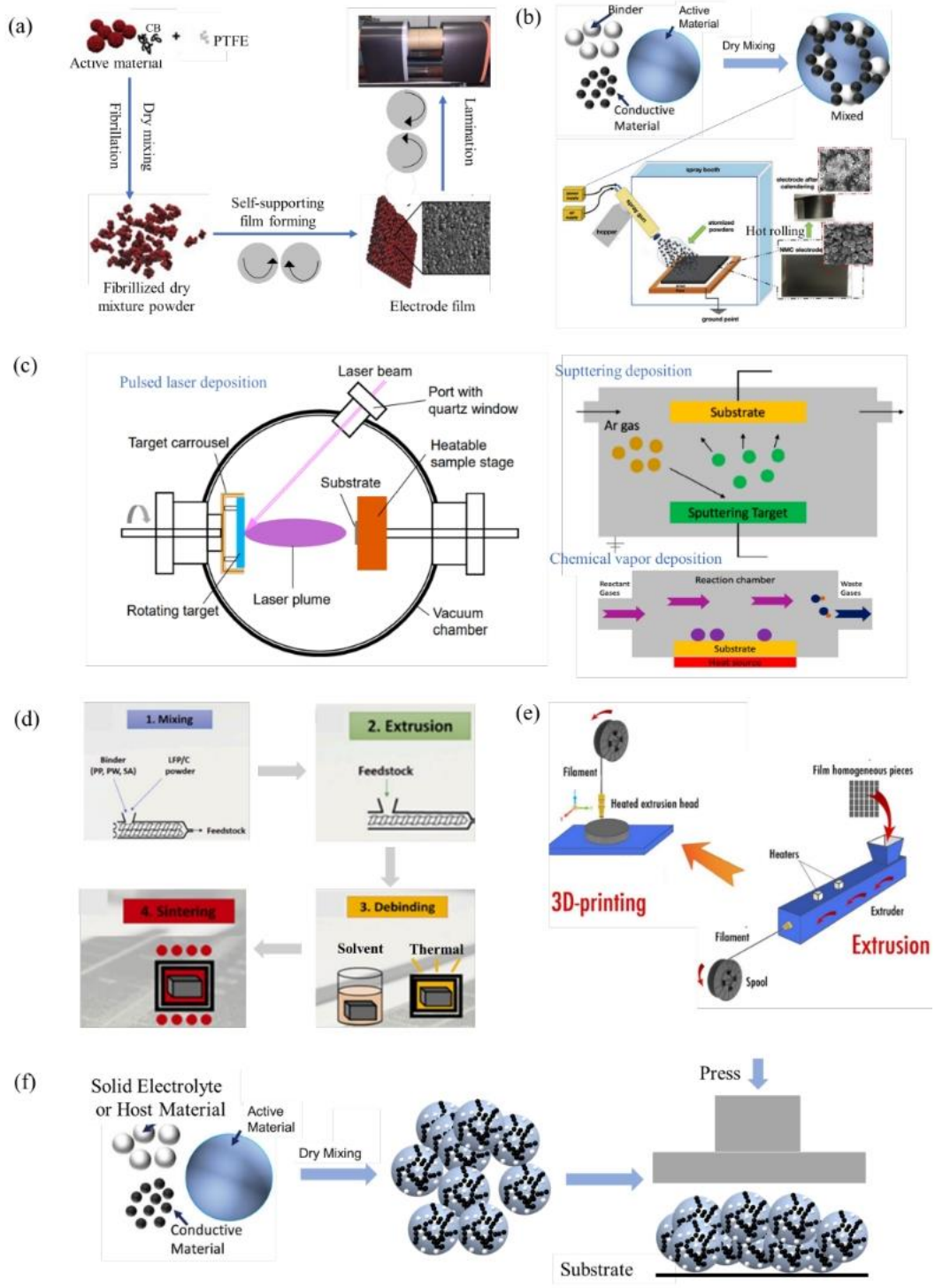

Figure 1.3 Schematic representation of 6 common procedures for solvent free electrode fabrication. (a) Polymer fibrillation; (b) dry spraying deposition; (c) physical vapor deposition, including pulsed laser deposition, sputtering deposition, and chemical vapor deposition; (d) melting and extrusion; (e) 3D printing; (f) direct pressing.

2.1 Polymer fibrillation

Pioneering polymer fibrillation procedure for electrode fabrication was developed by Maxwell Technologies for activated carbon electrode used in supercapacitor. Patents

have been granted with similar procedure[29-31]. The procedure involves the utilization of fibrillizable polytetrafluoroethylene (PTFE), which could be fibrillated under high shear force to generate fine fibrils. The obtained fibrils can bundle active material particles together and further be hot compressed to self-supporting electrode film. The electrode film is finally laminated on carbon coated current collector by hot rolling to form electrode. The roll-to-roll production way makes the procedure compatible with current commercial LiBs production facilities, thus could potentially replace SC procedure. Zhou et al. successfully scaled up this procedure to a pilot stage for fabrication of lithium iron phosphate (LFP) electrodes, where high-speed air blowing, hot-rolling, and hot overlying process were adopted, as shown in Figure 1.4a[32]. The jet mill with compressed dry air was used to stretch PTFE molecular chain. Cotton candy-like mixture was formed and then the mixture was hot-rolled twice at 180 ^{o}C to get free-standing electrode films. The final LFP cathode has high compact densities, almost 1.6 times higher than that of their SC counterparts. It was worth noting that 40% activated carbon was required to increase the flexibility of the LFP electrode, so the electrode was used in supercapacitors.

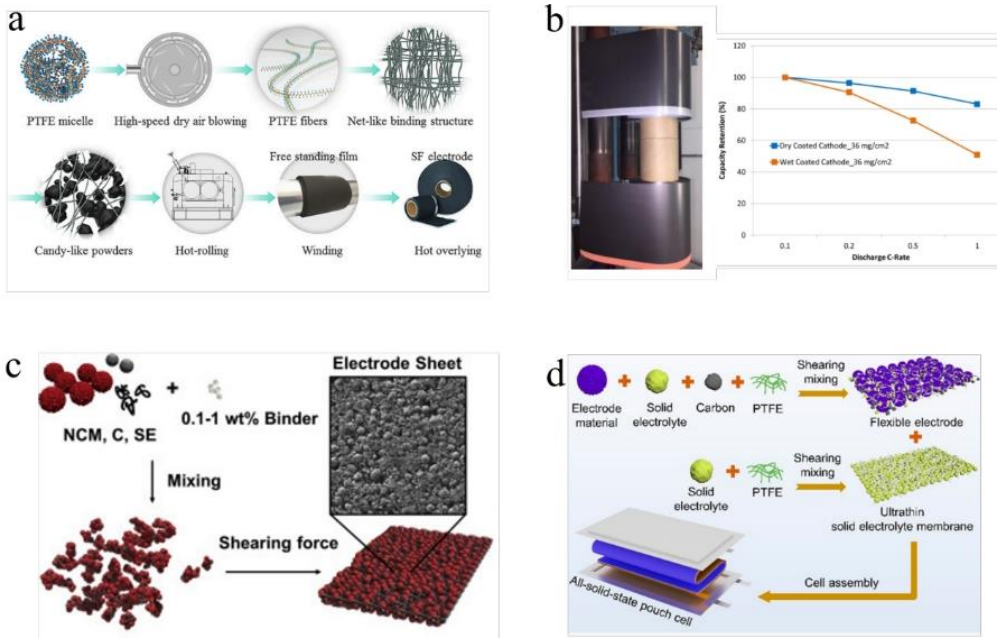

Figure 1.4 Schematic representation of the fabrication of SF electrode with PTFE fibrillation. (a) pilot scale LFP (40% activated carbon) electrode fabrication with high-speed air blowing to fibrillate PTFE; (b) SF graphite anode and NMC523 cathode with better rate capability compared to SC cathode; (c) non-porous NMC electrode fabrication with 0.1 wt% PTFE for ASSBs; (d) SF cathode, anode, and SEs

membranes fabrication with PTFE.

The lowest unoccupied molecular orbital (LUMO) of PTFE is very low, which can accept electrons easily, making PTFE instable in anode since it can be irreversibly reduced by lithium ion during the first lithiation process[33, 34]. Expanding PTFE fibrillation in SF anode fabrication is still a big challenge. Maxwell company expanded PTFE based SF procedure to the fabrication of both NMC cathode and graphite anode[35]. As shown in Figure 1.4b, NMC/graphite cells exhibited high-rate capability and decent cycling life with high mass loading. Good electrochemical performance and roll-to-roll manufacturing process make it easily implemented into commercial LiBs factories. The way they addressed the instability issue of PTFE in graphite anode was not explicitly explained. However, combining PTFE with another binder could be a practical strategy, where PTFE is used as processing aid to make self-supporting electrode film, while the second polymer acts as functional binder to keep the integrity of graphite anode after PTFE being decomposed.

Mechanical strength of self-supporting electrode film is critical for upscaling production since the film can be easily broken without the support of substrate. Increasing the degree of fibrillation of PTFE is one of most effective way to improve the mechanical strength of electrode film. Zhong et al. adopted different methods like high temperature, chemicals, and lubrication to activate PTFE to improve the mechanical strength of electrode film[36-38].

SF procedure is also promising for non-porous electrode fabrication for ASSBs since most solid electrolytes (SEs) are sensitive to moisture and polar solvents. Hippauf et al. applied this scalable SF procedure for NMC electrode fabrication for ASSBs (Figure 1.4c)[39]. PTFE powder was first mixed and sheared with NMC, SEs and carbon nanofiber (CNF) in an agate mortar until the formation of single flake. The flake was subsequently hot rolled several times to desired thickness. With the help of heating, the content of PTFE can be reduced to 0.1 wt %. The pouch cell showed decent cycling stability with 93.2% capacity retention after 100 cycles under the current of 0.7 mA/cm^2 without any artificial pressure. To overcome low initial coulombic efficiency (ICE)

caused by irreversible reaction of PTFE during the first lithiation process, low PTFE content (0.3%) was adopted for full cell configurations. 35% CNF was used as conductive additive to increase the electronic conductivity and accommodate the volume variations of graphite during charge/discharge process.

With a similar procedure, Li_3InCl_6@lithium cobalt oxide (LCO) electrode, graphite@Li_6PS_5Cl electrode, and electrolyte membranes were also fabricated, demonstrating both low thickness and high ionic conductivity at room temperature (Figure 1.4d)[40]. Using a 20 μm $Li_{6.5}La_3Zr_{1.5}Ta_{0.5}O_{12}$ (LLZTO) membrane as ceramic separator, the pouch cell with a high capacity NMC811 electrode displayed both acceptable cycling stability and unprecedented safety.

The scalability and compatibility make polymer fibrillation procedure promising to replace SC procedure. However, the available binders for the procedure are still narrow, only PTFE being reported so far. Developing fibrillizable binder with wide electrochemistry window for different battery systems is highly desirable.

2.2 Dry spraying deposition

Dry spraying deposition (DSD) is another popular SF procedure for electrode fabrication[41-43]. Ludwig et al. fabricated LCO electrode by integrating dry spray deposition and hot rolling, as schematically represented in Figure 1.5a[43]. A spraying gun was used to charge the fluidized dry particles. After being charged, the dry particles were drawn to the ground current collector and got deposited. A hot rolling process was followed to make the final electrode. The thickness and density of the electrode could be controlled by altering calendering pressure during hot rolling, along with multiple electrodes passing through the rollers until the desired values are obtained. The electrodes exhibited good flexibility as well as upscaling capability for 12-inch width sheet coating. The mechanical strength and electrochemical performance of dry manufactured electrode slightly outperformed SC electrodes due to uniform binder distribution. Physical model based on interfacial energies was developed by the same group to understand the mixing characteristics of the dry mixture[42]. The mixing

studies showed that functional electrodes can be manufactured with binders and conductive additives as low as 1 wt% due to the uniformly distributed binder and conductive additives on the surface of LCO particles. Electrochemical performance of dry manufactured electrode with reduced conductive additives and binder is promising, as the cells retained 77% initial capacity after 100 cycles under the current of 0.3C. The achieved electrochemical performance of the reduced binder and conductive additives in LCO electrode confirmed the well distributed binder and conductive additive throughout the electrode matrix. Al-Shroofy et al. reported the fabrication of NMC111 cathode utilizing a similar procedure as shown in Figure 1.5b[41]. Polyvinylidene fluoride (PVDF) and carbon black were used as binder and conductive additive, respectively. The NMC111, PVDF, and carbon black were first dry mixed and then sprayed onto an electrically grounded aluminum foil through electrostatically charged spraying gun. The cycling life of the dry electrode was better than their SC counterpart.

Molecular weight (MW) of binder can also affect the electrochemical performance and mechanical integrity of electrode in this procedure[44]. Wang et al. investigated the effects of MW of PVDF on the electrochemical performance and mechanical integrity of NMC111 electrode fabricated via dry spray deposition procedure. As shown in Figure 1.5c, the electrode with Alfa Aesar PVDF (low MW) has higher peel off strength than HSV 900 (high MW) due to increased interface between molten PVDF and aluminum substrate, while electrode fabricated with HSV 900 showed improved rate capability, especially at high C-rate. The microstructure and porosity of the PVDF layer depends strongly on the MW of PVDF. With increasing molecular weight, the PVDF layer on the NMC111 surface becomes more porous, improving the high-rate capability without decreasing binding strength and long-term cycling performance. Liu et al. successfully fabricated long cycle life (>650 cycles) NMC electrode at regular thickness (56 μm) with a similar procedure. Thick electrode up to 200 μm was also fabricated successfully, allowing further electrode design and development, which cannot be achieved by the SC procedure[45].

In addition to SF cathode fabrication, the procedure is also effective for anode

fabrication. Schälicke et al. reported fabrication of graphite anode with different fluorine thermal-plastic[46]. Just 2 seconds in the high voltage field enabled an average graphite loading of 11 mg/cm^2 (3.5m Ah/cm^2). Dry deposited film was further hot compressed for 2-5 minutes under high pressure. The electrode demonstrated comparable electrochemical performance with SC fabricated electrode.

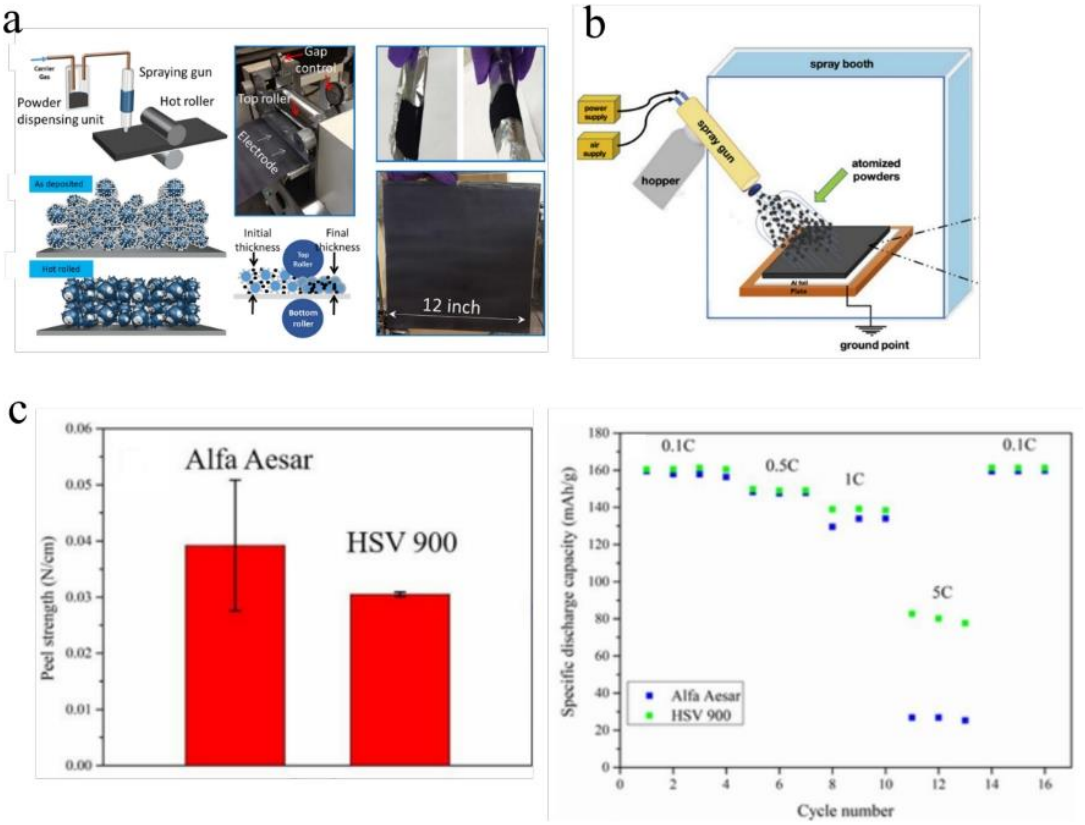

Figure 1.5 (a) Illustration of typical DSD process for electrode fabrication, including dry powder mixing, spraying system, and pressing part; (b) NMC cathode fabrication in large area with DSD procedure; (c) effect of molecular weight of the PVDF binder on the electrochemical performance and mechanical integrity of NMC111 cathode fabricated with DSD procedure.

Dry spraying deposition is versatile for electrode fabrication as it is compatible with all common active materials in LiBs. The challenges for this technology are upscaling and thickness controlling. The procedure is not compatible with current equipment used in LiBs production lines, and the efficiency is not comparable to SC process. Dry spraying deposition could be performed in the roll-to-roll way after active material deposition, which makes upscaling possible. However, research on dry spraying deposition was conducted only at laboratory scale so far. It is still challenging

to accurately control the thickness of fabricated electrode, even though the thickness could be adjusted through changing the number of compressing times, which is still highly dependent on the mass loading of initial dry powders.

2.3 Vapor deposition

In vapor deposition procedure, raw materials are vaporized and deposited onto substrate. The procedure was originally used to prepare coatings for metal tools in 1950s[47]. Vapor deposition includes magnetron sputtering, thermal evaporation, pulsed laser deposition, atomic layer deposition, etc. Kuwata et. al fabricated solid-state-thin-film-batteries consisting of an amorphous $Li_2O–V_2O_5–SiO_2$ SEs, crystalline $LiCoO_2$ cathode and amorphous SnO anode, respectively, using pulsed laser deposition technology, where the laser beam was focused onto the rotating target with an incident angle of 45º[48]. The substrate was placed 30-40 mm away from the target. The thin films were deposited with a continuous flow of O_2 gas at 0.2 Pa. Shiraki et. al further controlled the crystal orientation of LCO on the (110)-2×1 reconstructed substrate surfaces of Au and Pt with a similar procedure to obtain the most appropriate orientation for ion conduction. Epitaxial LCO thin films with polycrystalline $Li_{1.2}CoO_2$ as target were deposited with a thickness of 200 nm. The films were subsequently annealed at 650 °C in air to obtain high temperature LCO phase[49]. Ionized magnetron sputter deposition as another vapor deposition method can be applied with a relatively low temperature of 350 ºC[50]. The thin-film-batteries prepared by vapor deposition have good performance, such as high energy density[51-53], long cycling life[54], and improved rate capability[55, 56]. However, vapor deposition technology is only suitable for fabrication of electrode with small size, mainly for microelectronic devices and highly integrated circuits. The expensive equipment and complicated film forming process, high energy consumption, and low areal capacity limit its application in EVs or even 3C consumer electronics.

2.4 Hot melting and extrusion

Extrusion is wildly used for melt mixing of thermoplastics or kneading of ceramic pastes, where high polymer content is usually required. It is not compatible with

electrode fabrication since high loading of active materials is necessary for high energy density and low cost. To address the problem, many approaches have been tested, including addition of solvents and other additives[57, 58]. Sotomayor et al. were the first to use extrusion as SF method to fabricate electrode with lithium titanate (LTO) and LFP as active materials[59]. This process comprises of particle mixing, extrusion, debindering and sintering. A blend of thermoplastic polymers of polypropylene (PP), paraffin wax (PW) and stearic acid (SA) were used as sacrificial binder. The binders were first blended several times followed by the pelletization of the molten blend. The pellets were then introduced into a single-screw extruder where they were mixed again. After that, electrode sheets of various thicknesses could be obtained. The polymer blend was removed from the electrode by heating, which created pores inside the electrode. A double heating step in *n*-heptane was required to degrade the polymers. Finally, electrodes were sintered at high temperature to create cohesion between the remaining particles. The LFP/LTO cells were fabricated with areal capacity of 13.3 mAh/cm^2 and good cycling stability. This study proved that porous electrodes can be manufactured by SF extrusion even though much binder and high temperatures are required. A similar process was reported by Torre-Gamarra et al. to make binder free self-supporting thick LFP electrodes of approximately 500 µm with the same binder system, as depicted in Figure 1.6a[60]. In this study, binder and powders (LFP and conductive carbons) were first mixed at 180 ˚C for 40 min. Then, the pellets were introduced into an extruder where the temperature was elevated from 175 ˚C to 185 ˚C. A combination of solvent (*n*-heptane) and thermal (200-450 ˚C) debindering was adopted to remove the organic component from the electrode. The electrode was finally sintered at 650 ˚C. The high areal capacity electrode (13.7 mAh/cm^2) exhibited good cycling stability under low current. Reduction of binders' usage is critical for further application in practical electrode manufacturing.

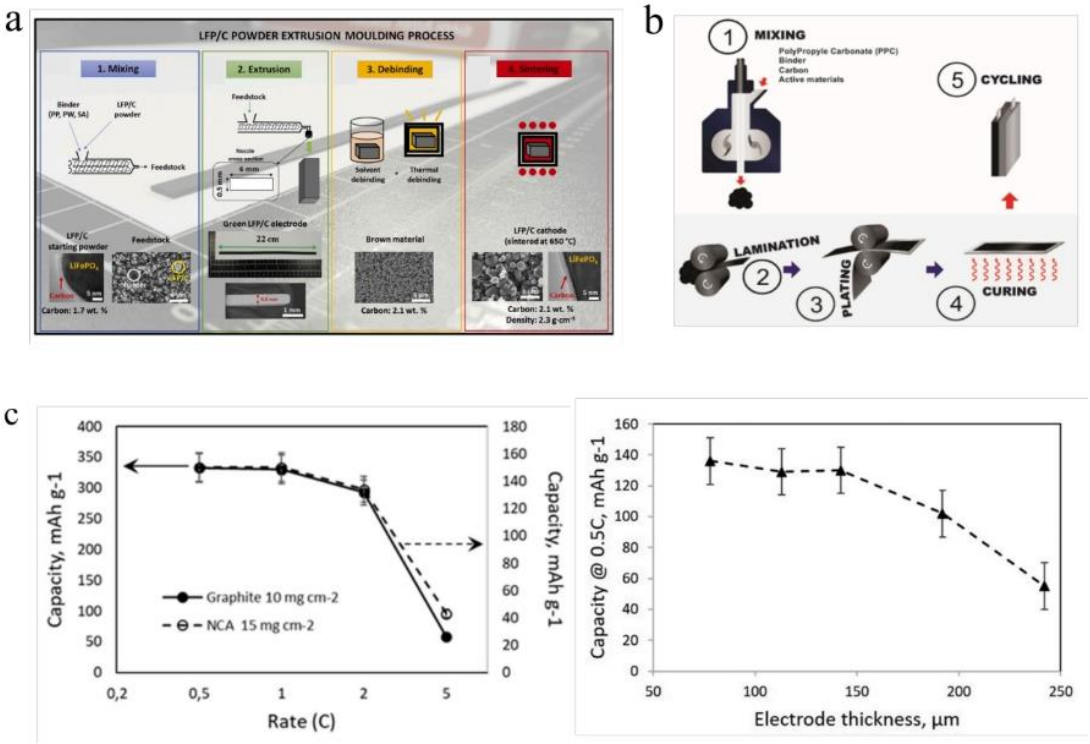

Figure 1.6 (a) Schematic representation of LFP electrode fabrication with PP, PW, SA binder system via melting and extrusion procedure; (b) LTO, LFP or NMC cathodes fabrication with the help of PPC as polymer processing aid through melting and extrusion procedure; (c) rate performance of NCA and graphite electrodes and specific capacity of NCA cathodes at different thickness.

The most recent use of SF extrusion was reported by Khakani et al.[61], where binder system consisted of polypropylene carbonate (PPC) and hydrogenated nitrile butadiene rubber (HNBR), as shown in Figure 1.6b. HNBR and PPC were first introduced into the internal mixer at 90 ˚C until a homogenous molten blend was obtained. Active materials (LTO, LFP or NMC) and conductive additives were then incorporated into the polymeric blend and mixed until properly dispersed. After that, the composite mixture was laminated to form self-supporting electrode films. This process was repeated several times until the desired thickness was reached. The electrode was subsequently laminated onto a carbon coated current collector. Finally, the electrode was heated to remove PPC at 230 ˚C. LFP, NMC111 cathodes and LTO anode were successfully fabricated with 77.5% active materials loading. Lithium nickel cobalt aluminum oxide (NCA) cathode and graphite anode with 90% active materials loading were fabricated by Astafyeva et al. with a similar procedure using PPC as sacrificial binder[62]. A large loading range from 4 to 40 mg could be achieved. High

capacity (over 5 mAh/cm^2) NCA cathode and graphite anode were fabricated. As shown in Figure 1.6c, NCA cathode exhibited a high specific capacity of 160 mAh/g with a loading of 15 mg/cm^2 (38% porosity) at 0.5C, and the specific capacity decreased to 100 mAh/g when the loading was increased to 46 mg/cm^2.

Melting and extrusion is a scalable procedure for electrode manufacturing with high loading. However, the extrusion is sensitive to particle size and needs accurate control of temperature, shear force, and time of extrusion[26]. Additionally, high consumption of polymers, tedious manufacturing process, high temperature required for debindering and sintering impede its further application in practical electrode manufacturing.

2.5 3D printing

Two different 3D printing techniques have been reported for electrode fabrication: liquid deposition modelling (LDM)[63, 64] and fused deposition modelling (FDM)[65]. LDM is solvent based technique and will not be further discussed here. For FDM, heating is applied to melt thermoplastic polymers. The molten thermoplastic polymers containing active materials and conductive additives are then horizontally deposited layer by layer to fabricate 3D electrodes[66, 67]. Trembacki et al. demonstrated through simulation that 3D battery design performs significantly better than 2D particle bed geometry with energy density improvements[68]. Pioneering work was reported by Foster et al. in 2017 for the application of FDM in LiBs, where thick 3D-printed anode (1 mm) discs were fabricated by operating a commercial graphene-based polylactic acid (PLA) filament (graphene/polylactic acid) as material source. Low discharge capacity of 15.8 mAh/g was obtained at low current density[69]. Ragones et al. pursued additional attempt for the development of PLA/LTO anode and PLA/LFP cathodes[70]. Separated electrode discs as well as spiral and double-spiral shaped current-collector/electrode (graphene-PLA/LTO-PLA) networks were obtained. Independent 3D-printed electrodes were tested in half-cell configuration. Cycling of cathodes resulted in capacities of 60, 50 and 20 mAh/g at current density of 9, 44 and 88 μA/cm^2, respectively. Reyes et al. recently reported 3D printing of LTO-LMO full cell, which

was conducted through the formulation of PLA/LTO/conductive additives and PLA/LMO/conductive additives filaments to feed a FDM 3D-printer[71]. The volumetric capacity of the full cell was 0.25 mAh/cm^3 at low current. Unfortunately, due to the printability requirements for FDM process, active material loading was kept relatively low, thus reducing the loading of active materials and severely impacting the electrochemical performance.

Nevertheless, the active materials loading can be improved by introducing a plasticizer[72]. With the help of plasticizer, Maurel et. al successfully increased graphite loading to 49.2% of total 3D printed electrode. Dichloromethane was used to dissolve PLA for better homogeneity of active materials, conductive additive, and plasticizer. This strategy is very useful to increase the loading of active material, although slurry preparation is necessary before extrusion. The same group extended this process to the fabrication of LFP/PLA and SiO_2/PLA 3D-printable filaments, which are utilized as cathode and separator in LiBs[73].

Utilizing 3D printing techniques, the electrode thickness and morphology could be accurately tailored for a specific application. However, similar to vapor deposition, currently the technology is not appropriate for large scale electrode fabrication but only for specifical scenarios, such as microelectronics and wearable devices[74].

2.6 Direct pressing

Direct pressing utilizes compressible materials as electrode host. The above 5 SF procedures involve dry coating or dry deposition process, which is skipped in direct pressing procedure. The dry powders are mixed and pressed directly to make the electrodes. In 2014, Han et. al reported a one-step and scalable synthesis of holey graphene without employing catalysts or any chemicals. The ultracapacitors based on holey-graphene showed improved volumetric capacitance compared to a normal, non-holey-graphene (Figure 1.7a)[75]. The same group used the synthesized holey-graphene as compressible host and conductive matrix to accommodate incompressible cathode and anode battery powders. The inherent nano-porosity facilitates the escape

of trapped gases upon compression, enabling the formation of binder-less and solventless composite electrodes. Different active materials, including NMC, LPF, LCO and holey graphene were blended and then pressed directly to form electrodes. LFP cathode has demonstrated good performance in half cells (Figure 1.7b)[76]. The holey graphene powder can be easily pressed into dense and strong monoliths with different shapes at room temperature without any solvents or binders, as illustrated in Figure 1.7c. This enables the fabrication of robust and dense graphene sheet exhibiting high density of 1.4 g/cm^3, excellent specific mechanic strength, good electrical and thermal conductivities, thus great potential as anode in LiBs[77].

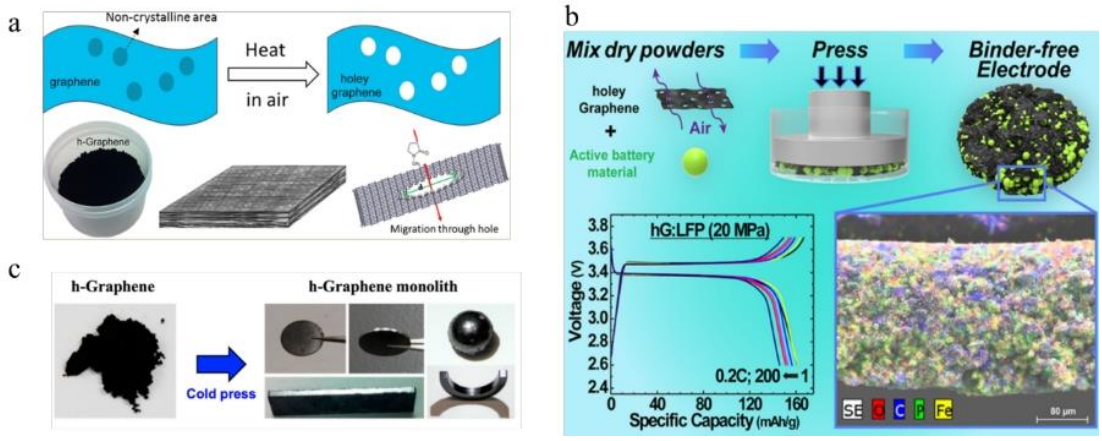

Figure 1.7 SF electrode fabrication based on compressible holey graphene. . (a) synthesis of holey graphene and the formation of dense structure; (b) LPF cathode fabrication by direct pressing with the help of compressible holey graphene; (c) fabrication of graphene monoliths with different shapes by direct pressing.

Direct pressing process has also been used in the fabrication of non-porous electrodes for ASSBs[78-83]. Kim et al. for this first time reported SF fabrication of LFP composite cathode for ASSBs via direct pressing[84]. The PEO and LiTFSI were first dissolved in ionic liquid $PYR_{1A}TFSI$ (A = 3 to 5) to form paste-like mixture, then LPF powder and conductive carbon were added and mixed within the paste to form a blend. The blend was annealed at high temperature overnight and then hot-pressed to form 1 mm thick strips of composite cathode. Finally, the strip was cold pressed to a thickness of 50 μm. Yubuchi et. al fabricated cathodes with $Lii_{0.5}Mn_{1.5}O_4$ particles, $80Li_2S{\cdot}20P_2S_5$ glass-ceramic electrolytes and acetylene black with a weight ratio of 30:70:6. The mixture were mixed using an agate mortar. A bilayer pellet (10 mm

diameter) consisting of a composite positive electrode (10 mg) and a glass-ceramic electrolyte (80 mg) was obtained by pressing at 360 MPa. Then indium foil was attached to the bilayer pellet by pressing at 240 MPa with two stainless steel rods[79]. Auvergniot et. al formulated positive composite electrodes using 38% active material (LCO, NMC111, or $LiMn_2O_4$), 57% Li_6PS_5Cl, and 5% vapor grown carbon fiber (VGCF) as conducting additive. The components were mixed by grinding in an agate mortar and then pressed under a pressure of 6.4 t/cm^2 to form composite positive electrode with a thickness of 90 μm[85].

Direct pressing is a simple and efficient procedure for electrode fabrication without dry coating process. However, the compatibility of pressing the dry mixture into electrodes in the roll-to-roll way, which is necessary for upscaling, is still questionable. Different SF procedures could have potential for different application. However, the adoption of roll-to-roll production makes fibrillation and dry powder spray deposition procedures compatible to the commercial LiBs production line. Considering the feasibility of upscaling production, the main features of the fibrillation and dry spraying deposition procedures were summarized in Table 1. For fibrillation procedure, only PTFE was reported so far. But the instability of PTFE in anode requires the exploration of fibrillizable polymer with wide electrochemistry window to replace PTFE. Dry spraying deposition is suitable for both cathode and anode, where PVDF was mostly used. After active materials deposition, both procedures experience hot pressing to make the final electrodes.

Table 1.1 Summary of polymer fibrillation and dry spray deposition procedures and their properties in LiBs.

Dry procedure	Binder	Electrodes	Main Performance	Temperature	Refereneces	Comments
PTFE Fibrillation	PTFE	LFP electrodes (40% activated carbon)	1.6 times higher compressed density	180 °C	Zhou et al.[32]	Instability issue of PTFE in anode should be addressed before the application of PTFE in anode. Exploring fibrillizable polymer with wide electrochemical window is favorable.
	PTFE	Hard carbon, Soft carbon	Comparable cycling life to SC procedure	160 °C	Zhang et al.[34]	
	PTFE	Graphite, NMC, silicon/graphite composite	High-rate capability NMC111/graphite full cell, 5 mAh/cm^2	120-160 °C	Duong et al.[35]	
Dry Spray Deposition	PVDF	LCO, NMC	Even binder distribution, better bonding strength	120-190 °C, 250 °C	Ludwig et al. [42, 43]	This procedure is appliable for both cathode and anode. The electrodes could be fabricated through roll-to-roll way after dry powder deposition.
	PVDF	NMC	300 cycles with 80% capacity fading	170 °C	Al-Shroofy et al.[41]	
	PVDF	NMC	PVDF with high molecular weight is preferable	200 °C	Wang et al. [44]	
	PVDF	NMC	200 µm electrodes	180 °C	Liu et al.[45]	
	FEP/THV	Graphite	Comparable electrochemical performance on electrodes and cells	170 to 300 °C.	Schälicke et al.[46]	

3. Advantages of SF procedure

In addition to energy saving and specific energy enhancement, electrode fabricated by SF procedure also have advantages including cost savings, low environmental footprint, and improved electrode quality, as summarized in Figure 1.8.

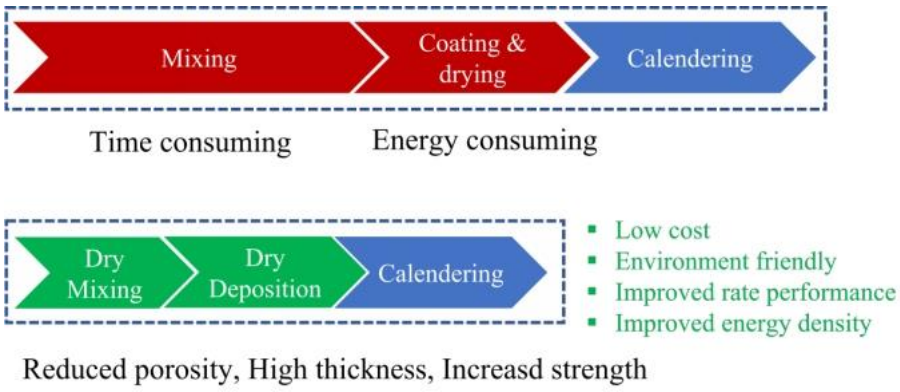

Figure 1.8 Comparison between SF and SC procedures, the advantages of SF procedure include cost saving, environment benefits, and improved electrode quality.

3.1 Cost saving

SF procedure can potentially lower the cost in three aspects, including less energy consumption, reduced raw materials usage, and less capital investment. The total cost is expected to decline by 10%-15% when SF procedure is applied[42].

3.1.1 Reduced Energy consumption

Mixing and coating-drying as well as NMP recovery are very expensive[86-88]. Energy consumption accounts for more than 47% of the electrode manufacturing cost[89]. For example, 10 kWh electricity is required to recycle one kg NMP[90]. Generally, it takes hours for slurry preparation with intense energy input, while it could take only minutes for dry mixing during SF procedure depending on the choice of mixers. Furthermore, no drying and NMP recovery processes are involved in SF procedure[39, 43]. Thus, a lot of energy can also be saved.

3.1.2 Less raw materials usage

Raw materials are most expensive part of LiBs, accounting for 60% of total cost[10, 91]. NMP used in SC procedure accounts for 1-2% of cell cost[88, 92], thus NMP alone can reduce cost by 1-2 %. Additionally, the amount of other inactive materials such as current collectors and separators can be reduced because it is easy to adopt thick electrode with SF procedure. For instance, the thickness of commercial graphite electrode is roughly 60-70 µm. If the thickness is increased to 120 µm, the amount of separator, current collector could be reduced to half.

3.1.3 Reduced capital cost

For SC procedure, large area of plant facilities is required to place coating machine and NMP recovery system, thus the capital invest is high. Coating machine is relatively expensive, which can also be avoided by applying SF procedure. NMP recovery system is also costly, typically 3-6 million USD for one GWh mass production line[93].

3.2 Environmental benign

CO_2 emission during coating and drying is around 1,000 kg for 10 kWh battery production line[94]. The demand of LiBs for EVs in 2030 is predicted to exceed one

TWh[95]. If all batteries are manufactured by SF procedure, skipping of coating and drying will help to reduce 100 million tons of CO_2 emission. Another environmental issue for LiBs production is potential NMP leakage. A complicated and expensive recovery system can reach 99% NMP recovery[90], however the remaining waste is still a threat to the environment. Leakage of NMP imposes high health risks to operators and can result in an explosion in the worst case when the NMP vapor concentration is too high.

3.3 Improved electrode quality

Performance of LiBs depends largely upon the quality of electrode. Different from SC procedure, the microstructures and morphology of SF electrode could be altered to improve areal capacity and other electrochemical properties. The SF procedure can improve the quality of electrodes from the following aspects.

3.3.1 Improved compressed density

Improved compressed density of electrodes can improve volumetric energy density of the LiBs because more active materials could be loaded within the same volume. High volumetric energy density is significant for application scenario with limited volumes like EVs and consumer electronics. For SC procedure, a lot of pores are left inside the electrodes after the evaporation of solvent, resulting in low compressed density even though the porosity decreases after the calendering. The relationship between porosity and compressed density of electrode was described by Equation 1 and 2:

$$\text{Porosity} = 1 - \frac{V1+V2+V3}{V} = 1 - \frac{V1+V2+V3}{\frac{W1+W2+W3}{V}} = 1 - \text{Compressed density} * \frac{W1\rho2\rho3 + W2\rho1\rho3 + W3\rho1\rho23}{\rho1\rho2\rho3(W1+W2+W3)} \quad \text{.....(1)}$$

$$\text{Compressed density} = (1 - \text{porosity}) * \frac{\rho1\rho2\rho3(W1+W2+W3)}{W1\rho2\rho3 + W2\rho1\rho3 + W3\rho1\rho2} \quad \text{.....(2)}$$

where W_1, W_2, W_3 and ρ_1, ρ_2, ρ_3 are weight and real density of active material, binder and conductive additive, respectively, while V_1, V_2, V_3 and V are the volume of active material, binder and conductive additive and electrode, respectively. For commercial LiBs, the porosity of electrodes is usually in the range of 30-45%[96]. High porosity decreases the volumetric energy density of LiBs. The compressed density achieved by

SF procedure could be much higher than SC procedure because of less pores inside the electrodes. For example, the compressed density of SF LFP-activated carbon electrode is almost 1.6 times of the SC counterpart[32].

3.3.2 Better rate capability

The binder is dissolved in solvent and forms compact insulating layers around active particles in SC procedure, which is detrimental for lithium-ion transport and results in deteriorative rate capability. When it comes to SF procedure, the binder is dry mixed with active materials and conductive additive, forming spot contact with active material particles. There is no insulating layer around active materials, resulting in better rate capability[97]. Additionally, less binder is used in SF procedure, in some case only 0.1%, which is also beneficial for rate capability[39]. As discussed above, SF electrodes generally have dense electrode structure, which also helps to increase the conductivity of electrode.

3.3.3 High areal capacity

The gradient binder distribution caused by solvent evaporation and low rate capability limits the thickness of SC electrode less than 100 μm[15]. However, if binder and active materials are dry mixed, the binder can distribute uniformly around the active particles. Effective ion transport helps the fabrication of thick electrode. The thickness of LPF electrode fabricated by melting and extrusion procedure can reach 500 μm with an specific capacity of 13.7 mAh/cm^2, much higher than electrode fabricated by SC procedure[60].

The specific energy of a cell is determined by the areal capacity of electrode to a large extent. The specific energy of prismatic cell was calculated as a function of areal capacity of graphite anode according to Equation 3:

$$\text{Specific Energy} = \frac{\text{capacity}_{NMC} * V_{nominal}}{\text{Cell weight}} = \frac{2 * S_{NMC} * H_{NMC} * \text{compressed density}_{NMC} * \text{loading}_{NMC} * \text{specific capacity}_{NMC} * V_{nominal}}{\text{Cell weight}} = \frac{2 * S_{NMC} * H_{NMC} * \text{compressed density}_{NMC} * \text{loading}_{NMC} * \text{specific capacity}_{NMC} * V_{nominal}}{\text{Weight}_{NMC\ cathode} + \text{Weight}_{Graphite\ anode} + \text{Weight}_{Electrolyte} + \text{Weight}_{separetor+current\ collector}}$$

$$= \frac{\frac{21376703699810}{57259}}{11568 + \frac{57259}{\text{Areal Capacity}}}\ \text{wh/kg} \quad \text{.....(3)}$$

where S_{NMC811}, H_{NMC811} and $V_{nominal}$ are the coated area of lithium nickel manganese cobalt oxide (NMC) electrode, thickness of single NMC electrode (current collector not included) and nominal voltage of the cell, respectively. Injection coefficient was set to 2.1 (ratio of electrolyte (g) to cell capacity (Ah)), which is the normal value for commercial NMC811 prismatic cells. The N/P ratio (ratio of anode capacity to cathode capacity) and the mass of current collector and separator was set to 1.1 and 0.1013 kg/m^2, respectively. The active material loading for both electrode is set to be 95%. The specific capacity for NMC811 and graphite are set to be 180 and 350 mAh/g, respectively. It is worth noting that the mass of packing materials was neglected intentionally, because it varies with the cell configuration and cell size. The specific energy in our study is a little higher than the actual situation. The specific energy increases with the enhancement of areal capacity very fast when areal capacity is less than 5 mAh/cm^2. The state-of-the-art commercial electrode has a specific capacity of 2-3 mAh/cm^2. SF procedure has advantage in fabricating very thick electrode, which could increase the energy density to very high level.

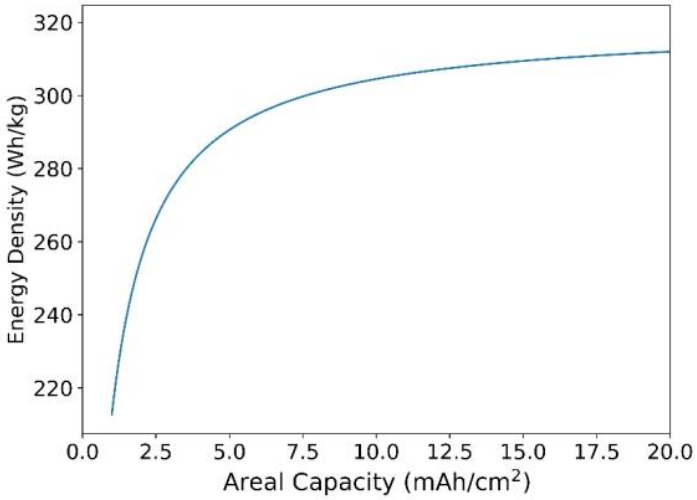

Figure 1.9 Specific energy of NMC811/graphite cells as a function of areal capacity of graphite anode.

3.3.4 Improved mechanical strength

Mechanical strength of LCO cathode manufactured by the dry spray technique with 5% PVDF reaches 148.8 kPa, while it is only 84.3 kPa by the SC procedure[43]. LCO cathode with only 1% PVDF demonstrated mechanical strength of 93.8 kpa, higher than

that of SC electrode at 83.4 kPa[42]. Binding strength is important for cycle life since losing contact between bulk electrode and current collector is one of the most common capacity failure mode of LiBs. Increased binding strength can also help to avoid powder fragmentation in the subsequent processes, which is favorable for increased yield and improved safety.

For SC procedure, binder is dissolved in solvent and floats with solvent during drying, especially under high temperature. The fast solvent evaporation results in gradient binder distribution along the radical direction of electrode. The low binder concentration in bottom sector and electrode bulk results in weak adhesion and cohesion. For the SF procedure, the binder was dry mixed with active materials and distributed evenly around active material. Uniformly distributed binder can increase contact between current collector and electrode film and contact among active particles. In addition to increased mechanical strength, uniform binder distribution can reduce the binder usage.

3.3.5 Reduced residuals

The residual solvent and other processing aid used during mixing cannot be removed thoroughly in the SC procedure, which can deteriorate the performance of LiBs[98, 99]. SF procedure completely avoids the residuals imposed during manufacturing and thus results in better cell performance.

3.3.6 Extended applications

The SF procedure could also be applied in prelithiation, where the lithiated silicon nanoparticles are used as prelithiation reagents (PreLi). However, Li_xSi is instable in common polar solvents like water used for commercial electrode production. Moreover, the slurry preparation is complicated and can lead to capacity loss of lithiated silicates, resulting in low prelithiation efficiency[100, 101]. Incorporating the SF procedure would therefore eliminate the need for slurry preparation and achieve efficient prelithiation with the lithiated silicon nanoparticles. Another common PreLi reagent is stabilized lithium metal powder (SLMP), which can only be used in non-polar solvents

like toluene[102, 103]. No solvent is used in SF procedure, and the PreLi reagents could be dry mixed directly with active material and conductive additives. SF procedure could also be applied in the fabrication of non-porous electrode used in ASSBs. Different SEs, especially sulfur electrolyte, are sensitive to polar solvents, which could be decomposed and result in short cycling life. On the other hand, it is crucial to fabricate thin, flexible, nonporous electrode sheets at large scale. Considering the fragility of electrode sheets fabricated by SC procedure, SF procedure can be advantageous in the fabrication of thin electrolyte films[27].

4. Challenges of SF procedure

SF procedure could fabricate electrode with improved quality at low cost. As one of the most promising techniques for electrode manufacturing, SF procedure has the potential to replace SC procedure used in the state-of-art commercial LiBs. However, some challenges need to be addressed before the new procedure could be commercialized.

4.1 Conductive network build up

Generally, different material of different sizes and density have the tendency to agglomerate, which is detrimental for the conductivity of electrode. Interfacial interactions between active material, binder and conductive additives are essential for uniform distribution of a dry mixture. Ideally, the binder decorates on active materials with limited agglomeration to obtain high mechanical strength with low content and conductive additive chains are necessary to enhance the electric conductivity of electrode without conductive additive agglomeration. The effect of surface energy and particle size on the property of dry mixture is to be further studied for the optimization of dry mixing procedure.

4.2 Adhesion and cohesion

Most of dry procedures undergo thermal activation, except for direct pressing with compressible host material, where the binder can be melted and possesses greater contact between particles and interface of electrode layer and current collector. The

adhesion and cohesion of dry procedure are higher than SC procedure. Further enhancement of the adhesion and cohesion is still highly desirable.

4.3 Constant mass loading

Constant mass loading of electrode is critical for consistent performance of LiBs. Generally, N/P ratio is set to more than 1.1 to get rid of lithium plating under fast charge operation[104]. If the deviation of mass loading is high, higher N/P ratio is required. For the SC procedure, the slurry with suitable viscosity was casted onto the current collector. The slurry has decent liquidity and the deviation of electrode thickness is less than 1 μm. Compared to slurry used in SC procedure, the dry mixture used in SF procedure has less fluidity, resulting in less constant active material loading. It is still challenging to get reliable SF procedure at the same level as SC procedure.

4.4 Binder selection

Different dry procedures require different binders. PVDF is more used for dry spraying deposition, while thermoplastic is used for 3D printing and melting extrusion process. Only PTFE has been used in polymer fibrillation so far. However, it is instable under low voltage range and cannot be used for LPF fabrication due to the hardness of LPF particles. Fibrillizable binder with good stability under large voltage window need to be explored. The binder for other dry procedures like 3D printing, melting extrusion, and dry spraying deposition need to be heated to above the melting point to increase contact. Developing suitable polymer binder with low melting point is beneficial for these SF procedures.

4.5 Production upscaling

Dry mixing is critical for SF electrode fabrication. Many different mixers could be used in lab scale for dry mixing such as ball mill[105] and blade mill[106], which are suitable for different active materials and binders. As discussed above, the different density and size of raw material makes it difficult to obtain homogenous dry mixture. The challenge thus becomes the preparation of homogenous dry mixture with minimum particle agglomeration.

5. Objectives of the study

This project is the result of cooperation between University of Stavanger (UiS) and Beyonder AS. Beyonder is a technology driving startup focus on new technology for energy storage. One of Beyonder's products is lithium-ion capacitors (LiCs), where activated carbon is used as cathode active material. High specific surface area makes activated carbon trend to adsorb moisture from environment, which is a big challenge for cell manufacturing because the required dry room with low dew point will consume a large amount of energy. Some companies are using SF procedure to produce activated carbon electrode, especially with the fibrillation of PTFE. As industrial PhD, this project not only want to explore new technology of lithium-ion batteries, but also want to make the contribution to the product development for Beyonder. There are many different SF procedures have been developed for electrodes manufacturing. However, most of those procedures have problems to be addressed before mass production. PTFE fibrillation is one of most promising SF procedures for electrode fabrication from the perspective of feasibility to upscale. Because the roll-to-roll production way makes it compatible to current lithium-ion batteries production line. SF electrode manufacturing has attracted tremendous attention from both academia and industry. Many big giants like Tesla, Volkswagen are also working on this procedure. However, there are still big gap when the procedure can be used for mass production. For instance, PTFE is not stable in anode caused by the low LUMO. PTFE is also not suitable for LFP electrode fabrication caused by the hardness of LPF particles.

How to make PTFE fibrillation-based SF full cell, including LFP and graphite electrodes is still a big challenge. This project focus on PTFE fibrillation-based procedure to explore its application in anode and cathode fabrication. We hope the results of this project can help accelerate the process using SF procedure to replace the-state-of-art energy and time-consuming slurry casting procedure.

References

[1] Dunn B, Kamath H, Tarascon J-M. Electrical energy storage for the grid: a battery of choices. Science. 2011;334:928-35.

[2] Whittingham MS. Ultimate limits to intercalation reactions for lithium batteries. Chemical reviews. 2014;114:11414-43.

[3] Zhang K, Han X, Hu Z, Zhang X, Tao Z, Chen J. Nanostructured Mn-based oxides for electrochemical energy storage and conversion. Chemical Society Reviews. 2015;44:699-728.

[4] Goodenough JB, Park K-S. The Li-ion rechargeable battery: a perspective. Journal of the American Chemical Society. 2013;135:1167-76.

[5] Thackeray MM, Wolverton C, Isaacs ED. Electrical energy storage for transportation—approaching the limits of, and going beyond, lithium-ion batteries. Energy & Environmental Science. 2012;5:7854-63.

[6] Zubi G, Dufo-López R, Carvalho M, Pasaoglu G. The lithium-ion battery: State of the art and future perspectives. Renewable and Sustainable Energy Reviews. 2018;89:292-308.

[7] Zhan C, Cai F, Amine K, Lu J. Advanced Lithium Batteries for Automobile Applications at ABAA-9. ACS Energy Letters. 2017;2:1628-31.

[8] Wood III DL, Wood M, Li J. Zhijia Du, Rose E Ruther, Kevin A Hays, Nitin Muralidharan, Linxiao Geng, Chengyu Mao, Ilias Belharouak. Perspectives on the relationship between materials chemistry and roll-to-roll electrode manufacturing for high-energy lithium-ion batteries, Energy Storage Materials. 2020;29:254-65.

[9] Schnell J, Günther T, Knoche T, Vieider C, Köhler L, Just A, et al. All-solid-state lithium-ion and lithium metal batteries–paving the way to large-scale production. Journal of Power Sources. 2018;382:160-75.

[10] Berckmans G, Messagie M, Smekens J, Omar N, Vanhaverbeke L, Van Mierlo J. Cost projection of state-of-th- art lithium-ion batteries for electric vehicles up to 2030. Energies. 2017;10:1314.

[11] Schmitt M, Baunach M, Wengeler L, Peters K, Junges P, Scharfer P, et al. Slot-die processing of lithium-ion battery electrodes—Coating window characterization. Chemical Engineering and Processing: Process Intensification. 2013;68:32-7.

[12] Schmitt M, Scharfer P, Schabel W. Slot die coating of lithium-ion battery electrodes: investigations on edge effect issues for stripe and pattern coatings. Journal of Coatings Technology and Research. 2014;11:57-63.

[13] Pettinger K-H, Dong W. When does the operation of a battery become environmentally positive? Journal of The Electrochemical Society. 2016;164:A6274.

[14] Li J, Fleetwood J, Hawley WB, Kays W. From Materials to Cell: State-of-the-Art and Prospective Technologies for Lithium-Ion Battery Electrode Processing. Chemical Reviews. 2021;122:903-56.

[15] Bryntesen SN, Strømman AH, Tolstorebrov I, Shearing PR, Lamb JJ, Stokke Burheim O. Opportunities for the State-of-the-Art Production of LIB Electrodes—A Review. Energies. 2021;14:1406.

[16] Stein M, Mistry A, Mukherjee PP. Mechanistic understanding of the role of evaporation in electrode processing. Journal of The Electrochemical Society. 2017;164:A1616.

[17] Rollag K, Juarez-Robles D, Du Z, Wood III DL, Mukherjee PP. Drying temperature and capillarity-driven crack formation in aqueous processing of Li-ion battery electrodes. ACS Applied Energy Materials. 2019;2:4464-76.

[18] Font F, Protas B, Richardson G, Foster JM. Binder migration during drying of lithium-ion battery electrodes: Modelling and comparison to experiment. Journal of Power Sources. 2018;393:177-85.

[19] Kumberg J, Müller M, Diehm R, Spiegel S, Wachsmann C, Bauer W, et al. Drying of Lithium-Ion Battery Anodes for Use in High-Energy Cells: Influence of Electrode Thickness on Drying Time, Adhesion, and Crack Formation. Energy Technology. 2019;7:1900722.

[20] Jaiser S, Müller M, Baunach M, Bauer W, Scharfer P, Schabel W. Investigation of film solidification and binder migration during drying of Li-Ion battery anodes. Journal of Power Sources. 2016;318:210-9.

[21] Singh DP, Mulder FM, Abdelkader AM, Wagemaker M. Facile Micro Templating LiFePO4 Electrodes for High Performance Li-Ion Batteries. Advanced Energy Materials. 2013;3:572-8.

[22] Singh M, Kaiser J, Hahn H. Thick electrodes for high energy lithium ion batteries. Journal of The Electrochemical Society. 2015;162:A1196.

[23] Du Z, Wood DL, Daniel C, Kalnaus S, Li J. Understanding limiting factors in thick electrode performance as applied to high energy density Li-ion batteries. Journal of Applied Electrochemistry. 2017;47:405-15.

[24] Kim Y, Drews A, Chandrasekaran R, Miller T, Sakamoto J. Improving Li-ion battery charge rate acceptance through highly ordered hierarchical electrode design. Ionics. 2018;24:2935-43.

[25] Hawley WB, Li J. Electrode manufacturing for lithium-ion batteries—Analysis of current and next generation processing. Journal of Energy Storage. 2019;25:100862.

[26] Verdier N, Foran G, Lepage D, Prébé A, Aymé-Perrot D, Dollé M. Challenges in solvent-free methods for manufacturing electrodes and electrolytes for lithium-based batteries. Polymers. 2021;13:323.

[27] Lu Y, Zhao C-Z, Yuan H, Hu J-K, Huang J-Q, Zhang Q. Dry electrode technology, the rising star in solid-state battery industrialization. Matter. 2022;5:876-98.

[28] Li Y, Wu Y, Wang Z, Xu J, Ma T, Chen L, et al. Progress in solvent-free dry-film technology for batteries and supercapacitors. Materials Today. 2022.

[29] Mitchell P, Zhong L, Xi X. Recyclable dry particle based adhesive electrode and methods of making same. Google Patents; 2008.

[30] Zou B, Zhong L, Mitchell P, Xi X. Dry-particle packaging systems and methods of making same. Google Patents; 2006.

[31] Mitchell P, Zhong L, Xi X, Zou B. Dry particle based adhesive and dry film and methods of making same. Google Patents; 2009.

[32] Zhou H, Liu M, Gao H, Hou D, Yu C, Liu C, et al. Dense integration of solvent-free electrodes for Li-ion supercabattery with boosted low temperature performance. Journal of Power Sources. 2020;473:228553.

[33] Li G, Xue R, Chen L. The influence of polytetrafluorethylene reduction on the capacity loss of the carbon anode for lithium ion batteries. Solid State Ionics. 1996;90:221-5.

[34] Zhang Y, Huld F, Lu S, Jektvik C, Lou F, Yu Z. Revisiting Polytetrafluorethylene Binder for Solvent-Free Lithium-Ion Battery Anode Fabrication. Batteries. 2022;8:57.

[35] Duong H, Shin J, Yudi Y. Dry electrode coating technology. 48th Power Sources Conference2018. p. 34-7.

[36] Zhong L, Qiu K, Zea M, Shaw E. Dry electrode manufacture by temperature activation method. Google Patents; 2020.

[37] Zhong L, Shaw E, Kim BK. Dry electrode manufacture with lubricated active material mixture. Google Patents; 2022.

[38] Zhong L. Low cost high performance electrode for energy storage devices and systems and method of making same. Google Patents; 2016.

[39] Hippauf F, Schumm B, Doerfler S, Althues H, Fujiki S, Shiratsuchi T, et al. Overcoming binder limitations of sheet-type solid-state cathodes using a solvent-free dry-film approach. Energy Storage Materials. 2019;21:390-8.

[40] Wang C, Yu R, Duan H, Lu Q, Li Q, Adair KR, et al. Solvent-Free Approach for Interweaving Freestanding and Ultrathin Inorganic Solid Electrolyte Membranes. ACS Energy Letters. 2021;7:410-6.

[41] Al-Shroofy M, Zhang Q, Xu J, Tao C, Cheng YT. Solvent-free dry powder coating process for low-cost manufacturing of LiNi 1/3 Mn 1/3 Co 1/3 O 2 cathodes in lithium-ion batteries. Journal of Power Sources. 2017;352:187-93.

[42] Ludwig B, Liu J, Chen IM, Liu Y, Shou W, Wang Y, et al. Understanding interfacial-energy-driven dry powder mixing for solvent-free additive manufacturing of li-ion battery electrodes. Advanced Materials Interfaces. 2017;4:1700570.

[43] Ludwig B, Zheng Z, Shou W, Wang Y, Pan H. Solvent-free manufacturing of electrodes for lithium-ion batteries. Scientific reports. 2016;6:1-10.

[44] Wang M, Hu J, Wang Y, Cheng Y-T. The Influence of Polyvinylidene Fluoride (PVDF) Binder Properties on LiNi0.33Co0.33Mn0.33O2 (NMC) Electrodes Made by a Dry-Powder-Coating Process. Journal of The Electrochemical Society. 2019;166:A2151-A7.

[45] Liu J, Ludwig B, Liu Y, Zheng Z, Wang F, Tang M, et al. Scalable Dry Printing Manufacturing to Enable Long-Life and High Energy Lithium-Ion Batteries. Advanced Materials Technologies. 2017;2:1700106.

[46] Schälicke G, Landwehr I, Dinter A, Pettinger K-H, Haselrieder W, Kwade A. Solvent-Free Manufacturing of Electrodes for Lithium-Ion Batteries via Electrostatic Coating. Energy Technology. 2020;8:1900309.

[47] Garcia J, Goto T. Proc. Conf. Chem. Vapor Deposition Refract. Metals. Alloys, Compounds, 1967 Proc. Conf. Chem. Vapor Deposition Refract. Metals. Alloys, Compounds, 1967, 161-173, 1967. Materials transactions. 2003;44:1717-28.

[48] Kuwata N, Kawamura J, Toribami K, Hattori T, Sata N. Thin-film lithium-ion battery with amorphous solid electrolyte fabricated by pulsed laser deposition. Electrochemistry Communications. 2004;6:417-21.

[49] Shiraki S, Oki H, Takagi Y, Suzuki T, Kumatani A, Shimizu R, et al. Fabrication of all-solid-state battery using epitaxial LiCoO2 thin films. Journal of Power Sources. 2014;267:881-7.

[50] Chiu K-F. Lithium cobalt oxide thin films deposited at low temperature by ionized magnetron sputtering. Thin Solid Films. 2007;515:4614-8.

[51] Yang G, Abraham C, Ma Y, Lee M, Helfrick E, Oh D, et al. Advances in Materials Design for All-Solid-State Batteries: From Bulk to Thin Films. Applied Sciences. 2020;10:4727.

[52] Patil A, Patil V, Shin DW, Choi J-W, Paik D-S, Yoon S-J. Issue and challenges facing rechargeable thin film lithium batteries. Materials research bulletin. 2008;43:1913-42.

[53] Chen MC, Chang C, Glover GH, Gotlib IH. Increased insula coactivation with salience networks in insomnia. Biological psychology. 2014;97:1-8.

[54] Bates J, Dudney N, Neudecker B, Ueda A, Evans C. Thin-film lithium and lithium-ion batteries. Solid state ionics. 2000;135:33-45.

[55] Lin J, Lin L, Qu S, Deng D, Wu Y, Yan X, et al. Promising Electrode and Electrolyte Materials for High-Energy-Density Thin-Film Lithium Batteries. Energy & Environmental Materials. 2022;5:133-56.

[56] Reyes Jiménez A, Klöpsch R, Wagner R, Rodehorst UC, Kolek M, Nölle R, et al. A step toward high-energy silicon-based thin film lithium ion batteries. ACS nano. 2017;11:4731-44.

[57] Seeba J, Reuber S, Heubner C, Müller-Köhn A, Wolter M, Michaelis A. Extrusion-based fabrication of electrodes for high-energy Li-ion batteries. Chemical Engineering Journal. 2020;402:125551.

[58] Dreger H, Bockholt H, Haselrieder W, Kwade A. Discontinuous and continuous processing of low-solvent battery slurries for lithium nickel cobalt manganese oxide electrodes. Journal of Electronic Materials. 2015;44:4434-43.

[59] Sotomayor ME, de La Torre-Gamarra C, Levenfeld B, Sanchez J-Y, Varez A, Kim G-T, et al. Ultra-thick battery electrodes for high gravimetric and volumetric energy density Li-ion batteries. Journal of Power Sources. 2019;437:226923.

[60] De La Torre-Gamarra C, Sotomayor ME, Sanchez J-Y, Levenfeld B, Várez A, Laïk B, et al. High mass loading additive-free LiFePO4 cathodes with 500 μm thickness for high areal capacity Li-ion batteries. Journal of Power Sources. 2020;458:228033.

[61] El Khakani S, Verdier N, Lepage D, Prébé A, Aymé-Perrot D, Rochefort D, et al. Melt-processed electrode for lithium ion battery. Journal of Power Sources. 2020;454:227884.

[62] Astafyeva K, Dousset C, Bureau Y, Stalmach SL, Dufour B. High Energy Li-Ion Electrodes Prepared via a Solventless Melt Process. Batteries & Supercaps. 2020;3:341-3.

[63] Sun K, Wei TS, Ahn BY, Seo JY, Dillon SJ, Lewis JA. 3D printing of interdigitated Li-Ion microbattery architectures. Advanced materials. 2013;25:4539-43.

[64] Fu K, Wang Y, Yan C, Yao Y, Chen Y, Dai J, et al. Graphene oxide-based electrode inks for 3D-printed lithium-ion batteries. Advanced Materials. 2016;28:2587-94.

[65] Maurel A, Grugeon S, Armand M, Fleutot B, Courty M, Prashantha K, et al. Overview on lithium-ion battery 3D-Printing By means of material extrusion. ECS Transactions. 2020;98:3.

[66] Carneiro OS, Silva A, Gomes R. Fused deposition modeling with polypropylene. Materials & Design. 2015;83:768-76.

[67] Too M, Leong K, Chua C, Du Z, Yang S, Cheah C, et al. Investigation of 3D non-random porous structures by fused deposition modelling. The International Journal of Advanced Manufacturing Technology. 2002;19:217-23.

[68] Trembacki B, Duoss E, Oxberry G, Stadermann M, Murthy J. Mesoscale electrochemical performance simulation of 3d interpenetrating lithium-ion battery electrodes. Journal of the Electrochemical Society. 2019;166:A923.

[69] Foster CW, Down MP, Zhang Y, Ji X, Rowley-Neale SJ, Smith GC, et al. 3D printed graphene based energy storage devices. Scientific Reports. 2017;7:1-11.

[70] Ragones H, Menkin S, Kamir Y, Gladkikh A, Mukra T, Kosa G, et al. Towards smart free form-factor 3D printable batteries. Sustainable Energy & Fuels. 2018;2:1542-9.

[71] Reyes C, Somogyi R, Niu S, Cruz MA, Yang F, Catenacci MJ, et al. Three-dimensional printing of a complete lithium ion battery with fused filament fabrication. ACS Applied Energy Materials. 2018;1:5268-79.

[72] Maurel A, Courty M, Fleutot B, Tortajada H, Prashantha K, Armand M, et al. Highly loaded graphite–polylactic acid composite-based filaments for lithium-ion battery three-dimensional printing. Chemistry of Materials. 2018;30:7484-93.

[73] Maurel A, Grugeon S, Fleutot B, Courty M, Prashantha K, Tortajada H, et al. Three-dimensional printing of a LiFePO4/graphite battery cell via fused deposition modeling. Scientific reports. 2019;9:1-14.

[74] Wang Y, Chen C, Xie H, Gao T, Yao Y, Pastel G, et al. 3D-printed all-fiber li-ion battery toward wearable energy storage. Advanced Functional Materials. 2017;27:1703140.

[75] Han X, Funk M, Shen F, Chen Y, Li Y, Campbell C, et al. Scalable Holey Graphene Synthesis and Dense Electrode Fabrication toward High-Performance Ultracapacitors. ACS nano. 2014;8:8255-65.

[76] Kirsch DJ, Lacey SD, Kuang Y, Pastel G, Xie H, Connell JW, et al. Scalable Dry Processing of Binder-Free Lithium-Ion Battery Electrodes Enabled by Holey Graphene. ACS Applied Energy Materials. 2019;2:2990-7.

[77] Han X, Yang Z, Zhao B, Zhu S, Zhou L, Dai J, et al. Compressible, Dense, Three-Dimensional Holey Graphene Monolithic Architecture. ACS nano. 2017;11:3189-97.

[78] Kim G-T, Appetecchi GB, Alessandrini F, Passerini S. Solvent-free, PYR1ATFSI ionic liquid-based ternary polymer electrolyte systems. Journal of Power Sources. 2007;171:861-9.

[79] Yubuchi S, Ito Y, Matsuyama T, Hayashi A, Tatsumisago M. 5 V class LiNi0. 5Mn1. 5O4 positive electrode coated with Li3PO4 thin film for all-solid-state batteries using sulfide solid electrolyte. Solid State Ionics. 2016;285:79-82.

[80] Otoyama M, Ito Y, Hayashi A, Tatsumisago M. Raman imaging for LiCoO2 composite positive electrodes in all-solid-state lithium batteries using Li2S–P2S5 solid electrolytes. Journal of Power Sources. 2016;302:419-25.

[81] Ito Y, Yamakawa S, Hayashi A, Tatsumisago M. Effects of the microstructure of solid-electrolyte-coated LiCoO 2 on its discharge properties in all-solid-state lithium batteries. Journal of Materials Chemistry A. 2017;5:10658-68.

[82] Yubuchi S, Nakamura W, Bibienne T, Rousselot S, Taylor LW, Pasquali M, et al. All-solid-state cells with Li4Ti5O12/carbon nanotube composite electrodes prepared by infiltration with argyrodite sulfide-based solid electrolytes via liquid-phase processing. Journal of Power Sources. 2019;417:125-31.

[83] Boulineau S, Tarascon J-M, Leriche J-B, Viallet V. Electrochemical properties of all-solid-state lithium secondary batteries using Li-argyrodite Li6PS5Cl as solid electrolyte. Solid State Ionics. 2013;242:45-8.

[84] Kim G-T, Appetecchi GB, Alessandrini F, Passerini S. Solvent-free, PYR1ATFSI ionic liquid-based ternary polymer electrolyte systems: I. Electrochemical characterization. Journal of Power Sources. 2007;171:861-9.

[85] Auvergniot J, Cassel A, Ledeuil J-B, Viallet V, Seznec V, Dedryvère R. Interface stability of argyrodite Li6PS5Cl toward LiCoO2, LiNi1/3Co1/3Mn1/3O2, and LiMn2O4 in bulk all-solid-state batteries. Chemistry of Materials. 2017;29:3883-90.

[86] Nelson PA, Gallagher KG, Bloom ID, Dees DW. Modeling the performance and cost of lithium-ion batteries for electric-drive vehicles. Argonne National Lab.(ANL), Argonne, IL (United States); 2012.

[87] Liu Y, Zhang R, Wang J, Wang Y. Current and future lithium-ion battery manufacturing. Iscience. 2021;24:102332.

[88] Wood III DL, Li J, Daniel C. Prospects for reducing the processing cost of lithium ion batteries. Journal of Power Sources. 2015;275:234-42.

[89] Yuan C, Deng Y, Li T, Yang F. Manufacturing energy analysis of lithium ion battery pack for electric vehicles. CIRP Annals. 2017;66:53-6.

[90] Ahmed S, Nelson PA, Gallagher KG, Dees DW. Energy impact of cathode drying and solvent recovery during lithium-ion battery manufacturing. Journal of Power Sources. 2016;322:169-78.

[91] Choi JW, Aurbach D. Promise and reality of post-lithium-ion batteries with high energy densities. Nature Reviews Materials. 2016;1:1-16.

[92] Li J, Lu Y, Yang T, Ge D, Wood III DL, Li Z. Water-based electrode manufacturing and direct recycling of lithium-ion battery electrodes—a green and sustainable manufacturing system. IScience. 2020;23:101081.

[93] Wood DL, Quass JD, Li J, Ahmed S, Ventola D, Daniel C. Technical and economic analysis of solvent-based lithium-ion electrode drying with water and NMP. Drying Technology. 2018;36:234-44.

[94] Zackrisson M, Avellán L, Orlenius J. Life cycle assessment of lithium-ion batteries for plug-in hybrid electric vehicles–Critical issues. Journal of Cleaner Production. 2010;18:1519-29.

[95] Curry C. Lithium-ion battery costs and market. Bloomberg New Energy Finance. 2017;5:4-6.

[96] Shearing PR, Brandon N, Gelb J, Bradley R, Withers P, Marquis A, et al. Multi length scale microstructural investigations of a commercially available Li-ion battery electrode. Journal of The Electrochemical Society. 2012;159:A1023.

[97] Wang Y, Zheng Z, Ludwig B, Pan H. Dry powder based electrode additive manufacturing. Google Patents; 2020.

[98] Zhou C, Bag S, Lv B, Thangadurai V. Understanding the role of solvents on the morphological structure and Li-ion conductivity of poly (vinylidene fluoride)-based polymer electrolytes. Journal of The Electrochemical Society. 2020;167:070552.

[99] Li J, Daniel C, An SJ, Wood D. Evaluation residual moisture in lithium-ion battery electrodes and its effect on electrode performance. MRS advances. 2016;1:1029-35.

[100] Zhao J, Lu Z, Liu N, Lee H-W, McDowell MT, Cui Y. Dry-air-stable lithium silicide–lithium oxide core–shell nanoparticles as high-capacity prelithiation reagents. Nature communications. 2014;5:1-8.

[101] Zhao J, Lu Z, Wang H, Liu W, Lee H-W, Yan K, et al. Artificial solid electrolyte interphase-protected Li x Si nanoparticles: an efficient and stable prelithiation reagent for lithium-ion batteries. Journal of the American Chemical Society. 2015;137:8372-5.

[102] Huang B, Huang T, Wan L, Yu A. Pre-lithiating SiO anodes for lithium-ion batteries by a simple, effective, and controllable strategy using stabilized lithium metal powder. ACS Sustainable Chemistry & Engineering. 2021;9:648-57.

[103] Forney MW, Ganter MJ, Staub JW, Ridgley RD, Landi BJ. Prelithiation of silicon–carbon nanotube anodes for lithium ion batteries by stabilized lithium metal powder (SLMP). Nano letters. 2013;13:4158-63.

[104] Kim C-S, Jeong KM, Kim K, Yi C-W. Effects of capacity ratios between anode and cathode on electrochemical properties for lithium polymer batteries. Electrochimica Acta. 2015;155:431-6.

[105] Helmers L, Froböse L, Friedrich K, Steffens M, Kern D, Michalowski P, et al. Sustainable Solvent-Free Production and Resulting Performance of Polymer Electrolyte-Based All-Solid-State Battery Electrodes. Energy Technology. 2021;9:2000923.

[106] Zhang Z, Wu L, Zhou D, Weng W, Yao X. Flexible sulfide electrolyte thin membrane with ultrahigh ionic conductivity for all-solid-state lithium batteries. Nano Letters. 2021;21:5233-9

Chapter 2: Revisiting Polytetrafluorethylene Binder for Solvent Free Lithium-Ion Battery Anode Fabrication

1. Introduction

Lithium-ion batteries (LIBs) dominate the market of portable consumer electronic devices since SONY Corporation launched the first commercial product in the 1990s. As the most studied energy storage devices, LIBs have attracted more and more attention. Their high operation voltage, high energy density, small self-discharge, high-rate performance, and long cycle stability make them especially attractive to electric vehicles (EVs)[1-5]. Nevertheless, transport electrification is one of the biggest challenges we face today[2]. There are three significant issues to be addressed for the widespread application of LIBs in EVs: safety, long driving range, and low cost[5,6]. In terms of safety and short driving range, one of the most promising solutions is all-solid-state batteries. Regarding the cost, the high cost of LIBs has become a bottleneck for its widespread application, as the cost of energy-storage systems must reduce to $\$125 kwh^{-1}$ to meet the economical requirements[7].

The cost of batteries mainly consists of two parts, i.e., raw materials and manufacturing costs. Reducing manufacturing energy consumption and increasing electrode thickness are two effective methods to lower the manufacturing cost of LIBs[7]. The fabrication of electrodes with the conventional slurry casting (SC) procedure involves mixing the active material, polymer binder, and conductive additive in water or *N*-methyl-pyrrolidone (NMP). After several hours of mixing, the slurry is cast on the current collector, dried, and rolled to form electrodes. NMP is the commonly used organic solvent in cathode fabrication, while water is used for anode. Dozens of meters long oven with a temperature higher than 120 ^{o}C is required in the process of drying for both anode and cathode. The energy consumed in slurry making and coating accounts for approximately 50% of all cell production processes in a 20.5 Ah, 3.7 V and 1 ppm production line[8]. Numerous research groups have explored the possibility of removing the solvent from the electrode fabrication process to reduce the manufacturing cost[9-11]. A solvent free (SF) electrode has been fabricated with the

help of laser technology. The laser is focused on the electrode material to achieve pulsed-laser deposition. However, the process requires high vacuum and extremely high annealing temperature while only forming thin films of the electrode[12,13]. Radio frequency magnetron sputtering method can be applied with a relatively low temperature substrate of 350 ^{o}C. However, expensive equipment and inert atmosphere are required, which limits its large-scale application[14]. $Li_4Ti_5O_{12}$ anodes were fabricated with the dry-spraying method, where the electrode component mixture was sprayed directly onto the current collector through the slot in N_2 atmosphere and subsequently isothermally hot-pressed several times[15]. Another common method for SF electrode fabrication is electrostatic spray deposition (ESD), for which high voltage was added between the deposition nozzle and the grounding current collector, and the deposition material is atomized. The charged particles are deposited onto the current collector and subsequently heat pressed, or heat rolled to form electrodes[16-18]. All these methods are either quite complicated or energy-consuming, not suitable for mass production.

Polytetrafluorethylene (PTFE) has also been demonstrated for SF electrode fabrication. Yang et. al fabricated SiO anode with PTFE and polyvinylidene fluoride (PVDF) using its sticky property, where PTFE, PVDF, SiO and acetylene black were dry mixed and pressed to form the final electrodes[19]. Another promising method for SF electrode fabrication is using fibrillizable polymer, in most cases polytetrafluorethylene (PTFE), to replace conventional soluble binder, where high shear, hot-rolling, and hot lamination processes were involved. PTFE can be stretched to form fibrils under high shear, which can act as a net to support active material and conductive additives. The mixture of the electrode component was hot-rolled after mixing under high shear to form a free-standing film and finally laminated with the current collector using hot-rolling again. Since Maxwell's company firstly revealed the SF electrode production process for supercapacitors using PTFE as the binder in 2004, the method attracted more and more attention with the widespread utilization of EVs[20]. However, the study mainly focused on electrodes applied in supercapacitors

or cathodes in LIBs due to its instability when applied in anodes[6,21]. The energy level of the lowest unoccupied molecular orbitals (LUMO) of PTFE is relatively low, which implies that PTFE accepts electrons readily, making it electrochemically unstable in an anodic environment[22,23]. For LIBs, the electrons are favorably transferred to the LUMO of PTFE to generate lithium fluoride and carbyne through a defluorination process[24-26]. The sub-micro scale carbyne is unstable and could be further decomposed to amorphous carbon, which cannot withstand the volume shrinkage and expansion in the process of discharge and charge, resulting in poor cycling stability[27-30].

Increasing the loading of active material is another important way to decrease manufacturing costs because less current collector, separators, and other auxiliary materials are required per unit capacity. However, the electrode kinetics is unfavourable for a thick electrode, resulting in poor C-rates performance. Moreover, the thick electrode is not compatible with the slurry-casting process. Breakdown of electrode and delamination of active material from the current collector caused by an uneven distribution of binder in the drying process limit the practical implementation of thick electrode. On the other hand, it is facile for thick electrode fabrication using a solvent free method since it avoids the drying process.

Therefore, developing a rapid and facile solvent free electrode fabrication method compatible with the current commercial LIBs production line is highly desired. PTFE has shown great potential for cathode production in LIBs and electrode fabrication in capacitors due to its compatibility with the current commercial production line[20,21]. Post-Li chemistries like Al or Zn are emerging as promising candidates for next-generation rechargeable batteries[31,32]. The application of the method could also be used for electrodes fabrication for these batteries. In this study, we successfully extended PTFE for solvent free anode fabrication. SF anodes with different active carbon materials including graphite, hard carbon and soft carbon were fabricated with PTFE as binder. The SF graphite anode was unstable, while SF hard carbon and SF soft carbon anode showed great long-term cycle life. Notably, the SF hard carbon electrode

with a high loading of 10.7 mg/cm^2 showed similar long-term cycling stability and better C-rates performance compared to the SC anodes, demonstrating its potential for large-scale production. To the best of our knowledge, it's the first time that the PTFE was utilized for solvent free anode fabrication. It was proposed that the long cycle life performance of SF hard carbon and SF soft carbon anode was attributed to the low volume variation during the charge/discharge process, and the electrodes were able to maintain their integrity even though PTFE was reduced to amorphous carbon.

2. Experimental

2.1. Primer coated current collector preparation

To increase the adhesion between electrode dry film and current collector, copper foil (10 μm) with primer was used as the current collector. The primer slurry was prepared by mixing polyacrylic acid (PAA), carbon black, Carbon nanotube (CNT, Lanxi Zhide Advanced Materials Co., Ltd, China) in deionized water. The weight ratio of PAA/ carbon black/CNT was 20/20/1. The prepared slurry was cast on copper foil with a doctor blade and subsequently dried in blast air oven at 40 ^{o}C for 10 min. The thickness of the primer layer is approximately 1 μm.

2.2. Electrodes fabrication

The commercial anode active material (graphite/soft carbon/hard carbon), carbon black, PTFE powder (MTI, China) were used directly for anode fabrication. A powder mixture was prepared by mixing the active material, carbon black, and PTFE powder in V-blender for 10 minutes. The weight ratio of active material/carbon black/PTFE was 90/5/5. Jet mill with 2 inches grinding chamber (Sturtevant, US) was adapted to apply high shear with the grinding and feeding pressure of 80 and 60 psi, respectively, to fibrillate PTFE. The free-standing film formed with the dry mixture fed through the gap of calendering rolls and then pressed under at temperature of 160 ^{o}C. The thickness of which was adjusted according to the gap of rolls of the calender machine with a speed of 10 cm/min. Finally, the free-standing film was laminated to the primer coated current collector using hot rolling at 160 ^{o}C. For comparison, SC anode was also fabricated by mixing active materials with carbon black, and aqueous carboxymethyl cellulose/styrene-butadiene rubber (CMC/SBR) binder (1:1, m:m) with the same

weight ratio as the SF anode. The prepared slurry was cast onto the copper foil (10 μm, Guangdong, China) by doctor blade coating technology. After drying in a blast air oven for 30 min at 40 ^{o}C, the electrode was rolled to designated thickness. Both electrodes were cut into a disc of 15 mm diameter and further dried in a vacuum oven at 120 ^{o}C for 12 hours before moving to half-cell assembly.

2.3. Hard carbon anode prelithiation

The half pouch cell was assembled with SF hard carbon electrode as the anode and lithium foil as the cathode. Before prelithiation, the pouch half-cell was aged for 12 hours with a fixture to apply pressure. First, the cell was current discharged to 0.01 V and then set to rest for 30 minutes, and finally current charged to 1.5 V. The pouch cell was disassembled and the SF anode was washed with diethyl carbonate (DEC) several times and then dried under room temperature in the glove box for further full cell assembly.

2.4. Cell assembly and electrochemical characterization

Both SF and SC half cells were assembled with 2032-coin cells (MTI, China) in an argon-filled glove box, where water and oxygen concentrations were less than 0.01 ppm. Cellulose film (Celgard, US), lithium foil (Sigma Aldrich, 600 μm) and 70 μL 1.2 M $LiPF_6$ in EC-EMC (30/70, v/v) with 2 wt.% vinylene and 10 wt.% fluoroethylene carbonate (FEC) were used as separator, encounter electrode and electrolyte, respectively. The full cells with NCM 523 electrode as cathode were assembled using the same method except with prelithiated SF hard carbon electrodes.

For the half cell, the galvanostatic charge/discharge tests were performed over a voltage range of 0.01–1.5 V under room temperature using an 8-channel battery analyzer (Neware, China). The C-rates conducted for rate performance testing ranged from 0.1C to 2C. All cells were aged under room temperature for 12 h before testing and underwent several formation cycles with the constant charge/discharge current of 0.05C/0.05C. The capacity retention was calculated based on the average delithiation capacity of the first three cycles in the subsequent cycles (excluding the formation cycles). For the full cell, the voltage range is 2.8 to 4.2V. Autolab was used for

electrochemical impedance spectroscopy (EIS) analysis with the frequence between 0.01Hz to 1MHz.

The pristine and cycled electrodes were observed using a scanning electron microscope (SEM). The cycled electrodes were charged to the fully delithiation state after cell cycling, followed by disassembling the cell, dipping the electrode into DEC solution for 2 h to remove any residual electrolyte, and finally left for drying at room temperature overnight in an argon-filled glove box for further ex-situ analysis.

2.5. Adhesion and mechanical strength characterization

Adhesion was tested using a tensile force machine (Dongri Instrument Co., Ltd). Electrodes with 20*50 mm dimension were fixed between two parallel holders by double-sided tape (Figure 2.1). The velocity is 50 mm/min. The same electrode stripes were used for mechanical testing.

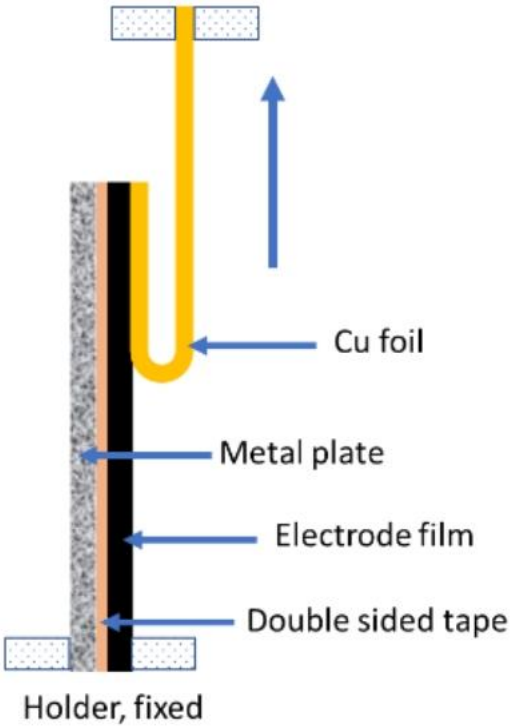

Figure 2.1. Graphical representation of peel off strength test with tensile machine.

3. Results and discussion

Graphite was firstly selected for the SF anode investigation due to its most widely application in commercial LIBs. The schematic illustration of SF graphite anode

fabrication is shown in Figure 2.2. Graphite, PTFE and carbon black were mixed for 10 minutes using a V-blender for the sake of uniform distribution of conductive additive. Then the mixed dry powder was fibrillated with a jet mill to form the dry mixture, and PTFE particles were stretched to fibrils by high shear force generated by high pressure dry compressed air. Therefore, PTFE fibrils hold graphite and carbon black together like a net structure. To increase the flexibility of the dry electrode film and the adhesion between the film and the current collector, the hot-pressing process with calendering machine was involved in both free-standing film formation and film and current collector lamination. The flexible nature of PTFE makes the free-standing film fairly soft, which can be bent and folded several times without any obvious electrode cracks or particles peeling off from the electrode film. The flexibility and mechanical strength of the dry electrode film indicates a high degree of fibrillation and good functionality of PTFE, making the method compatible with today's commercial roll to roll manufacturing process.

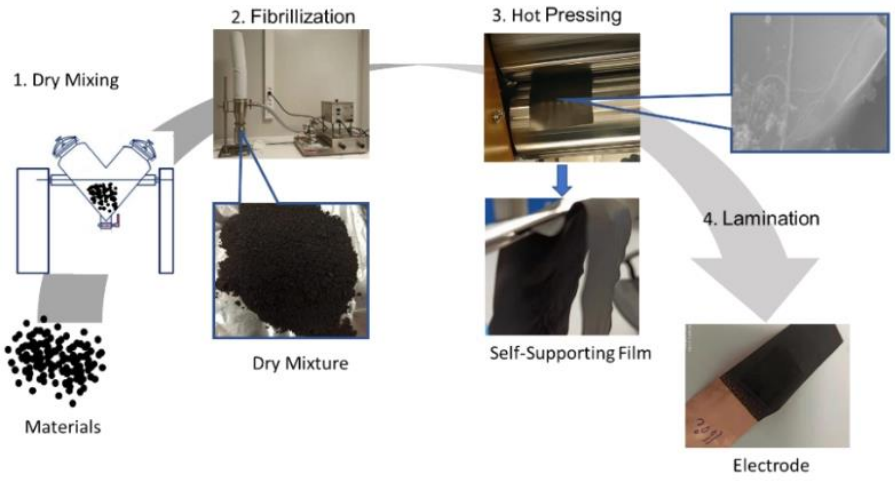

Figure 2.2 Schematic representation of SF anode fabrication procedure.

The adhesion strength between active materials layer and the current collector is a big issue for SF electrodes[33]. It is critical for the SF method since PTFE is insoluble, resulting in less contact area between the electrodes film and current collector. For better adhesion, a conductive adhesive primer coated copper foil was used as current collector. The optimal temperature for the graphite film to current collector lamination was also investigated. As shown in Figure 2.3, the adhesion increased from 16 to 21

N/m as the lamination temperature increased from 100 to 160 °C. When the lamination temperature was further increased to 180 °C, the adhesion didn't change a lot.

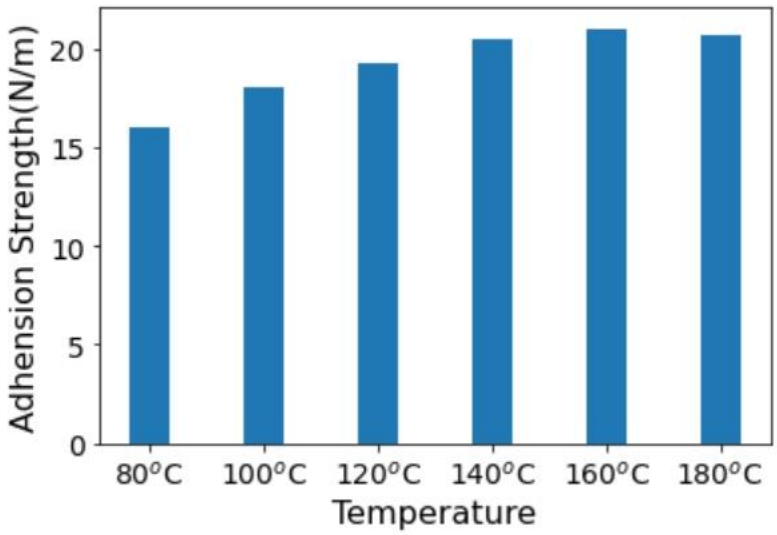

Figure 2.3 Adhesion strength at different lamination temperatures.

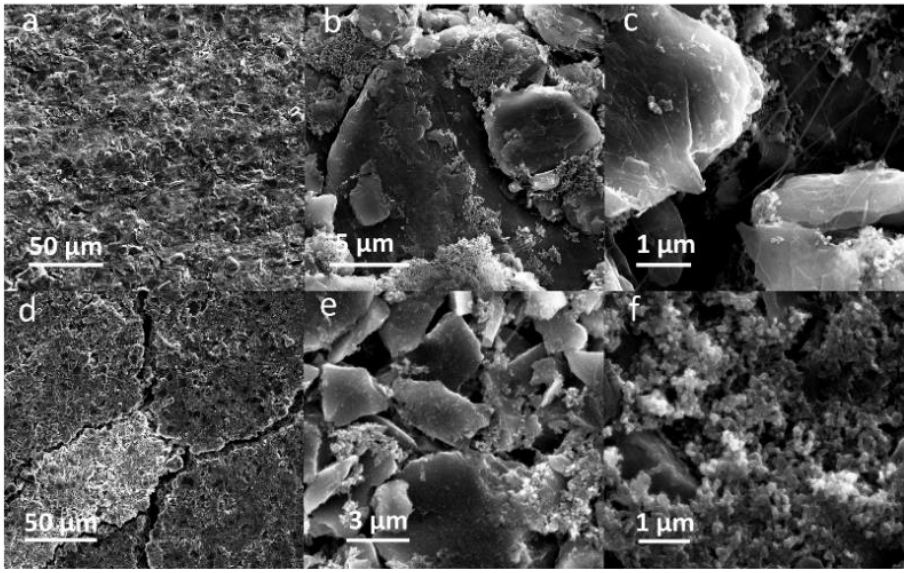

Figure 2.4 SEM images of pristine SF graphite anodes with different magnifications: (a) 1550x, (b) 16000x, (c) 45000x. SF graphite anodes after 100 cycles with different magnifications: (d) 1550x, (e) 23500x, (f) 50000 x.

The SEM-EDS mapping of pristine SF graphite electrode demonstrates that fluorine is uniformly distributed on the surface of the electrode (Figure 2.5), demonstrating even distribution of PTFE on the electrode. Figure 2.4a-c shows the SEM images of pristine SF graphite anode at different magnifications. The fibrils of PTFE could be observed from the top view of SEM images (Figure 2.4b, c) of the pristine graphite electrode,

which bundles graphite to form a net-like structure, ensuring the free-standing film with good mechanical stability with a tensile strength of 8N/m and good flexibility.

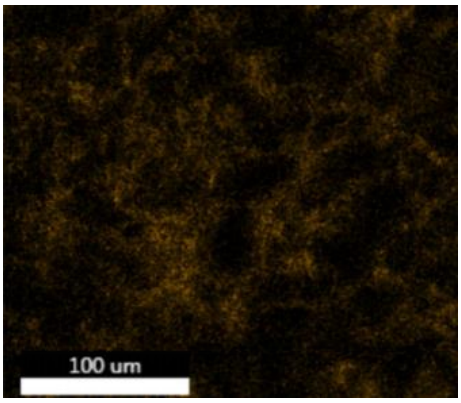

Figure 2.5 Fluorine element distribution on the surface of the pristine SF graphite anode from SEM-EDS.

The cycling stability of SF graphite anode was studied in half cells with a current of 0.1C at room temperature. It is worth mentioning that the areal loading of the SF graphite anode was 12.4 mg/cm^2, which was higher than the commercial one. As shown in Figure 2.6a, the capacity faded fast even under a small current, with only approximately 30% capacity retention after 35 cycles. The fast capacity fading could be ascribed to the reaction of PTFE and lithium ion in the first lithiation process. Most of the PTFE was reduced by lithium ion and the adhesion and cohesion degraded. The low initial coulombic efficiency (ICE) of 73% was also caused by the irreversible reaction(Figure 2.6b)[26], which was illustrated by Equation 1

$$-(-CF_2-)_n- + 2n\,Li \longrightarrow n\,C\,(amorphous) + 2n\,LiF \qquad (1)$$

It's worth noting that earlier studies demonstrated relatively stable cycling performance of PTFE based graphite anode using dry press procedure. The difference of stability could be ascribed to electrode fabrication procedure, electrode structure and testing condition[34-36]. According to the reports mentioned above, the graphite electrodes were fabricated by mixing PTFE with graphite and then dry pressed onto substrate, while we used high speed air to fibrillate PFTE. The fine PTFE fibrils in our

study has more chance to accept electrons and get reduced. High porosity could help to accommodate the volume variation of graphite electrodes during charge/discharge process[34]. Current density is another factor affecting the stability of electrodes. PTFE based graphite anodes is more stable under 0.1 mAh/cm^2 than that under 0.4 mAh/cm^2 [35]. A further factor which could degrade the stability of SF graphite electrodes in our research is the high active material loading and increased density of electrode (12.4 mg/cm^2, 1.68 g/cm^3). In summary, inferior stability of SF graphite electrodes in our system could ascribe to high loading of graphite, high pressed density and the easily reduction of fibrillated PTFE.

The irreversible capacity of the first cycle was 1260 mAh per gram of PTFE, resulting from the irreversible reaction of PTFE with lithium-ion and the solid electrolyte interphase (SEI) film formation in the first lithiation process. The reduction of PTFE was further confirmed by X-ray diffraction (XRD) characterization of pure PTFE powder, graphite powder and SF graphite electrode after first lithiation. The characteristic peak of PTFE at 18.2° was not identified for the SF graphite anode, demonstrating the reduction of PTFE (Figure 2.7). The results is consistent with those reported in literature[26]. The coulombic efficiency increased to more than 99% in the second cycle, indicating that most PTFE was reduced in the first cycle. The coulombic efficiency (CE) increased to 99.6% and 99.8% and maintained stable after 10 cycles and 20 cycles, respectively. The high CE implied that most inserted active lithium could be reversibly extracted, which was crucial for the long cycle life of electrodes. The high CE further verified that the capacity fading was mainly caused by the loss of contact of active material rather than the irreversible side reactions.

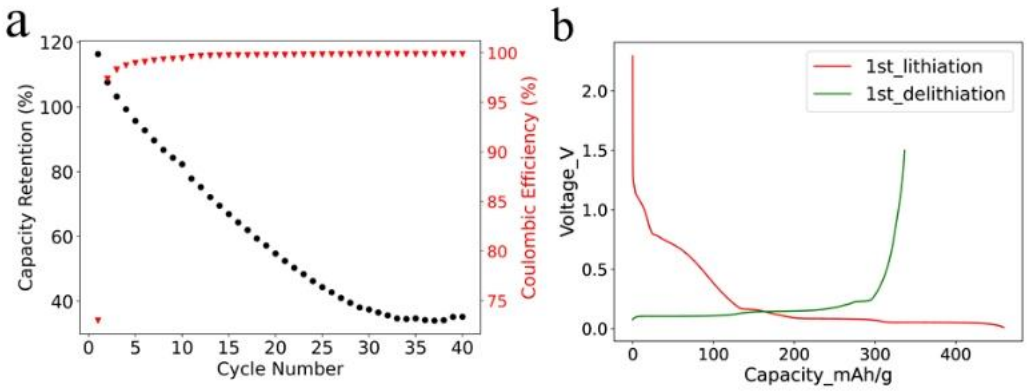

Figure 2.6 (a) Cycling performance of SF graphite with a current of 0.1C at room temperature; (b) Voltage-capacity curves for the first lithiation and delithiation processes.

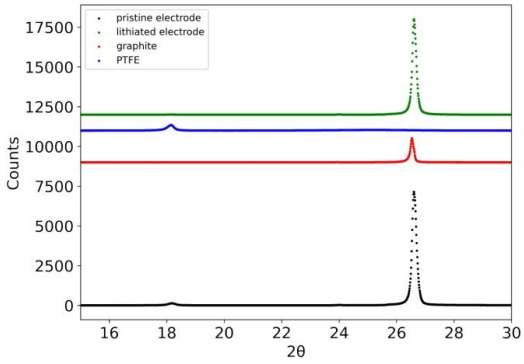

Figure 2.7 XRD characterization of pure PTFE powder, graphite powder, pristine SF graphite anode and SF graphite anode after first lithiation.

The morphology of the cycled SF graphite electrodes was observed by SEM to explore the capacity fading mechanism. As shown in Figure 2.4d, cracks could be observed from the top view of the cycled electrodes. There were no visible fibrils left (Figure 2.4e, f), indicating that most long PTFE fibrils was reduced to short carbyne. The cross-sectional SEM images (Figure 2.8a) showed that the electrode was uncompacted compared to the pristine one, losing contact of some active material to the electrode bulk parts or current collector. No obvious separation between electrode film and the current collector was observed, indicating good adhesion between the electrode film and the primer coated current collector. Considering that the graphite has a big volume variation during the charge/discharge process, the thickness of the SF graphite anode at different states were measured. The thickness of SF graphite anode for the pristine, after the first lithiation and after the first delithiation process was 84.2, 117.6, 98.6 μm, respectively (Figure 2.9). The thickness of the first lithiated anode

increased by 19.2% compared with the pristine one. Taking all these into consideration, the possible fading mechanism was that PTFE was reduced to carbyne with sub-micro dimension in the first lithiation process, which could be further decomposed to amorphous carbon[24,25,27,37]. The sub-micro scale carbyne and amorphous carbon cannot bind active materials together when the electrode has huge volume variation during cycling, losing the integrity and resulting in fast capacity fading[28-30].

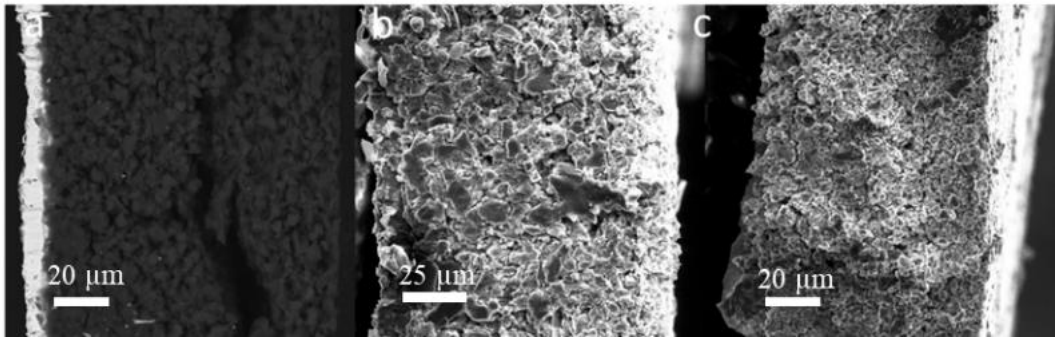

Figure 2.8 Cross sectional SEM images of SF anodes after 100 cycles: (a) graphite, (b) hard carbon, (c) soft carbon.

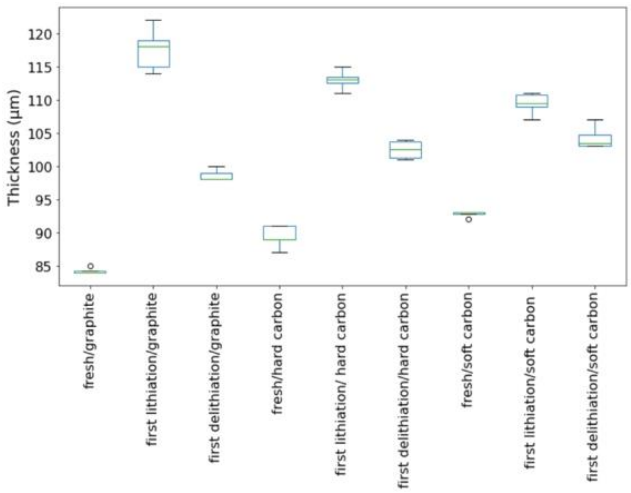

Figure 2.9 Thickness variation of various SF-anode at different stages.

As one alternative to graphite, hard carbon has the advantage of better rate performance as well as smaller volume variation during charge/discharge cycling[38-41]. To confirm our hypothesis on SF graphite fading mechanism, the cycling stability of SF hard carbon anode fabricated with the same procedure as SF graphite was studied in half cells with a current of 0.3C at room temperature. For comparison, SC hard carbon anodes with CMC/SBR as binder were also fabricated. Considering that the

electrode with high thickness is easily fabricated with our solvent free method, the areal loading, thickness and compacted density of the SF hard carbon anode is 10.7 mg/cm^2, 89.4 μm and 1.20 g/cm^3, respectively. While for the SC anodes, the areal loading, thickness and density of the electrode are 5.6 mg/cm^2, 74 μm and 0.76 g/cm^3, respectively. As shown in Figure 2.11a, the specific capacity for SF and SC hard carbon anode was 172 and 175 mAh/g at 0.05C. More than 80% capacity retention was obtained after 100 charges/discharge cycles for SF hard carbon anode. For the SC anode, capacity retention was lower at approximately 76% under the same condition. The CE was more than 99.5% and kept stable after the first 3 formation cycles for SF and SC anodes, demonstrating well reversible lithium insertion and extraction. It is worth noting that electrodes with high loading of 25 mg/cm^2 could also been fabricated with high flexibility (Figure 2.10).

Figure 2.10 Hard carbon electrode with high loading of 25 mg/cm^2.

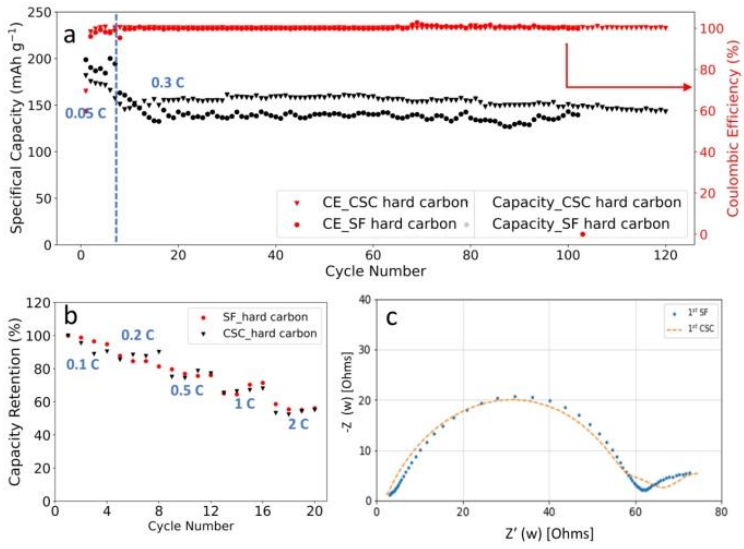

Figure 2.11 (a) Cycling performance and columbic efficiency of the SF hard carbon and SC electrodes cycled between 0.01 V and 1.5 V; (b) Rate capability of SF and SC hard carbon electrodes in the range of 0.1C to 2C in half cells; (c) EIS analysis of SF and SC hard carbon electrodes after formation.

C-rates performance comparison was also carried out with charge/discharge current in the range of 0.1C to 2C **(**Figure 2.11b**)**. For the SF hard carbon anodes, the electrode delivered a specific capacity of 159 $mAhg^{-1}$ at 0.1C. The capacity retentions were 86%, 75%, 67%, 54% at 0.2C, 0.5C, 1C, 2C, respectively. While the capacity retentions for the SC anode were 87%, 79%, 70%, and 55% at the same circumstance, which was comparable to the SF one. Considering that the SF anodes had higher loading and larger compacted density (1.20 g/cm^3 for the SF hard carbon anode compared to 0.76 cm^3 for the SC hard carbon anode), it is fair to conclude that the SF anode has better C-rates performance. Both PTFE and CMC/SBR are insulating, which is unfavourable for the conductivity of the electrode. For the SC anode, insulating CMC dissolved in water and form a compact insulating layer around hard carbon particles to block the conduction pathway, resulting in increased resistance and low C-rates performance. While in the SF anode, high C-rates performance was achieved due to reduced blocking of active material, which could be further ascribed to the fibrous nature of PTFE binder. The EIS results of SF and SC hard carbon electrodes after formation demonstrated that the two electrodes had similar resistance, which was consistent with the rate capability performance **(**Figure 2.11b and c**)**.

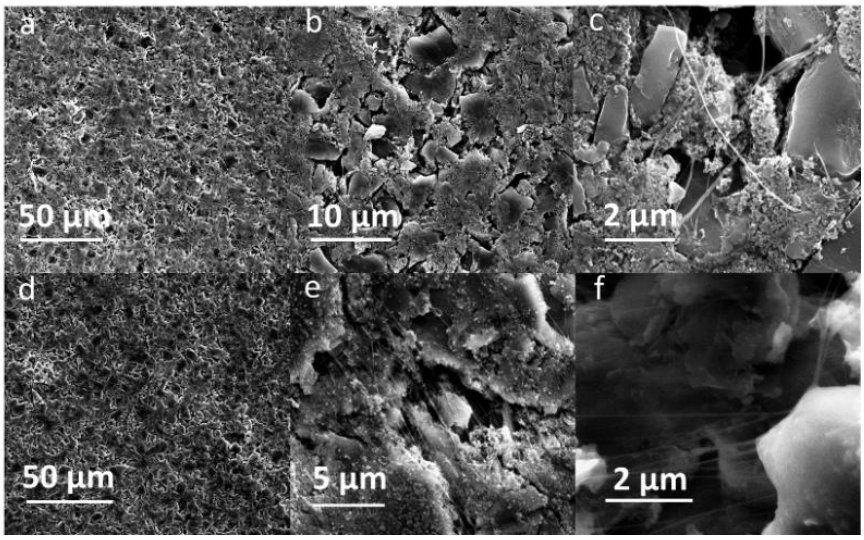

Figure 2.12 SEM images of pristine SF hard carbon anodes with different magnifications: (a) 1550x, (b) 7200, (c) 33000x. SF hard carbon anodes after 100 cycles with different magnifications: (d) 1550x, (e) 16000x, (f) 33000x.

Both pristine and cycled SF hard carbon electrodes were characterized by SEM imaging. The pristine SF hard carbon electrodes showed similar morphology as the SF graphite electrode (Figure 2.12a-c), as uniformly distributed PTFE fibrils could also be observed for the hard carbon anode. On the other hand, the cycled SF hard carbon electrode presented quite different morphology characteristics (Figures 2.12d-f). Unlike the cycled SF graphite anode (Figure 2.4d), no apparent cracks were observed for the SF hard carbon electrode and it maintained compact after 100 cycles (Figure 2.12d), demonstrating its good integrity. The fibril on the surface of active material disappeared, while there were still many fibrils left bridging the neighboring hard carbon particles. The different fibrils morphology of cycled SF hard carbon and graphite anodes was attributed to their different volume expansion during the charge process. PTFE was only reduced to carbyne when electron transfer happens, which meant that degradation will not occur when the fibrils do not contact the active materials directly. The fibrils were broken down in SF graphite anode due to the significant volume expansion during the first lithiation process. The broken fibrils fell on the surface of graphite and were further reduced to carbyne. However, in SF hard carbon anode, the low volume variation during the charge/discharge process indicated that the fibril bridging the adjacent hard carbon particles can keep their position and do not contact the active

material directly, therefore they had less possibility to be reduced to carbyne. This explains why only fibril bridging the adjacent hard carbon remained while the fibril on the surface of the particles disappeared. The thickness of the pristine, first lithiated and first delithiated SF hard carbon electrodes is 89.4, 111.3, 102.5 μm, respectively. Compared to the first delithated one, the thickness of the first lithiated SF hard carbon anode only increased 8.5%, which was much less than the SF graphite anode counterpart **(**Figure 2.9). The cross-sectional SEM image also showed the compact structure of the cycled electrode (Figure 2.8b). Voltage-capacity curves for SF and SC hard carbon electrodes were shown in Figure S5. The initial coulombic efficiency for SF and SC hard carbon electrodes was 57% and 73%, respectively. The low ICE of SF electrodes was ascribed to the irreversible reaction between active lithium and PTFE in the first lithiation process. The reaction capacity of PTFE to active lithium here was 1021 mAh/g, in line with the theoretical value of 1070 mAh/g[26]. A plateau around 0.85 V in the first lithiation process (Figure 2.13a) could also be attributed to the reaction between PTFE and lithium ions. The plateau did not appear in the second cycle of SF electrode or first cycle of SC electrode, which confirmed that the reaction is irreversible and was completed in the first lithiation process (Figure 2.13c, d). The plateau at approximately 0.95 V of the SC hard carbon electrode was ascribed to the formation of SEI film (Figure 2.13b). To further confirm the stability of PTFE, electrodes with 85% PTFE and 15% carbon black were fabricated with the similar procedure and half cells were assembled. Cyclic voltammogram (CV) was scanned at 0.5 mV/s (Figure 2.14). In the first cycle, there was a reduction peak at around 0.9 V, which could be ascribed to the irreversible reaction of PTFE and lithium ion. The CV results were consistent with the results of differential capacity (dQ/dV) and Voltage-Capacity curves in Figure 2.13.

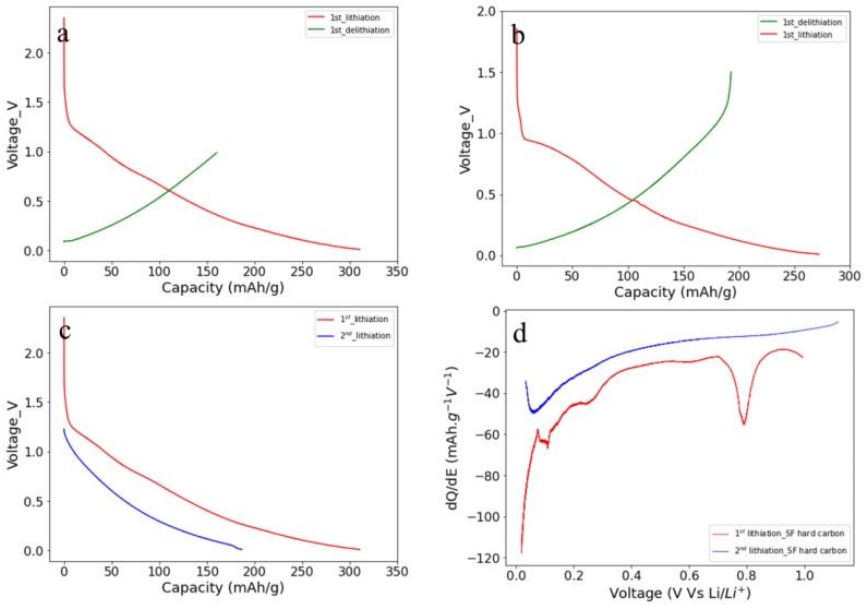

Figure 2.13 (a) First lithiation voltage-capacity curves for the SF hard carbon electrodes. (b) First lithiation voltage-capacity curves for the SC hard carbon electrodes. (c) Voltage-capacity curves for the SF hard carbon electrodes during the first and second cycles. (d) Differential capacity curves for the SF hard carbon electrodes during the first and second cycles.

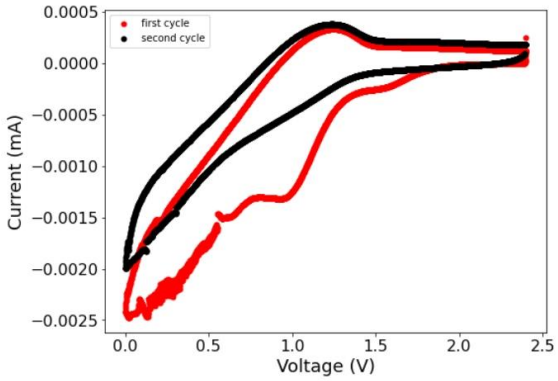

Figure 2.14 Cyclic voltammogram curves of PTFE electrodes scanned at 0.5 mV/s at the range of 0-2.4V.

To further clarify the relationship between the cycle life of the anodes and the volume variation of the active materials, the SF soft carbon anode was also fabricated and investigated with the same procedure. As shown in Figure 2.15, the SF soft carbon electrode showed comparative cycling performance to SF hard carbon anode, with roughly 80% capacity retention after 100 cycles under 0.3C. The low ICE of 72% is also ascribed to the irreversible reaction between PTFE and active lithium in the first lithiation process, similar with the SF graphite and hard carbon electrodes. The thickness of SF soft carbon anode was measured to be 92.8, 108.5 and 104.2 μm for pristine, first lithiation and first delithiation states, respectively. Similar SEM

morphology was observed for both pristine and cycled electrodes (Figure 2.16) compared to the SF hard carbon electrode. PTFE fibre was distributed evenly on the surface of soft carbon for the pristine electrode, and no apparent cracks were observed for the electrode after 100 cycles. The cross-sectional SEM images demonstrated the integrity of the electrode after 100 cycles (Figure 2.8c). The cycling performance and morphology study of SF soft carbon electrode further supports our hypothesis that the stability of SF hard carbon and soft carbon electrode is attributed to its low volume variation during the charge/discharge process.

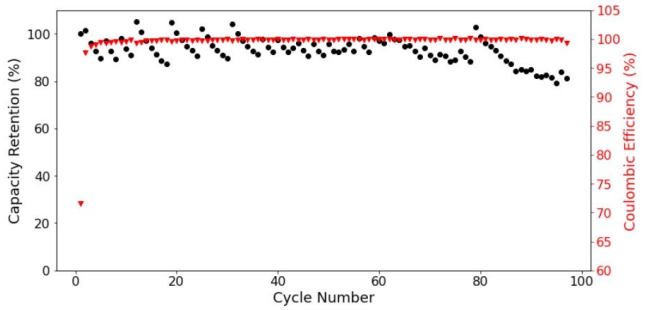

Figure 2.15 Capacity stability of SF soft carbon electrodes.

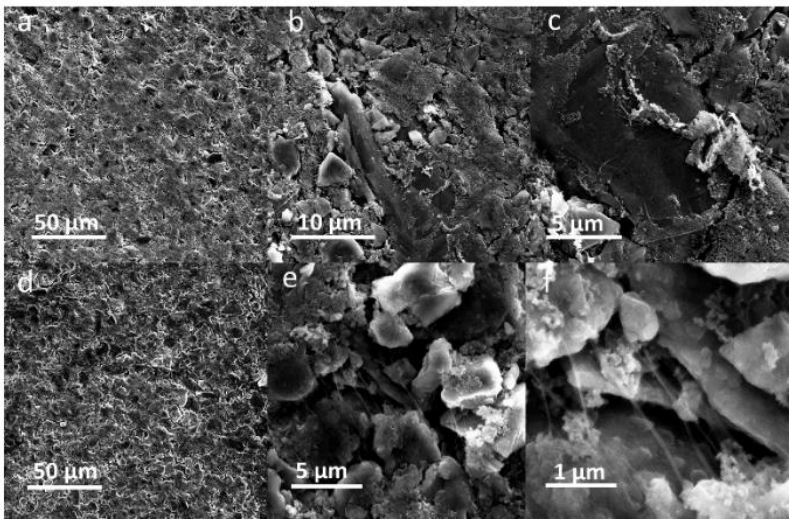

Figure 2.16 a, b, c) SEM images of pristine SF soft carbon anodes. d, e, f) SEM images of SF soft carbon electrodes after 100 cycles at different magnifications.

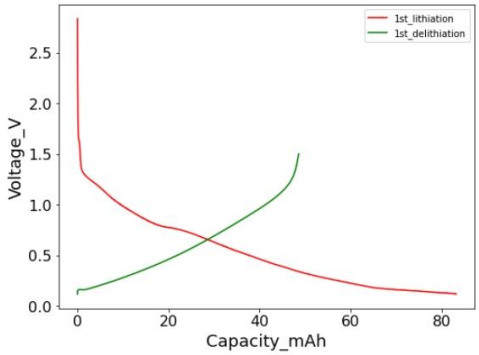

Figure 2.17 Voltage-capacity curves for the prelithiation process with lithium foil as lithium resource.

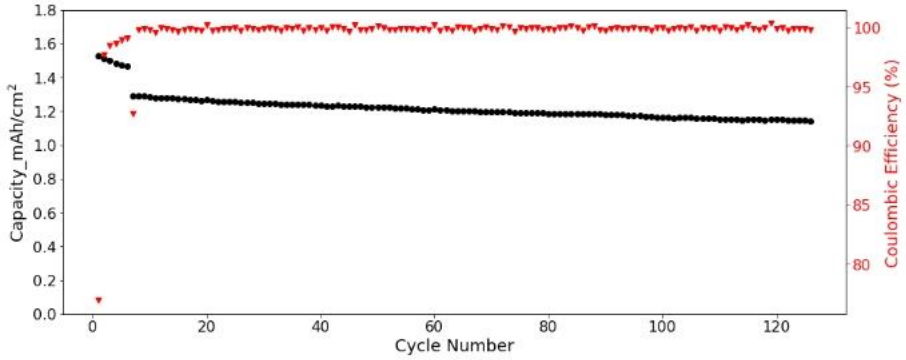

Figure 2.18 Cycling performance and columbic efficiency of the SF hard carbon electrode with NCM 523 as cathode under a current of 1/3 C in coin cell.

Full cells were assembled to further verify the cycling performance of SF hard carbon electrodes. Commercial NCM 523 electrodes were used as cathode. Considering the low ICE of SF hard carbon electrode, the SF hard carbon electrodes were prelithiated with electrochemical method before cell assembly. The Voltage-Capacity curve for the lithiation process was shown in Figure 2.17. For the cycling test, the cell went through 5 cycles activation process with a current of 0.05C/0.05C charge/discharge process. Then the cycling test was conducted under 1/3 C at room temperature. The SF hard carbon electrode demonstrated good stability with nearly 90% capacity retention after 120 cycles (Figure 2.18). With prelithiation, the ICE increased from 57% to 77%. The CE increased to more than 99% and was very stable after activation.

4. Conclusions

We successfully extended PTFE for solvent free anode fabrication. Anodes with different carbon active materials, i.e., graphite, hard carbon, soft carbon were fabricated,

and the stability of anodes was determined by the volume variation of the active materials during the charge/discharge cycling. The SF hard carbon anode and SF soft carbon anode demonstrated good cycle stability during charge /discharge process. The SF hard carbon anode revealed similar long-term cycling stability and comparative C-rates performance compared to the SC anode. The long cycling life of SF hard carbon and soft carbon anode was attributed to the low volume variation of the active materials during the charge and discharge process. The electrodes were able to keep their integrity even though PTFE was reduced to amorphous carbon. Electrodes with high thickness could easily be prepared using this method, which could decrease the manufacturing cost while increasing the energy density simultaneously. Furthermore, the method can be easily implemented on the existing commercial roll to roll production lines, demonstrating high potential for large-scale production.

References:

1. Marom, R.; Amalraj, S.F.; Leifer, N.; Jacob, D.; Aurbach, D. A review of advanced and practical lithium battery materials. *Journal of Materials Chemistry* **2011**, *21*, 9938-9954.

2. Etacheri, V.; Marom, R.; Elazari, R.; Salitra, G.; Aurbach, D. Challenges in the development of advanced Li-ion batteries: a review. *Energy & Environmental Science* **2011**, *4*, 3243-3262.

3. Obrovac, M.; Chevrier, V. Alloy negative electrodes for Li-ion batteries. *Chemical reviews* **2014**, *114*, 11444-11502.

4. Scrosati, B.; Garche, J. Lithium batteries: Status, prospects and future. *Journal of power sources* **2010**, *195*, 2419-2430.

5. Goodenough, J.B.; Park, K.-S. The Li-ion rechargeable battery: a perspective. *Journal of the American Chemical Society* **2013**, *135*, 1167-1176.

6. Hippauf, F.; Schumm, B.; Doerfler, S.; Althues, H.; Fujiki, S.; Shiratsuchi, T.; Tsujimura, T.; Aihara, Y.; Kaskel, S. Overcoming binder limitations of sheet-type solid-state cathodes using a solvent-free dry-film approach. *Energy Storage Materials* **2019**, *21*, 390-398.

7. Wood III, D.L.; Li, J.; Daniel, C. Prospects for reducing the processing cost of lithium-ion batteries. *Journal of Power Sources* **2015**, *275*, 234-242.

8. Pettinger, K.-H.; Dong, W. When does the operation of a battery become environmentally positive? *Journal of The Electrochemical Society* **2016**, *164*, A6274.

9. Hawley, W.B.; Li, J. Electrode manufacturing for lithium-ion batteries—Analysis of current and next generation processing. *Journal of Energy Storage* **2019**, *25*, 100862.

10. Verdier, N.; Foran, G.; Lepage, D.; Prébé, A.; Aymé-Perrot, D.; Dollé, M. Challenges in solvent-free methods for manufacturing electrodes and electrolytes for lithium-based batteries. *Polymers* **2021**, *13*, 323.

11. Lu, Y.; Zhao, C.-Z.; Yuan, H.; Hu, J.-K.; Huang, J.-Q.; Zhang, Q. Dry electrode technology, the rising star in solid-state battery industrialization. *Matter* **2022**, *5*, 876-898.

12. Shiraki, S.; Oki, H.; Takagi, Y.; Suzuki, T.; Kumatani, A.; Shimizu, R.; Haruta, M.; Ohsawa, T.; Sato, Y.; Ikuhara, Y. Fabrication of all-solid-state battery using epitaxial LiCoO2 thin films. *Journal of Power Sources* **2014**, *267*, 881-887.

13. Kuwata, N.; Kawamura, J.; Toribami, K.; Hattori, T.; Sata, N. Thin-film lithium-ion battery with amorphous solid electrolyte fabricated by pulsed laser deposition. *Electrochemistry Communications* **2004**, *6*, 417-421.

14. Chiu, K.-F. Lithium cobalt oxide thin films deposited at low temperature by ionized magnetron sputtering. *Thin Solid Films* **2007**, *515*, 4614-4618.

15. Park, D.-W.; Cañas, N.A.; Wagner, N.; Friedrich, K.A. Novel solvent-free direct coating process for battery electrodes and their electrochemical performance. *Journal of Power Sources* **2016**, *306*, 758-763.

16. Al-Shroofy, M.; Zhang, Q.; Xu, J.; Chen, T.; Kaur, A.P.; Cheng, Y.-T. Solvent-free dry powder coating process for low-cost manufacturing of LiNi1/3Mn1/3Co1/3O2 cathodes in lithium-ion batteries. *Journal of Power Sources* **2017**, *352*, 187-193.

17. Koike, S.; Tatsumi, K. Preparation and performances of highly porous layered LiCoO2 films for lithium batteries. *Journal of power sources* **2007**, *174*, 976-980.

18. Schälicke, G.; Landwehr, I.; Dinter, A.; Pettinger, K.-H.; Haselrieder, W.; Kwade, A. Solvent-Free Manufacturing of Electrodes for Lithium-Ion Batteries via Electrostatic Coating. *Energy Technology* **2020**, *8*, 1900309.

19. Yang, J.; Takeda, Y.; Imanishi, N.; Capiglia, C.; Xie, J.; Yamamoto, O. SiOx-based anodes for secondary lithium batteries. *Solid State Ionics* **2002**, *152*, 125-129.

20. Mitchell, P.; Xi, X.; Zhong, L.; Zou, B. Dry particle based electro-chemical device and methods of making same. **2005**.

21. Zhou, H.; Liu, M.; Gao, H.; Hou, D.; Yu, C.; Liu, C.; Zhang, D.; Wu, J.-c.; Yang, J.; Chen, D. Dense integration of solvent-free electrodes for Li-ion supercabattery with boosted low temperature performance. *Journal of Power Sources* **2020**, *473*, 228553.

22. Brodd, R.J.; Kozawa, A.; Yoshio, M. *Lithium-Ion Batteries: Science and Technologies*; Springer: 2009.

23. Wu, Q.; Zheng, J.P.; Hendrickson, M.; Plichta, E.J. Dry process for fabricating low cost and high-performance electrode for energy storage devices. *MRS Advances* **2019**, *4*, 857-863.

24. Shiraishi, S.; Kobayashi, T.; Oya, A. Electrochemical lithium ion doping and undoping behavior of carbyne-like carbon film electrode. *Chemistry letters* **2005**, *34*, 1678-1679.

25. Kastner, J.; Kuzmany, H.; Kavan, L.; Dousek, F.; Kürti, J. Reductive preparation of carbyne with high yield. An in situ Raman scattering study. *Macromolecules* **1995**, *28*, 344-353.

26. Li, G.; Xue, R.; Chen, L. The influence of polytetrafluorethylene reduction on the capacity loss of the carbon anode for lithium-ion batteries. *Solid State Ionics* **1996**, *90*, 221-225.

27. Kavan, L. Electrochemical carbon. *Chemical reviews* **1997**, *97*, 3061-3082.

28. Pan, B.; Xiao, J.; Li, J.; Liu, P.; Wang, C.; Yang, G. Carbyne with finite length: The one-dimensional sp carbon. *Science advances* **2015**, *1*, e1500857.

29. Nair, A.K.; Cranford, S.W.; Buehler, M.J. The minimal nanowire: Mechanical properties of carbyne. *EPL (Europhysics Letters)* **2011**, *95*, 16002.

30. Haley, M.M. On the road to carbyne. *Nature Chemistry* **2010**, *2*, 912-913.

31. Zheng, J.; Archer, L.A. Controlling electrochemical growth of metallic zinc electrodes: Toward affordable rechargeable energy storage systems. *Science Advances* **2021**, *7*, eabe0219.

32. Zheng, J.; Bock, D.C.; Tang, T.; Zhao, Q.; Yin, J.; Tallman, K.R.; Wheeler, G.; Liu, X.; Deng, Y.; Jin, S. Regulating electrodeposition morphology in high-capacity aluminium and zinc battery anodes using interfacial metal–substrate bonding. *Nature Energy* **2021**, *6*, 398-406.

33. Haselrieder, W.; Westphal, B.; Bockholt, H.; Diener, A.; Höft, S.; Kwade, A. Measuring the coating adhesion strength of electrodes for lithium-ion batteries. *International Journal of Adhesion and Adhesives* **2015**, *60*, 1-8.

34. Novák, P.; Scheifele, W.; Winter, M.; Haas, O. Graphite electrodes with tailored porosity for rechargeable ion-transfer batteries. *Journal of power sources* **1997**, *68*, 267-270.

35. Manev, V.; Naidenov, I.; Puresheva, B.; Pistoia, G. Effect of electrode porosity on the performance of natural Brazilian graphite electrodes. *Journal of power sources* **1995**, *57*, 133-136.

36. Manev, V.; Naidenov, I.; Puresheva, B.; Zlatilova, P.; Pistoia, G. Electrochemical performance of natural Brazilian graphite as anode material for lithium-ion rechargeable cells. *Journal of power sources* **1995**, *55*, 211-215.

37. Sun, Q.; Cai, L.; Wang, S.; Widmer, R.; Ju, H.; Zhu, J.; Li, L.; He, Y.; Ruffieux, P.; Fasel, R. Bottom-up synthesis of metalated carbyne. *Journal of the American Chemical Society* **2016**, *138*, 1106-1109.

38. Liao, X.; Yu, J.; Gao, L. Electrochemical study on lithium iron phosphate/hard carbon lithium-ion batteries. *Journal of Solid-State Electrochemistry* **2012**, *16*, 423-428.

39. Ni, J.; Huang, Y.; Gao, L. A high-performance hard carbon for Li-ion batteries and supercapacitors application. *Journal of Power Sources* **2013**, *223*, 306-311.

40. Fujimoto, H.; Tokumitsu, K.; Mabuchi, A.; Chinnasamy, N.; Kasuh, T. The anode performance of the hard carbon for the lithium-ion battery derived from the oxygen-containing aromatic precursors. *Journal of Power Sources* **2010**, *195*, 7452-7456.

41. Yang, J.; Zhou, X.-y.; Zou, Y.-l.; Tang, J.-j. A hierarchical porous carbon material for high power, lithium-ion batteries. *Electrochimica Acta* **2011**, *56*, 8576-858

Chapter 3: Leveraging Synergies by Combining Polytetrafluorethylene with Polyvinylidene Fluoride for Solvent-Free Graphite Anode Fabrication

1. Introduction

The implementation of lithium-ion batteries (LiBs) in electric vehicles (EVs) and stationary grids needs to overcome the bottlenecks of current LiBs, especially low energy density and high cost[1-3]. The manufacturing cost and energy density of LiBs are determined to a large extent by electrodes' chemical composition and manufacturing process[4, 5]. Commercial electrodes are fabricated via slurry casting (SC) procedure, where active material, binder and conductive additives are mixed with solvent, typically water for anode while N-methyl-2-pyrrolidone (NMP) for cathode, to form slurry with appropriate viscosity. The slurry is subsequently casted onto substrate with aluminiun foil for cathode and copper foil for anode, and then dried under high temperature followed by pressing with high pressure to get final electrodes. Ovens with dozens of metres are used to evaporate solvent in short time. The slurry preparation, coating and drying account for nearly 50% total energy consumption for LiBs production[6]. For the cathode side, complicated and expensive NMP recovery is required because it is hazardous to the environment. The high manufacturing cost caused by SC procedure has no doubt been an obstacle for widespread application of LiBs.

In addition to lowering energy consumption, reducing raw materials is another significant way to reduce the cost of LiBs because they account for approximately 60% of the total cost[7, 8]. Thick electrodes can lower bill of materials (BOM) cost and increase the energy density simultaneously because less auxiliary materials, including current collector, separator, tab and container material, are used for the same specific capacity. For the commercial graphite electrodes, the thickness of the electrode is less than 100 µm with areal capacity of 2-3 mAh/cm^2[9]. Increasing the areal capacity could drastically increase the energy density of the LiBs because more active materials are deployed within same cell volume. However, defects including electrode cracking, active powder drops and delamination of active materials from substrate caused by

uneven binder distribution limit the thickness of electrodes fabricated by SC procedure[10-13]. Removing solvent from the electrode fabrication is a promising solution to address the afore-mentioned issues.

Tremendous efforts are being dedicated to solvent free (SF) technology for electrode fabrication. Vapor deposition is utilized for SF thin electrodes fabrication, where raw materials are vaporized and deposited onto substrate. Vapor deposition includes magnetron sputtering, thermal evaporation, pulsed laser deposition, atomic layer deposition, etc. Kuwata et al. fabricated solid-state-thin-film-batteries consisting of $Li_2O–V_2O_5–SiO_2$ solid electrolyte (SE), $LiCoO_2$ (LCO) cathode and SnO anode using pulsed laser deposition technology, where the laser beam was focused onto the rotating target under vacuum[14]. Shiraki et al. controlled the crystal orientation of LCO with a similar procedure to obtain the most appropriate orientation for ion conduction[15]. Epitaxial LCO thin films with polycrystalline $Li_{1.2}CoO_2$ as target was deposited with a thickness of 200 nm. The films were subsequently annealed at 650 °C in air to obtain final LCO electrodes. Ionized magnetron sputter deposition can be applied with a relatively low temperature of 350 ^oC[16]. The thin-film-batteries prepared by vapor deposition exhibited good performance, such as high energy density[17, 18], long cycling life[19], and improved rate capability[20, 21]. However, vapor deposition technology is only suitable for the fabrication of electrode with small size, mainly for microelectronic devices and highly integrated circuits. The expensive equipment and complicated film forming process, high energy consumption, and low areal capacity limit its application in EVs or even 3C consumer electronics. Extrusion can be used for SF electrode fabrication with extra high thickness. Sotomayor et al. were the first to use extrusion as SF method to fabricate electrode with lithium titanate oxide (LTO) and lithium iron phosphate (LFP) as active materials[22]. This process comprises of particle mixing, extrusion, debindering and sintering. A blend of polypropylene, paraffin wax and stearic acid were used as sacrificial binder. A double heating step in *n*-heptane was required to degrade the polymers, and high temperature was applied to sinter electrode. The LFP/LTO cells with areal capacity of 13.3 mAh/cm^2

were fabricated and demonstrated good cycling stability. Melting and extrusion is a scalable procedure for electrodes manufacturing with high loadings. However, extrusion is sensitive to the particle size and needs accurate control of temperature, shear force, and time of extrusion[23]. Additionally, high consumption of polymers, tedious manufacturing procedure, high temperatures required for debindering and sintering processes impede its further application in practical electrode manufacturing.

Another promising procedure for SF electrode fabrication is using fibrillizable PTFE binder to replace conventional soluble binder. Dry mixing, fibrillation of PTFE, self-supporting electrode film formation and lamination are involved in this procedure. Maxwell Technology developed this procedure for activated carbon electrodes used for supercapacitors[24, 25]. Hippauf et al. applied this scalable SF procedure for lithium nickel cobalt manganese oxide (NCM) electrode fabrication for all-solid-state-batteries (ASSBs)[26]. PTFE powder was first mixed and sheared with NCM, SE and carbon nanofiber (CNF) in a mortar for one minute until the formation of single flake. The flake was subsequently hot rolled several times to desired thickness. The content of PTFE can be reduced to 0.1 wt%, which is beneficial for ion transport. The pouch cell showed decent cycling stability with 93.2% capacity retention after 100 cycles under the current of 0.7 mA/cm^2. Zhou et al. successfully scaled up this procedure to pilot stage for fabrication of LFP electrodes, where high-speed air blowing, hot-rolling, and hot overlying process were adopted[27]. The jet mill with high pressure dry air was used to extend PTFE molecular chain. Cotton candy-like mixture was formed, and the mixture was hot-rolled twice at 180 ^{o}C to form free-standing electrodes film employing a horizontal-type roller. The LFP cathode was fabricated with compact densities, almost 1.6 times higher than SC electrodes. 40% activated carbon was required to increase the flexibility of the LFP electrodes.

The lowest unoccupied molecular orbital (LUMO) of PTFE is low, making it easy to accept electrons and get reduced when used in anodes[28-30]. The instability issue of PTFE in SF anode fabrication is still a challenge. In our previous work, we successfully fabricated SF hard carbon/soft carbon anode with the fibrillation of

PTFE[31]. The SF hard carbon anodes demonstrated comparable cycling life to their SC counterparts, even though most PTFE fibrils was reduced at the first lithiation process. However, SF graphite anode exhibited fast capacity fading, resulting from the decomposition of PTFE and the big volume variation during charge/discharge process. To expand the application of this procedure to other anode active materials like graphite with big volume variation during charge/discharge process, PVDF has been reported to be promising to address the instability issue caused by the reduction of PTFE.

In this study, we successfully expanded PTFE for graphite anode fabrication with the help of PVDF. The SF graphite anode demonstrated good stability under high loading. Thick SF graphite anode (180 μm) could be easily fabricated, which could significantly increase specific energy of LiBs cell. The decent electrochemical performance and roll-to-roll production make the procedure has the potential to replace current commercial SC procedure.

2. Experimental

2.1 Dry mixing optimization

A conical mixer (Figure 3.1 in Supporting Information (SI), Xinyang, Wuxi, China) was used for dry mixing. Graphite (CP5H, Shanshan, Shanghai, China) and carbon black were baked at 150 ℃ overnight before mixing. The graphite, carbon black, PVDF (HSV900, Arkema, Colombes Cedex, France) were mixed with a mass ratio of 90:5:2. The mixing time and speed were screened to get optimal mixing parameters.

Figure 3.1 The conical mixer with a conical mixing cavity and is equipped with a central rotating shaft, which can rotate at a speed up to 30 m/s.

2.2 Electrodes fabrication

Figure 3.2 presented schematic process of SF PVDF graphite anode fabrication combining PTFE and PVDF. Graphite, PVDF, carbon black, PTFE powder (MTI, Shenzhen, China) were used directly for anode fabrication. A powder mixture was prepared by mixing graphite, carbon black, and PVDF in a conical mixer at a speed of 1200 r/min for 90 minutes. After that, PTFE powder was added to the mixture and mixed for 30 min using a V blender. The high-speed dry air was then applied using 2 inches grinding chamber jet mill (Sturtevant, Hanover, NC, US) to fibrillate PTFE to cotton candy like dry mixture. The weight ratio of graphite/carbon black/PVDF/PTFE was 90/5/2/3. For comparison, graphite anode without PVDF was fabricated by similar procedure with the weight ratio of 90/5/5 (graphite/carbon black/PTFE). The free-standing electrode film was formed when the dry mixture was hot rolled at 160 ºC using the calendering machine at a speed of 15 cm/min. The thickness of the electrode film was adjusted according to the gap between rolls of calender machine. The electrode film could be folded several times without any obvious cracks or defects, indicating good flexibility and mechanical strength, which is critical for upscaling production. Finally, the free-standing film was laminated to the carbon coated copper foil using hot rolling at 80 ºC before the electrode film was baked at 180 ºC for 10 min. For convenience, SF graphite anode with PVDF will be denoted as SF PVDF graphite anode, while SF graphite anode without PVDF will be denoted as SF graphite anode. For PTFE film fabrication, 80% carbon black was added to increase the electrical condicitivity: the PTFE powder and carbon black were mixed for 30 min in a kitchen mixer, then the mixture was grinded in an agata mortar until the formation of flake; finally, the flask was hot rolled using a calendering machine.

2.3 Cell assembly

Both half cells and full cells were assembled with 2032-coin cell parts (MTI, Shenzhen, China) in an argon-filled glove box, where water and oxygen concentrations were less than 0.01 ppm. Cellulose film (Celgard, Charlotte, NC, US), lithium foil (Sigma-alrich, 600 μm, Darmstadt, Germany) and 50 μL 1.2 M $LiPF_6$ in EC-EMC (3/7,

v/v) with 10 wt% fluoroethylene carbonate (FEC) were used as separator, encounter electrode and electrolyte, respectively. For full cell assembly, commercial lithium iron phosphate (LPF) electrodes from Beyonder AS (Norway) were used as cathode. The capacity ratio of anode (NP ratio) to cathode is 1.1:1.

2.4 Prelithiation

Single layer pouch cell was assembled with commercial LFP electrode as cathode, SF graphite electrode as anode, single polyethylene (PE) as separator, respectively. Commercial electrolyte (Tianci, Wuxi, China) was used directly. The pouch cell was aged for 12 h before charging to a certain state of charge (SOC). Thereafter, the cells were disassembled in glovebox and the lithiated SF graphite anodes were washed with dimethyl carbonate (DMC) several time and dried under room temperature for full cell assembly.

2.5 Electrochemical and morphological characterization

The galvanostatic charge/discharge tests were performed under room temperature using an 8-channel battery analyzer (Neware, Shenzhen, China). The voltage ranges were 0.01-1.5 V and 2.5-3.65 V for half cells and full cells, respectively. All cells were aged under room temperature for 12 h before testing and underwent several formation cycles. Cyclic voltammetry (CV) was carried out in the voltage range of 0.01-3.2 V at a scanning rate of 0.5 mV/s.

The pristine and cycled electrodes were characterized using a scanning electron microscope (SEM, Phenomenon LE). The cycled electrodes were charged to the fully delithiation state after cell cycling, followed by disassembling the cell, dipping the electrode into DMC solution for 2 h to remove any residual electrolyte, and drying at room temperature overnight in an argon-filled glove box for further ex-situ analysis.

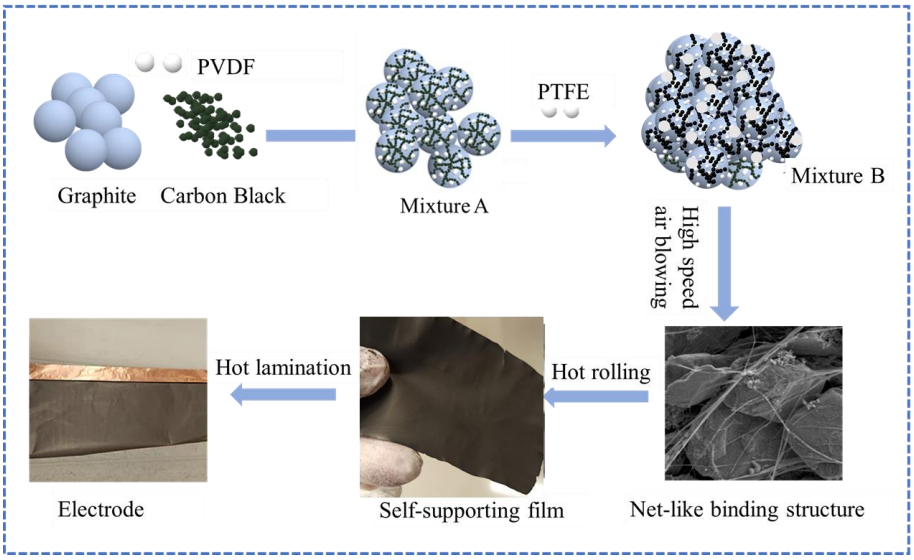

Figure 3.2 Schematic process diagram of SF PVDF graphite electrode fabrication based on PTFE fibrillation, including dry mixing, fibrillation, hot rolling and lamination.

3. Results and discussion

To study the stability of PTFE at anode, PTFE film with 80% carbon black were prepared. The film was used directly without current collector to assemble coin cells with lithium foil as counter electrode. The charge/discharge cycling test was conducted under a current of 1.2 mA/cm^2. As shown in Figure 3.3a, the capacity-voltage curves showed that PTFE delivered a capacity of 970 mAh/g at the first lithiation process, while the capacity of the first delithiation reduced to less than 20 mAh/g, demonstrating the irreversible reduction of PTFE during the first lithiation process. The lithiation and delithiation capacity in the second cycle is 191 and 97 mAh/g, respectively. The lithiation capacity in the second cycle is more than the delithiation capacity, which could be attributed to the reaction of PTFE with lithium ion in the lithiation process, because not all PTFE was reduced in the previous lithiation process. CV curves (Figure 3.3b) demonstrated that a reduction peak appeared at approximately 1 V in the first reduction cycle, which could be ascribed to the irreversible reaction of PTFE and lithium ion. The reduction peak became weaker in the following cycles, demonstrating that most PTFE was reduced in the first lithiation process. The CV result is consistent with charge/discharge cycling testing and earlier studies[28]. SEM was used to characterize the morphology of both pristine PTFE film and PTFE film after lithiation.

The PTFE fibrils are apparent from the pristine PTFE film (Figure 3.3c), while most of PTFE fibrils disappeared after lithiation (Figure 3.3d). SEM characterization further proved the irreversible reduction of PTFE during the first lithiation process.

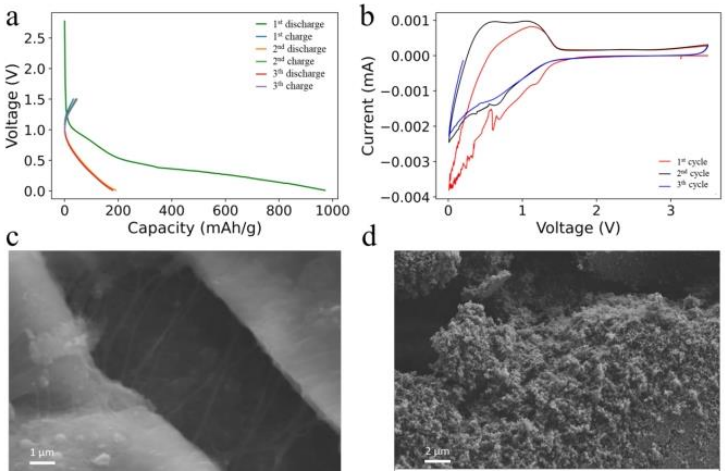

Figure 3.3 Stability analysis of PTFE at anode (a) capacity-voltage curves for PTFE film with 20% carbon black; (b) CV curves of PTFE film; (c) SEM image of pristine PTFE film; (d) SEM image of PTFE film after lithiation.

In dry mixing process, materials with different densities and sizes tend to agglomerate, which is detrimental to the electrical conductivity of electrodes and rate capability. Mixing parameters like mixing time and speed were screened and optimized. The dry mixture powder mixed under different speed and time were hot rolled under 120 ºC several times to get electrode film with a thickness of 100 µm. The ohmic resistances of electrode films obtained under different mixing condition were listed in Table 1. Surprisingly, the electrical conductivity didn't increase with mixing time or mixing speed. For instance, with a fixed speed of 1200 r/min, the resistance decreased from 1.831 to 1.412 mohm when increasing the mixing time from 30 to 90 minutes. The resistance didn't decrease with prolonged mixing time. The best conductivity was obtained after 90 min mixing under 1200 r/min mixing speed.

Table 3.1 Ohmic resistance of mixture A under different dry mixing time and speed (mohm).

Mixing Speed	30 min	60 min	90 min	120 min
400 (r/min)	3.766	3.125	2.785	2.042
800 (r/min)	2.015	1.827	1.679	1.594
1200 (r/min)	1.831	1.654	**1.412**	1.422
1400 (r/min)	1.733	1.615	1.448	1.437

To increase the adhesion between current collector and electrode film, 10 μm copper foil with primer was used as current collector. Slurry with poly (ethylene oxide) (PEO)/ carbon black mass ratio of 50/50 was prepared and casted onto Cu foil using doctor blade. The final primer thickness is 1 μm, which has negligible effects on the energy density of electrodes. The uniform distribution of carbon black on the surface of copper foil is evidence in Figure 3.4, which makes the primer coated current collector with comparable electroconductivity to bare copper foil. Hot rolling was deployed for the lamination of electrode film and primer coated Cu foil. The lamination temperature was screened from 40-160 ^{o}C. The maximum adhension was obtained at 80 ^{o}C. The adhesion increased from 2.3 to 6.8 N/m when the lamination temperature increased from 40 to 80 ^{o}C. The adhesion has negligible variation when the lamination temperature further increased. The improved adhesion with increasing temperature from 40-80 ^{o}C is ascribed to the melting of PEO, since PEO has melting point of about 70 ^{o}C. When the lamination temperature exceeds the melting point, PEO will have more contact area with electrode film. However, further increasing the temperature above the melting point cannot increase contact area, exhibiting little impact on adhesion strength.

SEM was also used to analyze the morphology of the pristine SF PVDF graphite anodes. The carbon black is distributed on the surface of graphite particles without obvious agglomeration, clarifying sufficient mixing of graphite and conductive additives (Figure 3.5a). No PVDF particles was observed, showing that most PVDF was melted around the surface of graphite particles. The PTFE fibrils could be observed (Figure 3.5a-c), which bundle with graphite to form a net-like structure, ensuring good mechanical strength of the film with a tensile strength of 7.8 N/m (100 μm) and good flexibility. The PTFE distributes evenly among the electrode, which was confirmed by the cross-sectional SEM images. SEM-EDS mapping of the pristine SF PVDF graphite electrode further confirmed that fluorine is uniformly distributed on the surface of the electrode (Figure 3.6). The SF graphite anodes without PVDF showed similar morphology (Figure 3.7a-c).

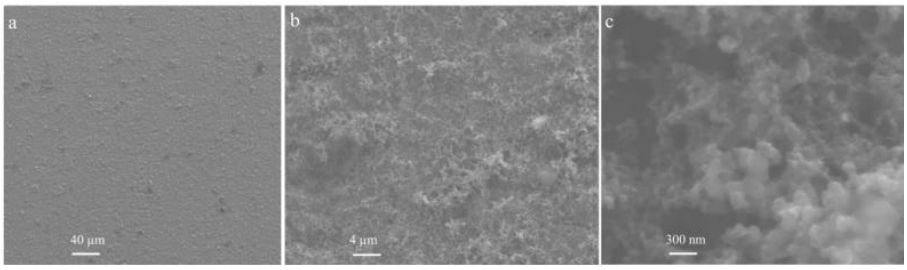

Figure 3.4 SEM images of carbon coated copper foil with different magnifications.

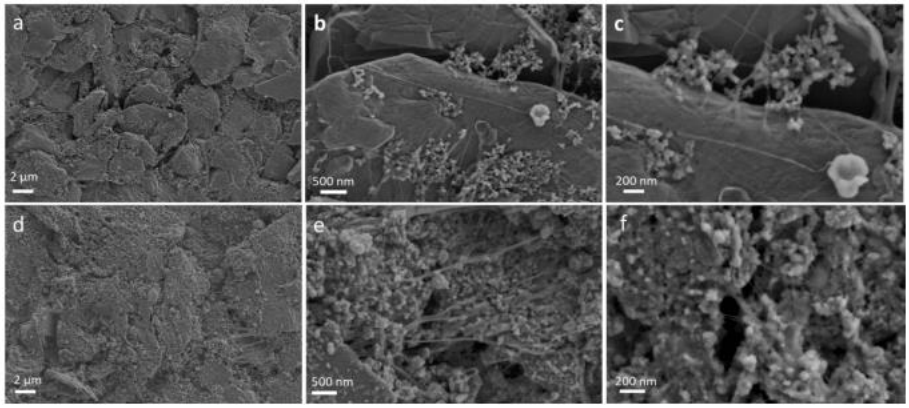

Figure 3.5 Top view of SEM images of pristine SF graphite anodes with different magnifications: (a) 10000x, (b) 50000x, (c) 100000x; SF graphite anodes after 100 cycles with different magnifications: (d) 10000x, (e) 50000x, (f) 100000x.

The cycling stability of SF PVDF graphite anode was studied in half cells with a current of 0.23 mA/cm^2 at room temperature. In contrast to fast capacity fading of SF graphite electrode (without PVDF) in our previous study[31], the capacity retention for SF PVDF graphite anode was more than 95% after 50 charge/discharge cycles with high areal capacity of 4.22 mAh/cm^2, as shown in Figure 3.8a. The low ICE of 85.6% is the result of irreversible reaction between PTFE and active lithium ion (Figure 3.8b). The coulombic efficiency (CE) increased to more than 99% from second cycle, indicating that most PTFE was reduced in the first cycle. The CE further increased to 99.7% at 10th cycle and kept stable after 10th cycle, proving the stability of SF PVDF graphite anode (Figure 3.8a).

The morphology of the cycled SF PVDF graphite electrodes was also studied to explore the stability mechanism, taking into consideration that most PTFE degraded. As shown in Figure 3.7d, e, apparent cracks could be observed from the top view of the cycled SF graphite anodes (without PVDF). There were almost no fibrils left (Figure

3.7f). Graphite has roughly 10% volume swelling and shrinking during lithiation and delithiation process[32, 33]. The reduction of PTFE makes the electrode unable to accommodate the volume variation and the electrode loses integrity, resulting in very fast capacity fading. However, no apparent cracks were observed from the top view of SF PVDF graphite anode after 100 charge/discharge cycling (Figure 3.5d-f). EDS-mapping also showed even distribution of fluorine after 100 cycles (Figure 3.9). The cross-sectional SEM images of cycled SF PVDF graphite anode (Figure 3.10d-f) further demonstrated that the electrodes maintain compact structure as good as the pristine one (Figure 3.10a-c), even though most PTFE fibrils was reduced. No obvious separation between electrode film and the current collector was observed (Figure 3.10d), indicating good adhesion between the electrode film and the primer coated current collector. Therefore, it could be proposed that the good stability of SF PVDF graphite anode was due to that PTFE acts as processing aid reagent in SF PVDF graphite anode, while PVDF acts as functional binder when PTFE is reduced in the first lithiation process.

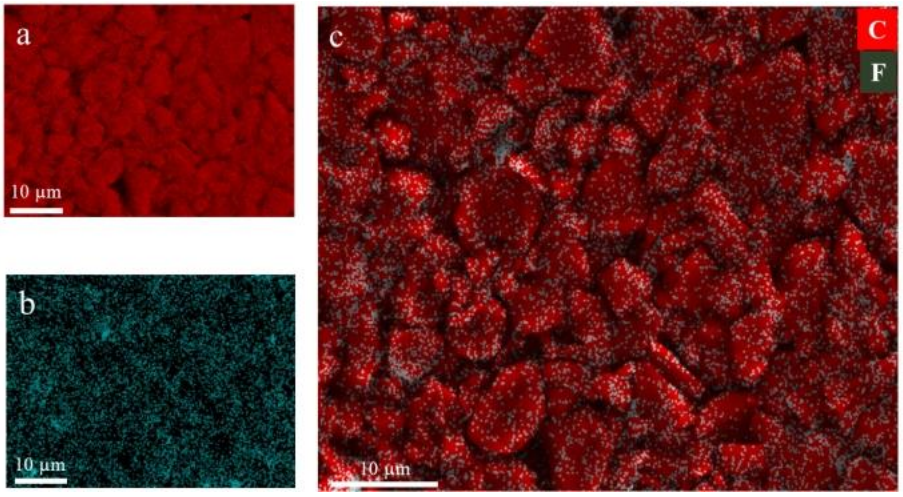

Figure 3.6 SEM-EDS mapping of fresh SF PVDF graphite anode (Graphite : Carbon black : PTFE : PVDF = 90 : 5 : 3 : 2). (a) carbon distribution; (b) fluorine distribution; (c) overlay of carbon and fluorine distribution.

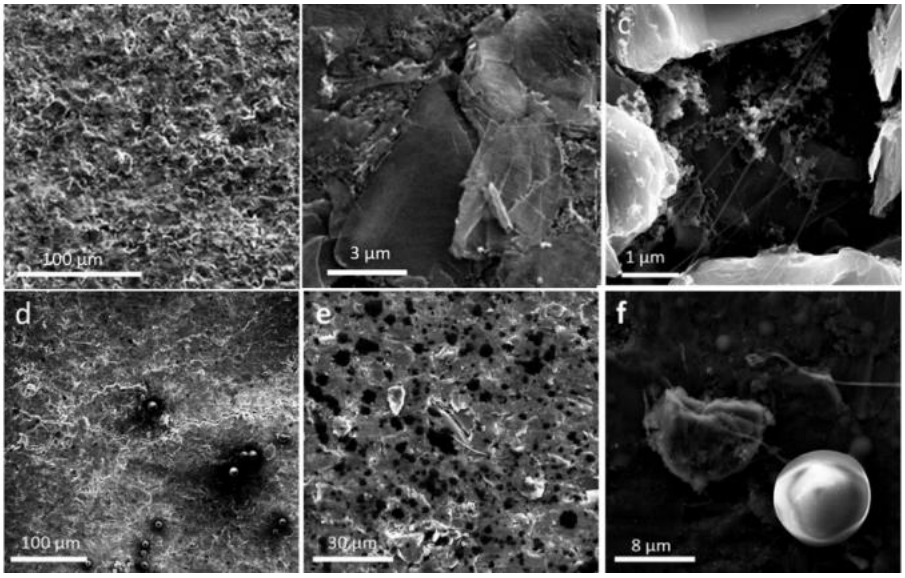

Figure 3.7 SEM of SF graphite anode under different magnification. a-c) Fresh electrodes. d-f) Electrodes after 100 charge/discharge cycling (Graphite/Carbon black : PTFE = 90 : 5 : 5).

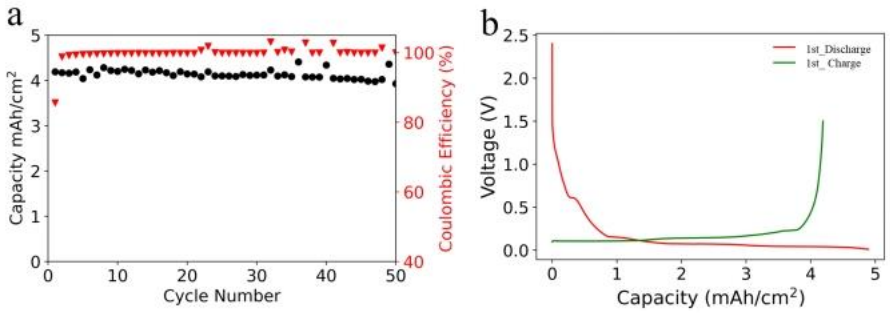

Figure 3.8 (a) Cycling performance of SF graphite anode at the current of 0.23 mA/cm^2 and room temperature; (b) voltage-capacity curves of SF graphite anode for the first lithiation and delithiation process.

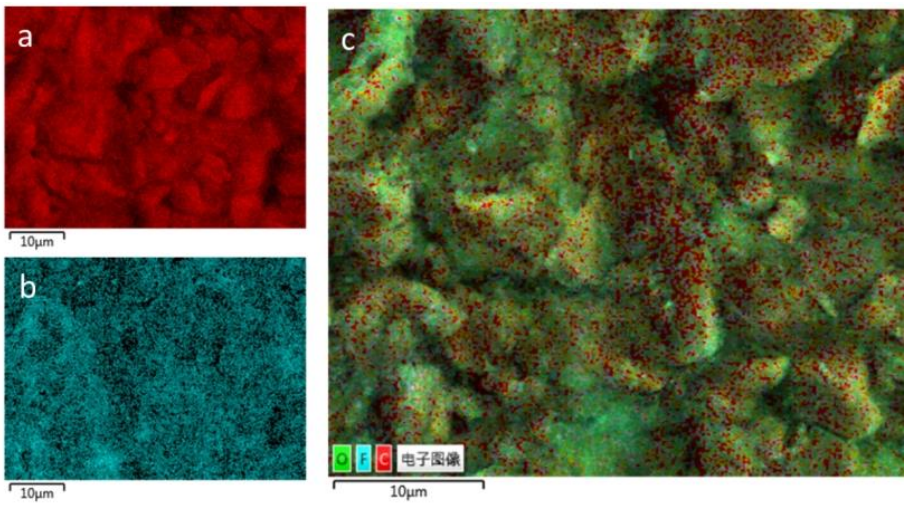

Figure 3.9 SEM-EDS of SF graphite anode after 100 charge/discharge cycles (graphite : carbon black : PTFE : PVDF = 90 : 5 : 3 : 2). (a) carbon distribution; (b) fluorine distribution; (c) overlay of carbon,

fluorine and oxygen distribution.

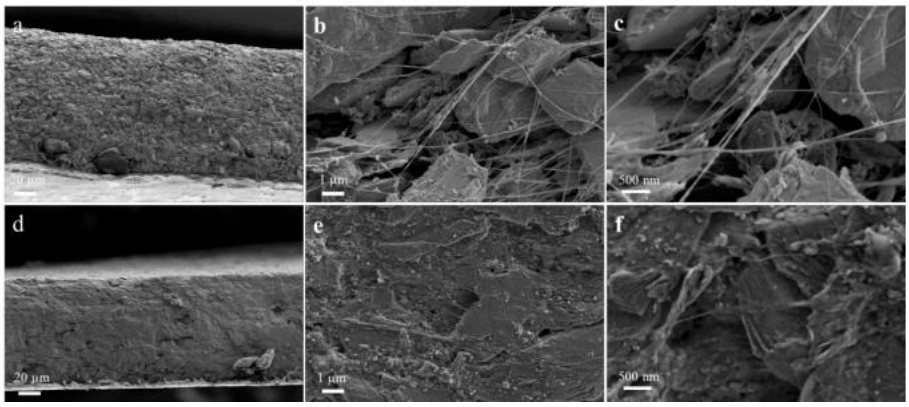

Figure 3.10 Cross-sectional SEM images of pristine SF PVDF graphite anodes with different magnifications: (a) 1000x, (b) 20000x, (c) 50000x; SF PVDF graphite anodes after 100 cycles with different magnifications: (d) 1000x, (e) 20000x, (f) 50000x.

In addition to energy saving, another big advantage of SF procedure is the deployment of thick electrode. We have previously fabricated SF PVDF electrode with areal capacity of more than 4.2 mA/cm^2 with excellent stability during cycling test. We further increased the graphite loading to 27 mg/cm^2 with a thickness of 180 µm (1.67 g/cm^3, 24% porosity). The high loading electrodes delivered an impressive areal capacity of 8.2 mAh/cm^2 (Figure 3.11a). The areal capacity of SF PVDF graphite anode in our study is not only much higher than commercial graphite electrodes, but also higher than many silicon-based anodes reported in literature[34-37]. The electrodes kept stable without obvious capacity fading for 15 cycles under a current density of 0.3 mA/cm^2 (Figure 3.11b). However, internal short circuit happened afterwards, which could be ascribed to the high pressure in coin cell resulting from thick electrode.

To explore the potential application of our extra high loading electrode for high energy density LiBs, specific energy of LFP/Graphite cells was calculated as a function of the areal capacity loading of graphite anode (Figure 3.11c). The N/P ratio (capacity of anode/capacity of cathode) was set to 1.1, and the amount of electrolyte was determined with injection coefficient of 3.5 (weight of electrolyte (g)/capacity of cell (Ah)), which is an average value for commercial LFP/Graphite prismatic cells. The detailed calculation method was clarified by Equation 1.

Cell energy density was calculated according to Equation 1:

$$\text{Energy density} = \frac{\text{capacity}_{LFP} * V_{nominal}}{\text{Cell weight}} = \frac{2 * S_{LFP} * H_{LFP} * \text{compressed density}_{LFP} * \text{loading}_{LFP} * \text{specific capacity}_{LFP} * V_{nominal}}{\text{Cell weight}} =$$

$$\frac{2 * S_{LFP} * H_{LFP} * H_{LFP} * \text{loading}_{LFP} * \text{compressed density}_{LFP} * V_{nominal}}{\text{Weight}_{LFP\ cathode} + \text{Weight}_{LFP\ cathode} + \text{Weight}_{LFP\ cathode} + \text{Weight}_{electrolyte} + \text{Weight}_{separetor+current\ collector}}$$

$$= \frac{2137670}{10570 + \frac{114S195}{\text{Areal Capacity}}} \quad \text{.....(1)}$$

where S_{LFP}, H_{LFP} and $V_{nominal}$ are the area of LFP electrode, thickness of single LPF electrode (current collector not included) and nominal voltage of LPP/Graphite cell, respectively. It is worth emphasizing that the weight of packing materials was ignored intentionally because it varies a lot along the cell configuration. Hence the specifical energy in our calculation will be slightly higher than the actual value. Figure 3.11c shows that the energy density of LFP/Graphite cells increases fast with the enhancement of areal capacity of graphite anodes when the areal capacity is less than 10 mAh/cm^2. However, the energy density increase becomes flat when further increase the areal capacity.

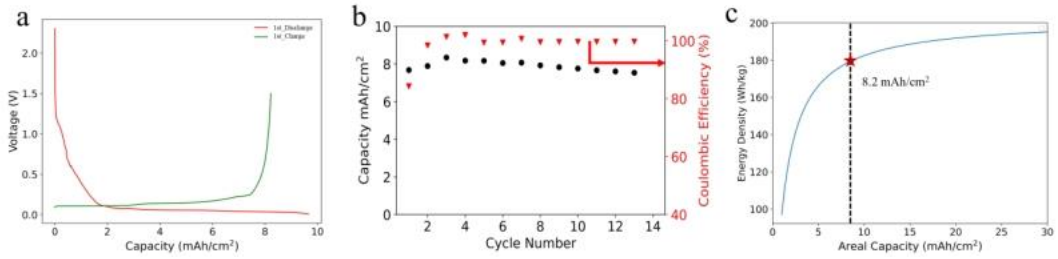

Figure 3.11 (a) Voltage-capacity curves for the first lithiation and delithiation process; (b) cycling of SF graphite with high loading of 27 mg/cm2, 180 μm under the current of 0.3 mA/cm2; (c) specific energy as a function of areal capacity of graphite anode (parameters used in the calculation were listed in Table 3.2).

Table 3.2 Parameters used for the calculation of cell (LFP/Graphite) energy density as a function of areal capacity of graphite.

Items	Thickness (μ)	Density (g/cm^3)	Specific capacity (mAh/g)	Loading	Comments
Copper foil	6	8.96	/	/	/
Aluminum foil	13	2.7	/	/	/
Separator	13	0.962	/	/	Polypropylene
Graphite	/	1.7	350	95%	/
LFP	/	/	140	95%	N/P ratio = 1.1
Electrolyte	/	/	/	/	3.5g /Ah

The irreversible reduction of PTFE in the first lithiation process could result in low

ICE in full cells. The theoretical irreversible lithiation capacity is approximately 1000 mAh/g. In our study, 2% of PTFE was used, which will reduce the capacity to 20 mAh per gram of electrode. The specific capacity of commercial graphite is around 350 mAh/g. 6% energy density will be lost due to the utilization of 2% PTFE. Therefore, prelithiation is an effective method to compensate lithium consumption caused by the reaction of PTFE and lithium ion. The ICE as well as cycling life can also be improved by addition of extra lithium inventory. Prelithiation was conducted with a similar procedure as reported in our previous work[31]. The pouch cell was charged to 2.7 V with the capacity of 1.1 mAh/cm^2 (Figure 3.12a). Full cell with LFP cathode was assembled with capacity ratio of anode to cathode (N/P ratio) at 1.1:1. The ICE increased to 89% in full cells (Figure 3.12a), which is at similar level as the commercial cells. It's worth noting that the ICE could be further increased by the adjustment of the depth of prelithiation. The prelithiated SF graphite anodes with PVDF showed good stability with about 80% discharge capacity retention after 110 cycles under a current of 0.7 mA/cm^2 (Figure 3.13). The CE increased to 99.5%, 99.7% and maintained stable after cycle 10 and 20, respectively.

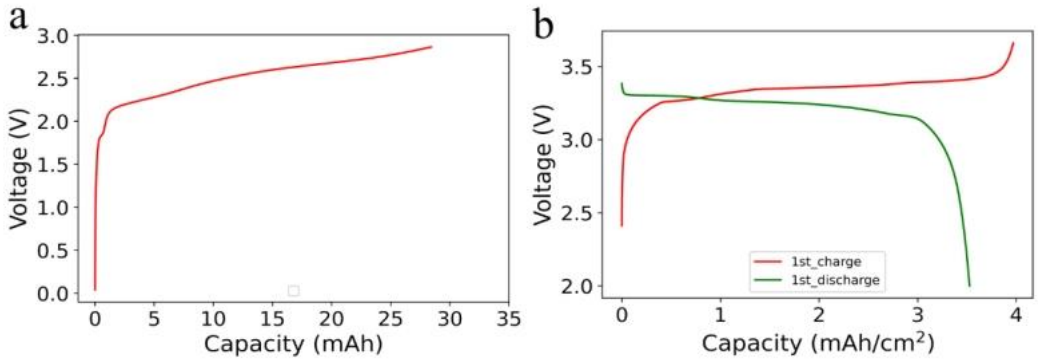

Figure 3.12 Prelithiation of SF graphite anode. (a) charge curve of prelithiation with LFP as lithium source; (b) capacity-voltage curve of prelithiated SF graphite in full cell with LFP as cathode.

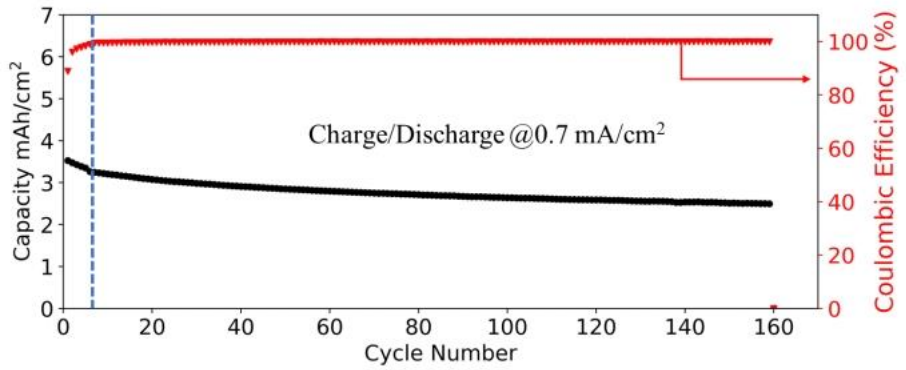

Figure 3.13 Cycling of prelithiated SF PVDF graphite with LFP as cathode under the current of 0.7 mA/cm^2.

4. Conclusions

We successfully expanded PTFE for SF graphite anodes fabrication with synergistic effect of PVDF as the dual binder. Thanks to the binding capability of PVDF, the electrodes were able to keep their integrity even though most PTFE was reduced in first lithiation process. The electrode shows good stability with high loading of 15 mg/ cm^2 and more than 95% capacity retention after 50 cycles. The electrodes with extra high loading could be easily prepared, which could lower the manufacturing cost while increase the energy density simultaneously. Furthermore, the method can be conveniently implemented on the existing commercial roll-to roll production line, demonstrating high potential for large-scale production.

References:

[1] D. Bresser, S. Passerini, B. Scrosati, Energy & Environmental Science 9 (2016) 3348-3367.

[2] J.B. Goodenough, K.-S. Park, Journal of the American Chemical Society 135 (2013) 1167-1176.

[3] M.M. Thackeray, C. Wolverton, E.D. Isaacs, Energy & Environmental Science 5 (2012) 7854-7863.

[4] G. Patry, A. Romagny, S. Martinet, D. Froelich, Energy Science & Engineering 3 (2014) 71-82.

[5] J. Kasemchainan, P.G. Bruce, Johnson Matthey Technology Review 62 (2018) 177-180.

[6] K.-H. Pettinger, W. Dong, Journal of The Electrochemical Society 164 (2016) A6274-A6277.

[7] G. Berckmans, M. Messagie, J. Smekens, N. Omar, L. Vanhaverbeke, J. Van Mierlo, Energies 10 (2017) 1314.

[8] J.W. Choi, D. Aurbach, Nature Reviews Materials 1 (2016) 1-16.

[9] S.N. Bryntesen, A.H. Strømman, I. Tolstorebrov, P.R. Shearing, J.J. Lamb, O. Stokke Burheim, Energies 14 (2021) 1406.

[10] M. Stein, A. Mistry, P.P. Mukherjee, Journal of The Electrochemical Society 164 (2017) A1616.

[11] K. Rollag, D. Juarez-Robles, Z. Du, D.L. Wood III, P.P. Mukherjee, ACS Applied Energy Materials 2 (2019) 4464-4476.

[12] F. Font, B. Protas, G. Richardson, J.M. Foster, Journal of Power Sources 393 (2018) 177-185.

[13] J. Kumberg, M. Müller, R. Diehm, S. Spiegel, C. Wachsmann, W. Bauer, P. Scharfer, W. Schabel, Energy Technology 7 (2019) 1900722.

[14] N. Kuwata, J. Kawamura, K. Toribami, T. Hattori, N. Sata, Electrochemistry Communications 6 (2004) 417-421.

[15] S. Shiraki, H. Oki, Y. Takagi, T. Suzuki, A. Kumatani, R. Shimizu, M. Haruta, T. Ohsawa, Y. Sato, Y. Ikuhara, Journal of Power Sources 267 (2014) 881-887.

[16] K.-F. Chiu, Thin Solid Films 515 (2007) 4614-4618.

[17] G. Yang, C. Abraham, Y. Ma, M. Lee, E. Helfrick, D. Oh, D. Lee, Applied Sciences 10 (2020) 4727.

[18] A. Patil, V. Patil, D.W. Shin, J.-W. Choi, D.-S. Paik, S.-J. Yoon, Materials research bulletin 43 (2008) 1913-1942.

[19] J. Bates, N. Dudney, B. Neudecker, A. Ueda, C. Evans, Solid state ionics 135 (2000) 33-45.

[20] J. Lin, L. Lin, S. Qu, D. Deng, Y. Wu, X. Yan, Q. Xie, L. Wang, D. Peng, Energy & Environmental Materials 5 (2022) 133-156.

[21] A. Reyes Jiménez, R. Klöpsch, R. Wagner, U.C. Rodehorst, M. Kolek, R. Nölle, M. Winter, T. Placke, ACS nano 11 (2017) 4731-4744.

[22] M.E. Sotomayor, C. de La Torre-Gamarra, B. Levenfeld, J.-Y. Sanchez, A. Varez, G.-T. Kim, A. Varzi, S. Passerini, Journal of Power Sources 437 (2019) 226923.

[23] N. Verdier, G. Foran, D. Lepage, A. Prébé, D. Aymé-Perrot, M. Dollé, Polymers 13 (2021) 323.

[24] P. Mitchell, L. Zhong, X. Xi, Recyclable dry particle based adhesive electrode and methods of making same, Google Patents, 2008.

[25] P. Mitchell, X. Xi, B. Zou, L. Zhong, Dry particle packaging systems and methods of making same, Google Patents, 2006.

[26] F. Hippauf, B. Schumm, S. Doerfler, H. Althues, S. Fujiki, T. Shiratsuchi, T. Tsujimura, Y. Aihara, S. Kaskel, Energy Storage Materials 21 (2019) 390-398.

[27] H. Zhou, M. Liu, H. Gao, D. Hou, C. Yu, C. Liu, D. Zhang, J.-c. Wu, J. Yang, D. Chen, Journal of Power Sources 473 (2020) 228553.

[28] G. Li, R. Xue, L. Chen, Solid State Ionics 90 (1996) 221-225.

[29] R.J. Brodd, A. Kozawa, M. Yoshio, Lithium-Ion Batteries: Science and Technologies, Springer, 2009.

[30] Q. Wu, J.P. Zheng, M. Hendrickson, E.J. Plichta, MRS Advances 4 (2019) 857-863.

[31] Y. Zhang, F. Huld, S. Lu, C. Jektvik, F. Lou, Z. Yu, Batteries 8 (2022) 57.

[32] L. Mickelson, H. Castro, E. Switzer, C. Friesen, Journal of the Electrochemical Society 161 (2014) A2121.

[33] T. Ohzuku, N. Matoba, K. Sawai, Journal of Power sources 97 (2001) 73-77.

[34] P. Li, J. Hwang, Y. Sun, Nano/microstructured silicon–graphite composite anode for high-energy-density Li-ion battery. ACS Nano 13: 2624–2633, 2019.

[35] T. He, J. Feng, Y. Zhang, L. Zu, G. Wang, Y. Yu, J. Yang, Advanced Energy Materials 8 (2018) 1702805.

[36] M.-G. Jeong, H.L. Du, M. Islam, J.K. Lee, Y.-K. Sun, H.-G. Jung, Nano Letters 17 (2017) 5600-5606.

[37] M. Ko, S. Chae, J. Ma, N. Kim, H.-W. Lee, Y. Cui, J. Cho, Nature Energy 1 (2016) 1-8.

Chapter 4: Solvent-free Lithium Iron Phosphate Cathode Fabrication with the Fibrillation of Polytetrafluoroethylene

1. Introduction:

Lithium-ion batteries (LiBs) dominate consumer electronics for their high energy density, long cycling life, high power and good reliability[1]. Recently, LiBs are attracting even more attention owing to specific energy improvement and cost reduction, especially in transportation sector[2,3]. Replacing internal combustion engine with energy storage systems (ESSs) like batteries is critical to reduce CO_2 emission and alleviate climate change issue[4]. However, the high cost and limited energy density of commercial LiBs impede further deployment of LiBs in electric vehicles (EVs)[5]. The cost of LiBs is mainly from raw materials and manufacturing. The manufacturing cost is determined by electrode manufacturing process[6]. Currently, electrode of commercial LiBs is fabricated by slurry casting (SC) procedure, where active material, conductive additives and polymer binder are mixed in solvent (water for anode and N-methyl-2-pyrrolidone (NMP) for cathode) to form slurry with appropriate viscosity[7,8]. The slurry is subsequently casted onto substrate (copper foil for anode and aluminum foil for cathode) and dried with the same coating machine thereafter. The drying process is complicated where dozens meters long ovens under high temperature consume huge amount of energy[7,9]. In addition, uneven binder distribution resulting from binder floating with quick solvent evaporation during drying process limits the fabrication of thick electrode. Another issue for SC procedure is toxicity of NMP for cathode fabrication, where organic solvent leakage is inevitable even with complicated and expensive NMP recovery system[10].

Fabricating electrode without solvent to get rid of drying process can save much energy and improve the energy density of the LiBs simultaneously with the adoption of high active material loading design[7,11,12]. There are many different SF procedures for electrode fabrication including dry powder deposition, polymer fibrillation, chemical or physical vapor deposition, 3 D printing, melting and extrusion, direct pressing[13]. Polymer fibrillation is one of the most promising SF procedures when

taking the feasibility of upscaling into consideration. Fibrillation under high shear force makes PTFE the most used polymer for fibrillation-based SF electrode fabrication, especially for activated carbon electrode. The lowest unoccupied molecular orbit (LUMO) of PTFE is not only lower than common polymer binder like PVDF, CMC, but also lower than common solvent like ethylene carbonate (EC) used in electrolyte. The low LUMO makes PTFE has the tendency to accept electrons to get reduced[14]. In our previous studies, we have succeeded in expanding PTFE fibrillation to the SF hard carbon and graphite anode fabrication, even though the PTFE is instable in anode[11]. Maxwell company had successfully fabricated lithium nickel manganese cobalt oxide (NMC)/graphite LiBs based on PTFE fibrillation[15]. SF NMC/graphite cells exhibited high-rate capability and decent cycling life with high mass loading. Good electrochemical performance and roll-to-roll manufacturing process make the procedure compatible to commercial LiBs production line. SF procedure is also promising for non-porous electrode fabrication for all-solid-state-batteries (ASSBs) since most solid electrolytes (SEs) are sensitive to moisture and polar solvents[13]. Hippauf et al. applied this scalable SF procedure for NMC electrode fabrication with 0.1% PTFE, the content of which is the lowest ever reported[16]. However, the limited reserves, unbalanced distribution and high cost of noble metal, especially cobalt make NMC based LiBs unsustainable. In contrary, lithium iron phosphate (LFP) is much cheaper with longer cycling life and higher safety but with low specific energy and poor rate-performance[17-19]. As new structure like cell to pack (CTP), cell to chassis (CTC) developed, the system integration degree of batteries pack increased a lot and the LFP LiBs have gained more attention[20,21].

SF procedure can well overcome the shortcomings of LFP electrode. On the one hand, spot contact between PTFE fibrils and LPF particles facilitates the ion transportation to increase the rate performance. On the other hand, adoption of thick LFP electrode can increase the specific energy of LFP cells. However, the PTFE fibrillation procedure is not suitable for LFP electrode fabrication caused by the hardness of LFP particles. Large amounts of additives are required to make the self-

supporting LFP electrode film. For example, 40% activated carbon was added to increase the flexibility of the LFP electrode when PTFE was used for LPF electrode fabrication[22]. Fabricating LFP electrodes with PTFE fibrillation will be great favor to develop LiBs with low cost and good performance.

In this study, we fabricate LFP electrode successfully with the help of carbon nanotubes (CNT). The CNT on the one hand can increase the conductivity of the electrode. On the other hand, CNT acts as matrix to hold LFP particles, where PTFE powders are able to be further fibrillated to ensure the formation of self-supporting LPF electrode film during hot rolling process. SF LFP/hard carbon full cells are fabricated successfully and demonstrate good stability. With the help of prelithiation, the initial coulombic efficiency (ICE) of SF LFP/hard carbon cells are increased to close to100%. The SF LFP/hard carbon full cells also demonstrate decent stability with more than 95% capacity retention after 50 cycles under the current of 0.5C in coin cells. The electrodes are fabricated through roll-to-roll process, which is compatible to current LiBs production line, making the method promising to replace current SC procedure for commercial LiBs.

2. Experimental section

2.1 Electrodes fabrication

Figure 1 presented schematic procedure of SF LFP cathode fabrication with PTFE fibrillation. LFP (Shanshan, Shanghai, China), CNT (Sigma-aldrich, Germany), PTFE powder (MTI, Shenzhen, China) were used directly for electrode fabrication. A powder mixture was prepared by mixing LFP and CNT in a conical mixer at a speed of 1400 r/min for 60 minutes. After that, PTFE powder was added to the mixture and mixed for another 20 min using a V blender. The high-speed dry air was then applied using 2 inches grinding chamber jet mill (Sturtevant, Hanover, NC, US) to fibrillate PTFE to cotton candy like dry mixture. The weight ratio of LFP/CNT/PTFE was set to 90/5/5. The free-standing electrode film was formed when the dry mixture was hot rolled at 160 ^{o}C using a calendering machine at a speed of 15 cm/min. The thickness of the electrode film was adjusted according to the gap between rolls of calendering machine

and the times the electrode film going through the gap of rolls. Finally, the free-standing film was laminated to the carbon coated aluminum foil (13 μm, Nanoblue, Dongguan, China) using hot rolling at 80 °C. For PTFE film fabrication, 80% carbon black was added to increase the electronic conductivity. The PTFE powder and carbon black were mixed for 30 min in a kitchen mixer, then the mixture was grinded in an agate mortar until the formation of flake; finally, the flask was hot rolled using a calendering machine. SF hard carbon electrode was fabricated with similar method in our previous study with hard carbon: carbon black: PTFE: PVDF = 90: 5: 3: 2. The thickness of SF hard carbon electrode was 120 μm with the capacity of 3.7 mA/cm^2.

To compare the performance of SF LFP electrode, SC LFP electrode was also fabricated. LFP, PVDF and CNT were mixed in NMP with same mass ratio of SF procedure. The slurry was casted onto same Al foil and dried. The SC LFP was subsequently calendered with the capacity of 1.6 mAh/cm^2.

2.2 Cell assembly

Both half cells and full cells were assembled with 2032-coin cell parts (MTI, Shenzhen, China) in an argon-filled glove box, where water and oxygen concentrations were less than 0.01 ppm. For half cells, two layers cellulose film (Celgard, Charlotte, NC, US), lithium foil (Sigma-Aldrich, 600 μm, Darmstadt, Germany) and 50 μL 1.2 M $LiPF_6$ in EC-EMC (3/7, v/v) with 10 wt% fluoroethylene carbonate (FEC) were used as separator, counter electrode and electrolyte, respectively. For full cell assembly, SF hard carbon electrodes were used as anode. The capacity ratio of anode to cathode (N/P ratio) was set to 1.1:1.

2.3 Prelithiation

Single layer SF Hard carbon electrode with size of 5*5 cm was assembled into monolayer pouch cell with lithium foil as counter electrode. The separator and electrolyte were similar with these used in coin cells. The pouch cell was discharged under the current of 0.3 mA/cm^2 with the lithiation capacity of 3 mAh/cm^2. The pouch cell was disassembled in glovebox and the prelithiated hard carbon electrode was

washed with DMC and dried under room temperature overnight in glovebox. The prelithiated hard carbon electrode was further assembled with SF LFP electrode to full SF LFP/hard carbon cell.

2.4 Electrochemical and morphological characterization

The galvanostatic charge/discharge tests were performed under room temperature using an 8-channel battery analyzer (Neware, Shenzhen, China). The cutoff voltage was set between 2.5 to 3.65 V for half cells. All cells were aged under room temperature for 12 h before testing and underwent several formation cycles. Cyclic voltammetry (CV) scanning was carried out in the voltage range of 2-3.8 V at a scanning rate of 0.5 mV/s.

The pristine and cycled electrodes were characterized using a scanning electron microscope (SEM, Phenomenon LE). The cycled electrodes were charged to the fully delithiation state after cell cycling, followed by disassembling the cell, dipping the electrode into DMC solution for 2 h to remove any residual electrolyte, and drying at room temperature overnight in an argon-filled glove box for further ex-situ analysis.

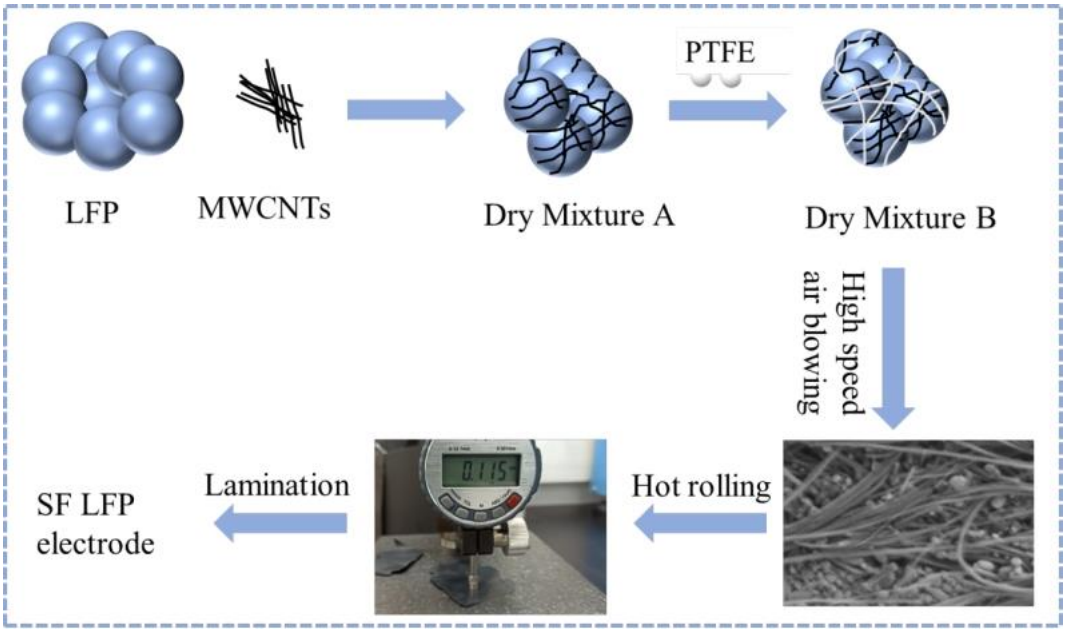

Figure 4.1 Schematic diagram of SF LFP electrode fabrication based on PTFE fibrillation, including dry mixing, fibrillation, hot-rolling and lamination.

3. Results and discussion

According to our previous studies and other publication, PTFE is instable in anode.

The stability of PTFE in cathode is waiting for further clarification. PTFE film was prepared and coin cells were assembled with PTFE film as cathode and lithium foil as counter electrode. The charge/discharge testing was conducted from 2-4 V under 1 mA/cm^2. In contrast to the results from 0-1.5V, the capacity of PTFE film is only 1.5 mAh/g, which is ascribed to capacitance of carbon black. The negligible capacity of PTFE demonstrated stability of PTFE within 2-4 V (Figure 4.3a). X-ray diffraction (XRD) characterization was conducted on both pristine and cycled SF LFP electrode. The peak at around 19° attributed to PTFE remained after lithiation. (Figure 4.3b). The pristine and cycled PTFE film were also observed under SEM (Figure 4.2 c, d). After three charge/discharge cycling, the PTFE fibrils maintained their structure. The results from electrochemical capacity, XRD and morphology analysis were consistently proved the stability of PTFE in cathode.

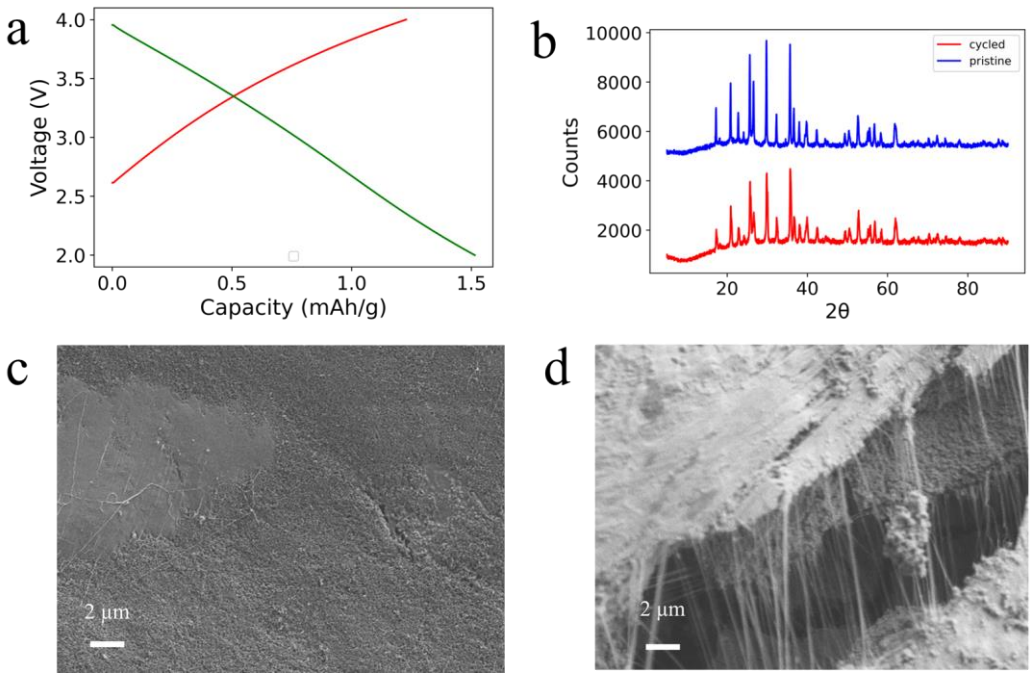

Figure 4.2 Stability study of PTFE used in cathode. (a) capacity-voltage curves of PTFE film. (b) XRD comparison between pristine and cycled SF LFP electrode; (c) SEM morphology of pristine PTFE film; (d) SEM morphology of PTFE film after cycling

PTFE fibrillation has been used for NMC electrode fabrication both for LiBs and ASSBs. However, there is no PFTE fibrillation based LFP electrode for LiBs reported so far. We first tried LFP electrode fabrication with the weight ratio of LFP /activated

carbon /PTFE = 47.5 /47.5 /5. The activated carbon was added to increase the flexibility of electrode. The activated carbon and LPF were mixed first and PTFE powder was subsequently added to form dry mixture. The dry mixture was fibrillated through a jet mill with grinding pressure of 80 Psi to get cotton candy like dry mixture. The mixture was thereafter hot rolled several times to form a self-supporting electrode film. After that, the electrode film was laminated with carbon coated aluminum foil with the same hot roller to get the final SF LFP-AC electrode. The coin cells were assembled with lithium foil as counter electrode and cycled under the current of 1C. The curves of capacity-voltage have the mixing characteristics of capacitance and batteries (Figure 4.3a) with the capacity of 1.1 mAh/cm^2. The voltage increases linearly with capacity from 2-3.4V, resulting from capacitance of activated carbon. After that, a charge plateau appears at 3.45V, which is ascribed to the faradaic reaction of LFP. The half cells have good stability with 90% capacity retention after 100 charge/discharge cycling under the current of 1.2 mA/cm^2 (Figure 4.3b). After 100 cycles, the capacity faded fast. When disassemble the coin cell after 100 cycles, the electrode and separator were dry without obvious electrolyte observed. The fast capacity fading could attribute to the consumption of electrolyte since just 50 μm electrolyte injected in the coin cell.

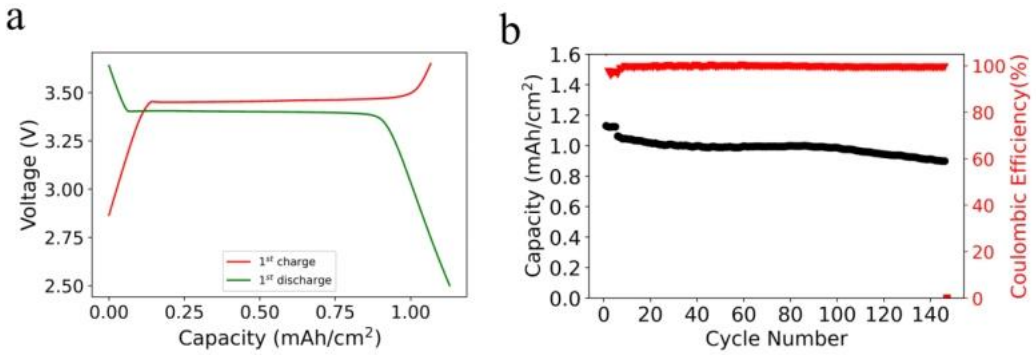

Figure 4.3 (a) stability of SF LFP-AC half cells under the current of 1.2 mA/cm2; (b) capacity-voltage curves for SF LFP-AC half cells.

The PTFE fibrils could be observed on the surface of pristine LPF-AC electrode under SEM (Figure 4.4 a, b). Activated carbon acts as conductive additive to keep the good conductivity network of the electrode to ensure good performance of SF LPF-AC electrode under high current (Figure 4.4c). However, activated carbon has low density

and high specific surface area, which will result in low specific energy and moisture absorption. The compressed density of LFP-AC electrode is only 1.6 g/cm^3, which is significantly lower than LFP electrodes (2.1-2.2 g/cm^3).

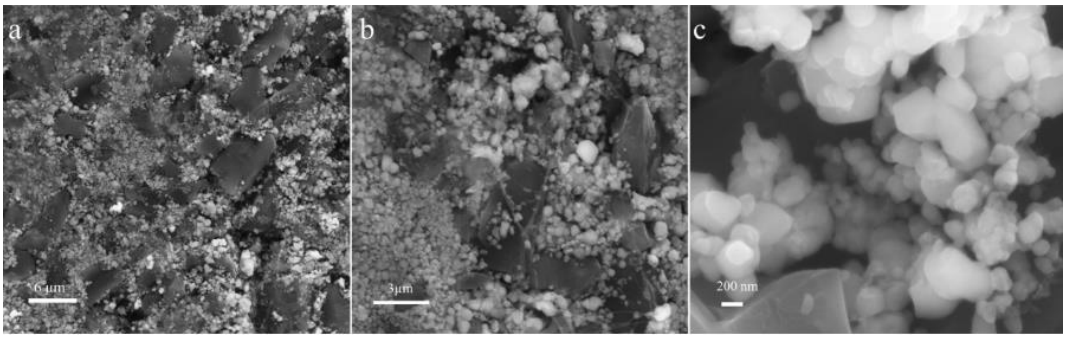

Figure 4.4 SEM images of pristine LFP-AC electrodes with different magnification. (a) x4000, (b) x10000; (c) x50000.

Fabricating SF LFP electrode basing on PTFE fibrillation for LiBs is waiting further exploration. We first tried SF LFP electrode fabrication without activated carbon, the mixture (LFP: carbon black: PTFE = 85: 10: 5) was hot rolled under the same condition of LFP-AC electrode. Out of our expectation, the rolls were stuck by the dry mixture powder. To form self-supporting electrode film, further fibrillation of PTFE is necessary when the mixture was compressed through the calendering rolls. The hardness of LFP particles prevent the tangent motion of calendering roll to PTFE particles, failing to further fibrillate PTFE. While in the case of carbon materials like graphite, the material itself is soft. When the dry mixture was compressed through calendering rolls, PTFE along with active material have opposite motion direction with rolls to get PTFE further fibrillated, ensuring the formation of self-supporting electrode film. For LFP-AC electrodes, the tap density of activated carbon (0.67 g/cm^3) is much smaller than LPF (1.3 g/cm^3). With 47.5% percent of activated carbon, the volume of activated carbon is much greater than LPF. The activated carbon acts as matrix to offer relative opposite motion of PTFE and roll when the dry mixture was compressed under calendering machine.

Different carbon materials including CNT, conductive graphite, carbon black were screened with different mass ratio. Self-supporting LFP electrode film was formed only with CNT with the carbon content is 10%, while other carbon materials just got rolls

stuck during hot-rolling process. The tap density of carbon black, CNT and conductive graphite are 0.16, 0.025 and 0.96 g/cm^3, respectively. The low tap density of CNT makes it has more relative volume ratio with same weight ratio. The relative high tap density of conductive graphite and carbon black make them insufficient to offer shear force during hot rolling. When further increase carbon black to 20%, self-supporting LFP electrode film with some cracks could be formed. The key parameter for carbon materials to assist LFP electrode film formation is the tap density. Regarding conductive graphite, no LFP electrode film could be formed even the content of graphite was increased to 40%. The minimum amount of different carbon materials required for LFP film formation was listed in Table 4.1. The lower tap density of carbon material, the less carbon material required to form LFP film.

Table 4.1 Carbon materials screening for SF LFP electrode fabrication

Table 4.1 Carbon materials screening for SF LFP electrode fabrication

Carbon materials	Tap density (g/cm^3)	Weight ratio (%)	Electrode formation	Comments
Carbon black	0.16	40	√	Flexible film
		20	√	Film with cracks
		10	×	Failed
CNT	0.025	40	√	Flexible film
		20	√	Flexible film
		10	√	No cracks or holes
		5	√	No cracks or holes
Conductive graphite	0.96	40	×	Film with cracks and holes
		20	×	Failed
		10	×	Failed

The mechanical strength of electrode film, which is critical for upscaling production, is determined by the fibrillation degree of PTFE powder. The temperature has huge effect on the property of PTFE[23-25]. The PTFE has a well-ordered hexgonal crystal structure at the temperature below 19 ℃, the hard PTFE particles will slide past each

other when shear force applied without being fibrillated. In the temperature between 19 to 30 ℃, the crystalline PTFE turns into hexagonal phase. Further heating PTFE to higher temperature, PTFE converts into a disordered pseudo-hexagonal phase with molecule chain packed loosely. The higher temperature, the easier the PTFE will be fibrillated before reaching to its melting point. To get the optimal mechanical strength of electrode film, the temperature was screened from 40 to 160 ℃ during hot rolling. The electrode film cannot be formed below 90 ℃. The tensile strength of obtained electrode film increase along the temperature enhancement between 100 to 160 ℃. The thickness of electrode film was reduced to 125 μm after pressing several times. The compressed density of the electrode film was 2.0 g/cm^3, which is similar with commercial LFP electrode (2.1-2.2 g/cm^3). The electrode film was subsequently laminated onto carbon coated aluminum foil.

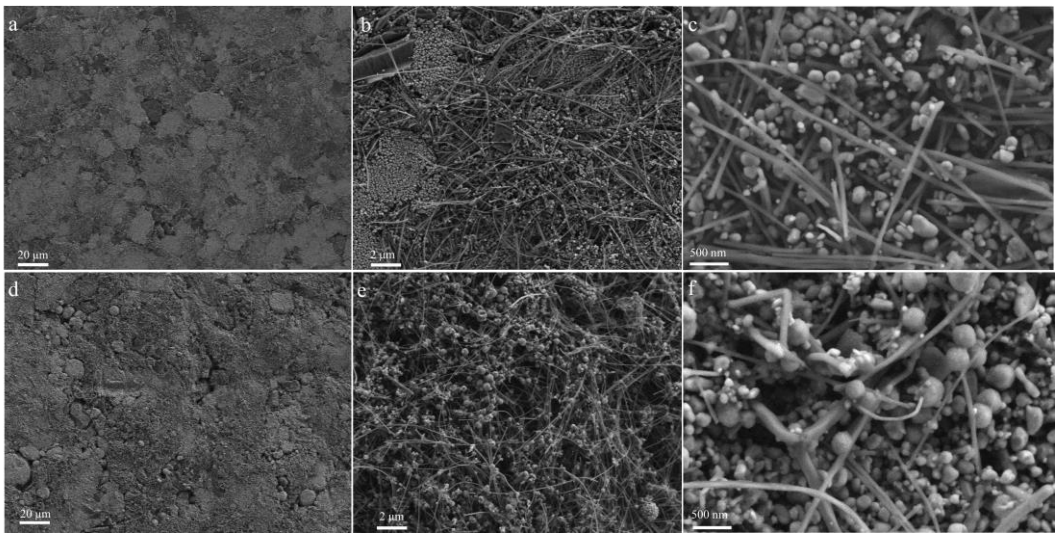

Figure 4.5 SEM images of pristine SF LFP electrode with different magnification. (a) x1000; (b) x5000; (c) x10000; SEM images of SF LFP electrode after 50 cycles. (d) x1000; (e) x5000; (f) x10000.

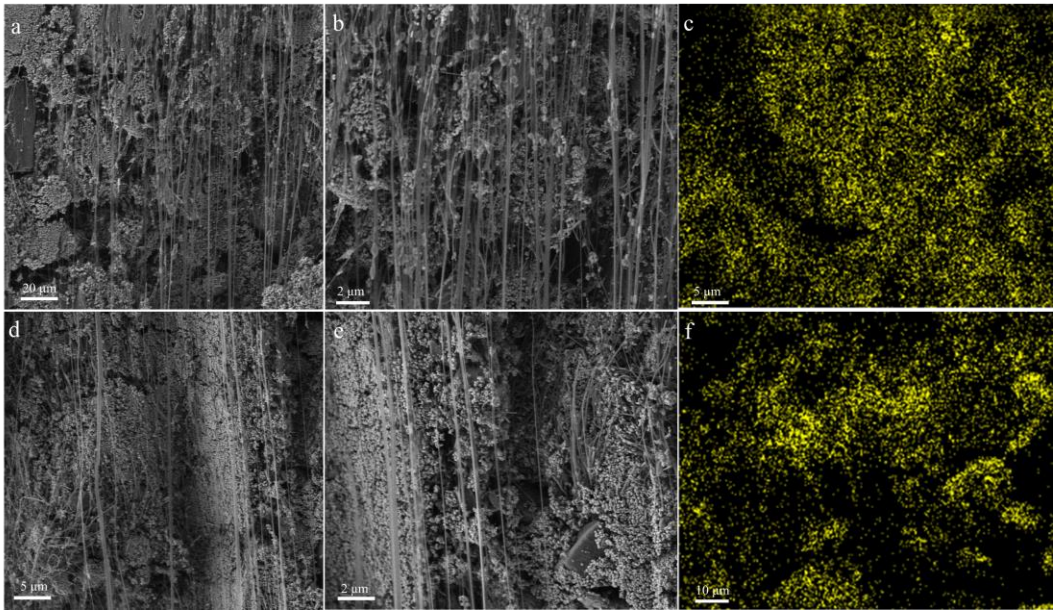

Figure 4.6 Cross section SEM images of pristine SF LFP electrode. (a) x1000; (b) x5000; (c) EDS mapping of Fluorine from pristine SF LFP electrode; SEM images of SF LFP electrode after 50 cycles. (d) x1000; (e) x5000; (f) EDS mapping of Fluorine from cycled SF LFP electrode.

PTFE fibrils were observed from fresh LFP electrode, demonstrating good fibrillation of PTFE (Figure 4.5a). LFP powders were distributed in the matrix of CNT (Figure 4.5b, c), enabling good conductivity and mechanical strength of the electrode. PTFE fibrils were more visible from the cross-sectional images (4.6a, b). EDS-mapping of pristine LFP electrode demonstrated the uniform distribution of PTFE, which is the guarantee of good mechanical strength of electrode film (4.6c).

The cycling stability of SF LFP electrode was studied in half cells with the specific capacity of 3.1 mAh/cm^2. LFP delivered the capacity of 142 mAh/g under the current of 0.6 mA/cm^2 with ICE of 95.6%, which is similar with commercial LFP electrode at room temperature (Figure 4.7a). The capacity retention was 80% after 40 charge/discharge cycles under the current of 1.7 mA/cm^2 (Figure 4.7b). However, after 40 cycles, the capacity fade very fast. When the coin cells were disassembled, there was no obvious cracks observed from LFP electrode. But the electrode and separator were dry and lithium electrode was pulverized. The fast capacity fading was mainly caused by the pulverization of lithium foil and electrolyte consumption. The cycled LFP electrode was characterized under SEM, the structure of LFP electrode was well

remained (Figure 4.5d-f). The cross-section observation and EDS mapping of the cycled electrode also similar with pristine SF LFP electrode (Figure 4.6 d-f). The cycled SF LFP electrode was assembled with new lithium foil and separator into coin cells and the capacity recovered to more than 95% of initial capacity. There are no obvious capacity fading during first several cycling (Figure 4.7 c). Those results demonstrated the good stability of SF LFP electrode even under high loading and current density.

To compare, LFP electrodes were fabricated through SC procedure. What is worth mentioning is that the materials loading of slurry casting procedure is 11.5 mg/cm^2 (1.6 mA/cm^2), which was much smaller than that of SF LPF electrode. When we try to increase the loading of SC electrode, cracks appeared after compressing. In contrast to SF LFP electrode, the SC LFP electrode delivered specific capacity of 138 mAh/g under the same current density. To further compare the rate-capability of two different electrodes, the capacity was tested under different current density from 0.08mA to 1.6mA/cm^2. The SF LFP electrodes showed higher rate-capability performance that SC LFP electrode (Figure 4.8 a). The capacity retention for SF electrode were 99.8, 99.1, 98.1, 95.0% under 0.16, 0.32, 0.8, 1.6 mA/cm^2, respectively, while the capacity retention for SC electrode were 98.6, 96.2, 91.7, 87.1% under same current density. Electrochemical impedance spectroscope (EIS) analysis was conducted to further explain the different performance of SF and SC LFP electrodes. For both pristine electrodes and electrodes after formation, the charge transfer resistances of SC electrodes are larger than SF LFP electrodes (Figure 4.8 b, c). The EIS results were consistent with rate performance. The different binding mechanism of PTFE fibrillation-based SF procedure facilitates better rata performance, where the spot contact of PTFE fibrils and LFP particles is beneficial for charger transfer and resulting good rata-capability. While in the case of SC procedure, PVDF was first dissolved in NMP. The PVDF formed a compact insulating layer around LFP particles, which is detrimental for charge transfer.

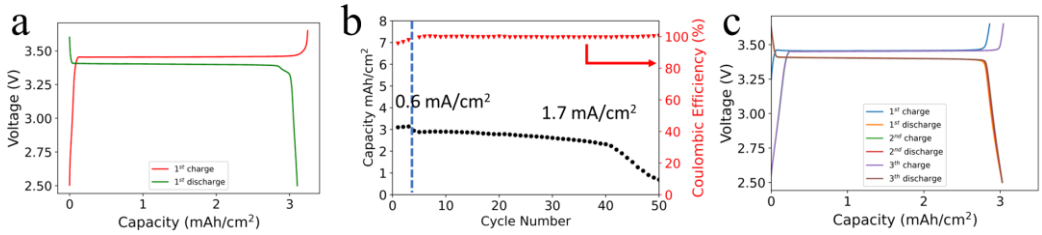

Figure 4.7 (a) Capacity-voltage curves for SF LFP half cells. (b) Stability of SF LFP half cells under the current of 1.7 mA/cm^2; (c) capacity recovery of cycled SF LFP electrode.

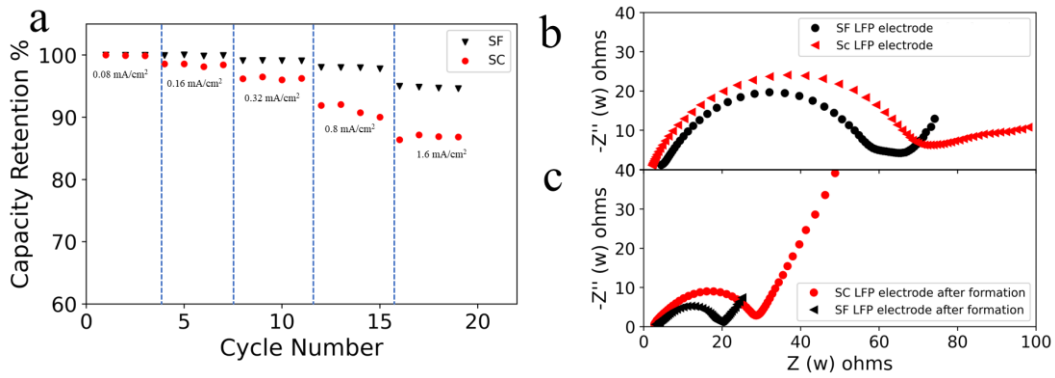

Figure 4.8 (a) Rate performance comparison between SF and SC LFP electrode under different current density; (b) EIS comparison between pristine SF and SC LFP electrodes in half cells; (b) EIS comparison between SF and SC LFP electrodes after formation in in half cell.

Hard carbon has low volume variation during charge/discharge process, ensuring longer cycling life than graphite electrode[26-28]. According to our previous study, PTFE fibrillation-based SF hard carbon electrode demonstrated good stability. Full cells were assembled with SF hard carbon electrodes and SF LFP electrodes. The SF hard carbon electrode was fabricated with similar procedure reported in our previous study, where 2% of PVDF and 3% PTFE were used as binder. The N/P ratio of the full cell was set to 1.2 (the areal capacity of hard carbon and LFP electrodes were 3.7 and 3.1 mAh/cm^2, respectively). Hard carbon has low ICE, which impedes its application in commercial LiBs[29,30]. The reaction between PTFE and lithium ion at first lithiation process make the ICE even lower. However, with the help of prelithiation, we can get rid of low ICE issue. And the ICE is adjustable according to the depth of prelithiation.

Single layer pouch cells were assembled with lithium foil as counter electrode. The hard carbon electrode was lithiated with the capacity of 2 mA/cm^2. The prelithiated SF hard carbon electrode was assembled into full coin cells with SF LFP electrodes as

cathode. Pristine and lithiated hard carbon electrodes was observed under SEM from both top view and cross section. Similar with our previous studies, PTFE fibrils tie up hard carbon particles together to form compact structure (Figure 4.9a-c and Figure 4.10a, b). After lithiation, most of PTFE fibrils decomposed (Figure 4.9d-f), but the electrodes kept their integrity with the help of PVDF (Figure 4.10 d, e). There were not much different between the fluorine distribution between pristine and lithiated hard carbon electrode from EDS mapping (Figure 4.10 c, f), demonstrating good stability of SF hard carbon electrode under the condition of prelithiation.

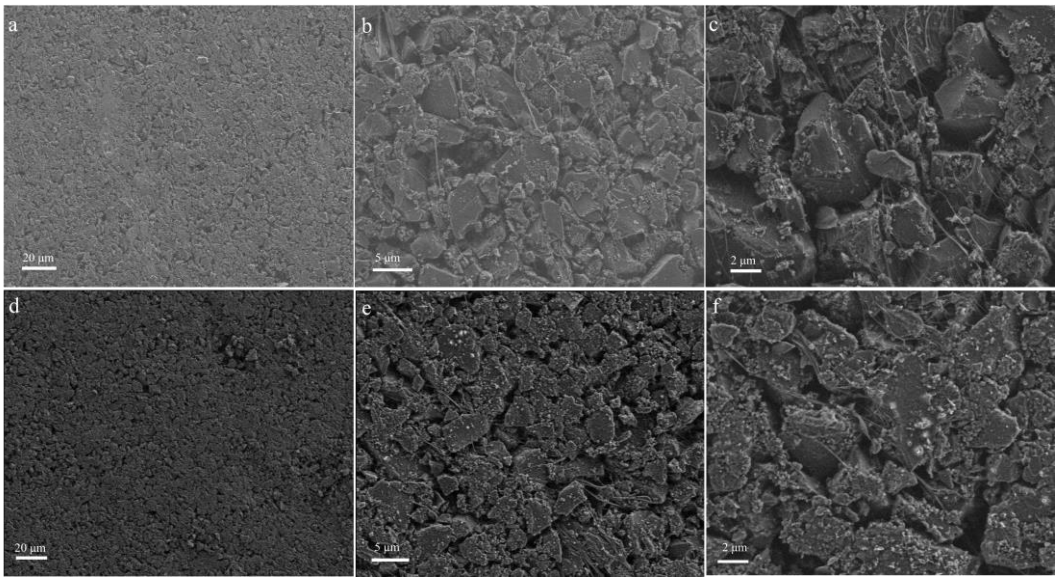

Figure 4.9 Top view SEM images of pristine hard carbon electrodes with different magnification. (a) 1000x, (b) 5000x, (c) 10,000x. Top view SEM images of prelithiated hard carbon electrodes with different magnification. (d) 1000x, (e) 5000x, (f) 10,000x.

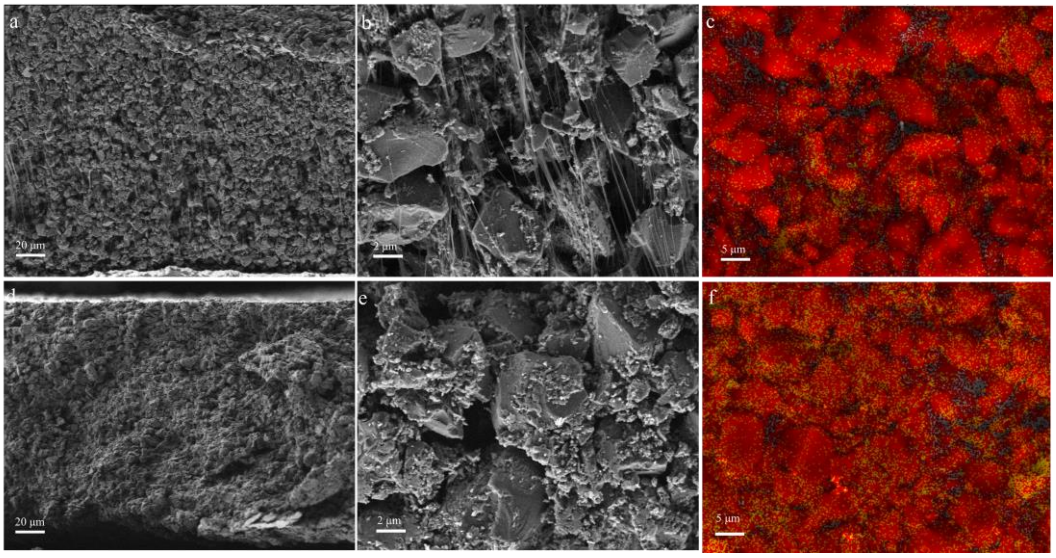

Figure 4.10 Cross section SEM images of pristine hard carbon electrode with magnification. (a) 1000x, (b) 10,000x, (c) EDS mapping of fluorine in cross section. Cross section SEM images of prelithiated hard carbon electrode with magnification. (a) 1000x, (b) 10,000x, (c) EDS mapping of fluorine in cross section.

X-ray photoelectron spectroscope (XPS) analysis was conducted to monitor the PTFE decomposition from SF hard carbon and SF LFP electrodes. The peak from F 1s in 689.2 eV in pristine hard carbon electrode was attributed to CF_2 (Figure 4.11a). After lithiation, new peak appeared at 686.9 eV belongs to LiF, which was the decomposition product of PTFE (Figure 4.11b). The same peak from PTFE appears in SF LFP electrode (Figure 4.11c)). After many cycles, the peak kept, demonstrating stability of PTFE in cathode. The new peak from 684.4 eV was attributed to PF_6^- from electrolyte.

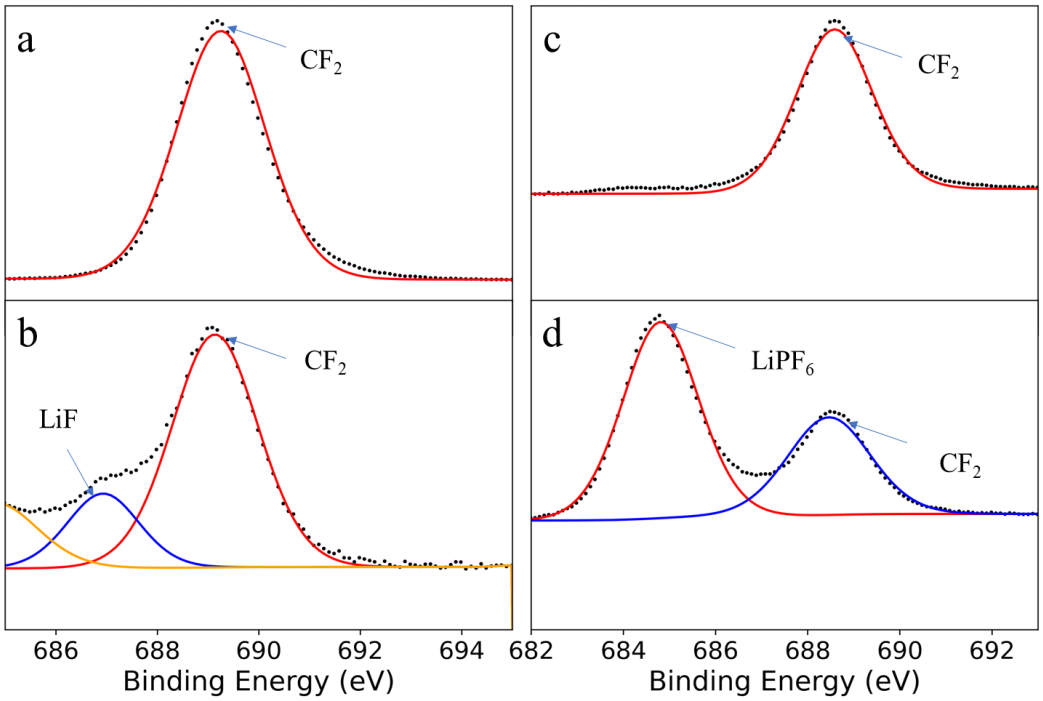

Figure 4.11 XPS analysis of F 1s with different electrode. (a) pristine SF hard carbon electrode, (b) prelithiated SF hard carbon electrode, (c) pristine SF LFP electrode, (d) cycled SF LFP electrode.

The cycling stability testing was performed under 0.5 C at room temperature. As shown in Figure 4.12a, the ICE of the full cell was close to 100% with the help of prelithiation. The full cells have good stability with more than 95 % capacity retention after 50 cycles (Figure 4.12 b). The average coulombic efficiency (CE) for first 50 cycles was more than 99.95%, which demonstrating the formation of stable SEI.

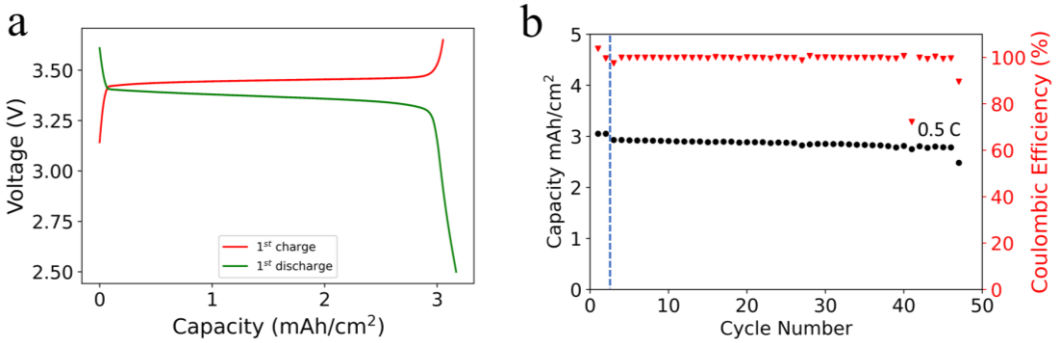

Figure 4.12 (a) Capacity-voltage curves for SF LFP/hard carbon cells; (b) stability of SF LFP/hard carbon cells under 0.5C.

4. Conclusion

PTFE fibrillation-based SF LFP electrode was successfully fabricated with the help of CNT, where CNT act as conductive additive and matrix to hold LFP particles to ensure the further fibrillation of PTFE when pressed through calender machine, simultaneously. The SF LFP electrode demonstrated good stability and better rate-capability than SC counterparts because of good conductivity of CNT and spot contact between PTFE fibrils and LFP particles. With the help of prelithiation, the ICE of SF LFP/hard carbon cells was increased to 100% and showed decent cycling stability under the current of 1.5 mA/cm^2 with more than 95% capacity retention after 50 cycles. The simple fabrication procedure and good performance of SF LFP/hard carbon cells makes it promising to replace current slurry casting procedure for commercial LiBs.

References

1. Whittingham, M.S. Ultimate limits to intercalation reactions for lithium batteries. *Chemical reviews* **2014**, *114*, 11414-11443.

2. Chen, W.; Liang, J.; Yang, Z.; Li, G. A review of lithium-ion battery for electric vehicle applications and beyond. *Energy Procedia* **2019**, *158*, 4363-4368.

3. Laadjal, K.; Cardoso, A.J.M. Estimation of lithium-ion batteries state-condition in electric vehicle applications: issues and state of the art. *Electronics* **2021**, *10*, 1588.

4. Matteson, S.; Williams, E. Learning dependent subsidies for lithium-ion electric vehicle batteries. *Technological Forecasting and Social Change* **2015**, *92*, 322-331.

5. Li, J.; Du, Z.; Ruther, R.E.; An, S.J.; David, L.A.; Hays, K.; Wood, M.; Phillip, N.D.; Sheng, Y.; Mao, C. Toward low-cost, high-energy density, and high-power density lithium-ion batteries. *Jom* **2017**, *69*, 1484-1496.

6. Ryu, H.-H.; Sun, H.H.; Myung, S.-T.; Yoon, C.S.; Sun, Y.-K. Reducing cobalt from lithium-ion batteries for the electric vehicle era. *Energy & Environmental Science* **2021**, *14*, 844-852.

7. Hawley, W.B.; Li, J. Electrode manufacturing for lithium-ion batteries—Analysis of current and next generation processing. *Journal of Energy Storage* **2019**, *25*, 100862.

8. Liu, H.; Cheng, X.; Chong, Y.; Yuan, H.; Huang, J.-Q.; Zhang, Q. Advanced electrode processing of lithium ion batteries: A review of powder technology in battery fabrication. *Particuology* **2021**, *57*, 56-71.

9. Wood, D.L.; Quass, J.D.; Li, J.; Ahmed, S.; Ventola, D.; Daniel, C. Technical and economic analysis of solvent-based lithium-ion electrode drying with water and NMP. *Drying Technology* **2018**, *36*, 234-244.

10. Wang, M.; Dong, X.; Escobar, I.C.; Cheng, Y.-T. Lithium Ion Battery Electrodes Made Using Dimethyl Sulfoxide (DMSO)—A Green Solvent. *ACS Sustainable Chemistry & Engineering* **2020**, *8*, 11046-11051.

11. Zhang, Y.; Huld, F.; Lu, S.; Jektvik, C.; Lou, F.; Yu, Z. Revisiting Polytetrafluorethylene Binder for Solvent-Free Lithium-Ion Battery Anode Fabrication. *Batteries* **2022**, *8*, 57.

12. Li, Y.; Wu, Y.; Wang, Z.; Xu, J.; Ma, T.; Chen, L.; Li, H.; Wu, F. Progress in solvent-free dry-film technology for batteries and supercapacitors. *Materials Today* **2022**.

13. Lu, Y.; Zhao, C.-Z.; Yuan, H.; Hu, J.-K.; Huang, J.-Q.; Zhang, Q. Dry electrode technology, the rising star in solid-state battery industrialization. *Matter* **2022**, *5*, 876-898.

14. Wu, Q.; Zheng, J.P.; Hendrickson, M.; Plichta, E.J. Dry process for fabricating low cost and high performance electrode for energy storage devices. *MRS Advances* **2019**, *4*, 857-863.

15. Duong, H.; Shin, J.; Yudi, Y. Dry electrode coating technology. In Proceedings of the 48th Power Sources Conference, 2018; pp. 34-37.

16. Hippauf, F.; Schumm, B.; Doerfler, S.; Althues, H.; Fujiki, S.; Shiratsuchi, T.; Tsujimura, T.; Aihara, Y.; Kaskel, S. Overcoming binder limitations of sheet-type solid-state cathodes using a solvent-free dry-film approach. *Energy Storage Materials* **2019**, *21*, 390-398.

17. Quan, J.; Zhao, S.; Song, D.; Wang, T.; He, W.; Li, G. Comparative life cycle assessment of LFP and NCM batteries including the secondary use and different recycling technologies. *Science of The Total Environment* **2022**, *819*, 153105.

18. Ioakimidis, C.S.; Murillo-Marrodán, A.; Bagheri, A.; Thomas, D.; Genikomsakis, K.N. Life cycle assessment of a lithium iron phosphate (LFP) electric vehicle battery in second life application scenarios. *Sustainability* **2019**, *11*, 2527.

19. Wang, Z.; Yuan, J.; Zhu, X.; Wang, H.; Huang, L.; Wang, Y.; Xu, S. Overcharge-to-thermal-runaway behavior and safety assessment of commercial lithium-ion cells with different cathode materials: A comparison study. *Journal of Energy Chemistry* **2021**, *55*, 484-498.

20. Chen, S.; Zhang, G.; Wu, C.; Huang, W.; Xu, C.; Jin, C.; Wu, Y.; Jiang, Z.; Dai, H.; Feng, X. Multi-objective optimization design for a double-direction liquid heating system-based Cell-to-Chassis battery module. *International Journal of Heat and Mass Transfer* **2022**, *183*, 122184.

21. Altenburg, T.; Corrocher, N.; Malerba, F. China's leapfrogging in electromobility. A story of green transformation driving catch-up and competitive advantage. *Technological Forecasting and Social Change* **2022**, *183*, 121914.

22. Zhou, H.; Liu, M.; Gao, H.; Hou, D.; Yu, C.; Liu, C.; Zhang, D.; Wu, J.-c.; Yang, J.; Chen, D. Dense integration of solvent-free electrodes for Li-ion supercabattery with boosted low temperature performance. *Journal of Power Sources* **2020**, *473*, 228553.

23. Blumm, J.; Lindemann, A.; Meyer, M.; Strasser, C. Characterization of PTFE using advanced thermal analysis techniques. *International Journal of Thermophysics* **2010**, *31*, 1919-1927.

24. Villani, V. A study on the thermal behaviour and structural characteristics of polytetrafluoroethylene. *Thermochimica Acta* **1990**, *162*, 189-193.

25. Ochoa, I.; Hatzikiriakos, S.; Mitsoulis, E. Paste extrusion of polytetrafluoroethylene: temperature, blending and processing aid effects. *International Polymer Processing* **2006**, *21*, 497-503.

26. Wang, K.; Xu, Y.; Wu, H.; Yuan, R.; Zong, M.; Li, Y.; Dravid, V.; Ai, W.; Wu, J. A hybrid lithium storage mechanism of hard carbon enhances its performance as anodes for lithium-ion batteries. *Carbon* **2021**, *178*, 443-450.

27. Xie, L.; Tang, C.; Bi, Z.; Song, M.; Fan, Y.; Yan, C.; Li, X.; Su, F.; Zhang, Q.; Chen, C. Hard Carbon Anodes for Next-Generation Li-Ion Batteries: Review and Perspective. *Advanced Energy Materials* **2021**, *11*, 2101650.

28. Alvin, S.; Cahyadi, H.S.; Hwang, J.; Chang, W.; Kwak, S.K.; Kim, J. Revealing the intercalation mechanisms of lithium, sodium, and potassium in hard carbon. *Advanced Energy Materials* **2020**, *10*, 2000283.

29. Ren, N.; Wang, L.; He, X.; Zhang, L.; Dong, J.; Chen, F.; Xiao, J.; Pan, B.; Chen, C. High ICE Hard Carbon Anodes for Lithium-Ion Batteries Enabled by a High Work Function. *ACS Applied Materials & Interfaces* **2021**, *13*, 46813-46820.

30. Shen, Y.; Qian, J.; Yang, H.; Zhong, F.; Ai, X. Chemically prelithiated hard-carbon anode for high power and high capacity Li-ion batteries. *Small* **2020**, *16*, 1907602.

Chapter 5: Conclusion and Future Perspectives

5.1 Conclusion

In this project, PTFE fibrillation-based SF procedure was successfully expanded to the fabrication of anode (hard carbon, soft carbon and graphite) and LFP cathode. Basing on different characterizations and analysis, the failure mechanism of SF graphite anode was proposed that the PTFE was reduced by lithium ion to amorphous carbon at first lithiation process. The nano size amorphous carbon lost the binding function during following charge/discharge process. Large volume swelling and shrinking of SF graphite electrode during charge/discharge process make the electrode lose its integrity, resulting in fast capacity fading. For hard carbon and soft carbon, the SF electrodes can keep their integrity even though the PTFE is reduced to amorphous carbon because of the limited volume variation during charge/discharge process. Basing on the understanding of failure mechanism, dual binder system was adopted to alleviate fast capacity fading issue of SF graphite anode. PVDF was combined with PTFE to ensure stability of SF graphite anode, where PTFE acts as an aid reagent to form self-supporting electrode, while PVDF acts as real functional binder, which can keep the electrode integrity when PTFE was decomposed.

PTFE based SF procedure was further expanded to SF LFP electrode fabrication. CNT was used on the one hand as conductive additive to increase the conductivity of LFP electrode. On the other hand, CNT acts as matrix for LFP particles. The CNT matrix enables the relative movement to ensure the further fibrillation of PTFE to form self-supporting electrode films. With the help of 5% CNT, SF LFP electrode was fabricated and showed decent electrical chemical performance. SF LFP/hard carbon full cells were fabricated. With the help of prelithiation, ICE was increased to nearly 100%, which can increase more than 10% of the specific energy since the ICE for cells without prelithiation is usually less than 90%. The SF full cells demonstrated impressive cycling life, with more than 95% of capacity retention after 50 cycles under 0.5C under room temperature in coin cells. The degree of PTFE fibrillation has most effect on the quality of electrode film. The temperature was screened to promote PTFE fibrillation to ensure

good mechanical strength.

5.2 Future perspectives

The roll-to-roll production way makes PTFE fibrillation-based SF technology promising to replace SC procedure for electrode manufacturing. However, most of the SF electrode fabrication are still conducted in laboratory scale. It is paramount to speed up the commercialization of SF procedure by combining fundamental research and engineering studies.

Generally, PTFE fibrillation-based SF procedure is compatible to current LiBs production line. The difference is that dry mixer for SF procedure replaces planetary mixer for SC procedure. A special feeding system is also required to make the self-supporting electrode film. Currently, there is no mature equipment for those process. Designing and manufacturing new equipment with high system integration degree is highly desirable to fabricate electrode at high speed, which is significant to reduce manufacturing cost. The equipment with special function integrated is also important, for example heating is required for electrode film formation.

In addition to normal electrode fabrication, the potential applications of SF procedure in ASBBs and other process like prelithiation in LiBs make it even more competitive. For example, using prelithiation reagents is promising strategy for prelithiation. However, most of prelithiation reagents is not suitable for slurry preparation process because of their high activity. For instance, stabilized lithium metal powder (SLMP) used as prelithiation reagents at anode is instable in water. Another interesting prelithiation reagent for anode is lithiated silicon, which is not stable in most polar solvent but could keep stable in air. At cathode side, lithium rich material Li_5FeO_4 (LFO) is candidate for prelithiation reagent. But it's difficult to make cathode slurry with LFO caused by high pH value. PTFE fibrillation-based SF procedure is will convenient for prelithiation with lithium rich materials as prelithiation reagents. Developing new materials, such as fibrillizable polymers with wide applicable electrochemical window to replace PTFE is also highly desirable since PTFE is instable

in anode.